Master Sciences de la Matière
École normale supérieure de Lyon
Université Claude Bernard Lyon 1

Notes - Spring 2017
Yann-Edwin KETA
M1 Physique

Numerical analysis of jamming criticality for spheroidal particles

Project supervised by:

Peter OLSSON
peter.olsson@tp.umu.se
tél. +46 90 7865046
Institutionen för fysik
Umeå universitet
SE-90187 Umeå, Sweden
http://physics.umu.se/

Contents

Introduction

Granular materials are ubiquitous in nature and are the second-most manipulated material in industry [1]. These are non-thermal systems, *i.e.* their kinetic energy vanishes in absence of an external drive. Despite their relative simplicity, they exhibit a wide range of interesting – even fascinating – behaviours [2].

Granular matter can show either liquid-like or solid-like properties under different experimental conditions. This transition from a flowing state to a rigid state is known as the *jamming transition*, and has been the subject of much recent work. Understanding why and how these materials transition from one of this state to the other is indeed of great theoretical interest, *e.g.* understanding the mechanisms which govern jamming in athermal macroscopic systems may help us to understand how supercooled liquid freeze into a frozen glass [3].

Numerical shearing simulations of non-rotating frictionless soft-core disks have been proven particularly efficient to study the jamming transition [4, 5]. Our present report aims to present the methods which have been employed in such studies and to show how they can and have been modified and enriched to study more general rotating frictionless soft-core spheroids (*ie.* ellipsoids of revolution), both prolate – elongated – and oblate – flattened.

Computer programs were written in MATLAB language for evaluation of the methods then in C language for performance (speed of execution). All the code developed specifically for this project is available on GitHub, in the repository yketa/shear_ellipsoids. Simulations with 64 and 1024 particles were run on 1 and 4 cores respectively on computers provided by the Department of Physics at Umeå University. Simulations with 16384 particles were run on 12 cores on the supercomputer provided by the Swedish National Infrastructure for Computing (SNIC) at High Performance Computing Center North (HPC2N).

This report is organised as follows. In chapter 1, we show how quaternions are used to numerically integrate rigid body rotation equations. In chapter 2, we briefly introduce ellipsoids and present different numerical methods to determine if and how they overlap. In chapter 3, we more thoroughly describe the jamming transition, as well as the models and methods we have used, modified and improved. In chapter 4 we present and discuss our numerical results.

Appendices provide theoretical backgrounds on objects and theories we use throughout this report. Appendix A is a theoretical introduction to quaternions. Appendix B is a demonstration of the Euler's equation describing the rotation of a rigid body. Appendix C is a theoretical introduction to ellipsoids. Appendix D is an introduction to renormalisation group theory and aims to show how this theory allows us to make scaling assumptions.

1 | Quaternions

Our goal here is to present quaternions and how they can be implemented in numerical simulations to solve rigid body rotation equations.

1.1 Interest of quaternions

1.1.1 Quaternions

Please find in appendix A a complete presentation of ellipsoids.

Quaternions are an extension of complex numbers which can be written

$$q = q_0 + \sum_{i=1}^{3} q_i e_i, \text{ with } \begin{cases} e_m^2 = -1 \\ e_m e_n = \varepsilon_{mnk} e_k \quad , m \neq n \end{cases} \text{ and } q_0, q_1, q_2, q_3 \in \mathbb{R} \tag{1.1}$$

and can therefore be associated to $\mathbb{R}^4$ vectors.

We can show that any rotation in the 3-dimensional space can be expressed as the action of some unit quaternion, *i.e.* a quaternion associated to a vectos of the unitary hypersphere in $\mathbb{R}^4$.

1.1.2 Theoretical interest

The intrinsic geometry of the rotation group is that of a sphere, therefore it is more natural to use quaternions to represent rotations like it is more natural rectangular coordinates to represent translations [6].

Furthermore, quaternions allow us to represent the orientation with a single vector and are safe from gimbal lock which results from the alignment of two of the three axes of rotation, causing the loss of one degree of rotational freedom, while Euler angles and rotation matrix are not [7].

1.1.3 Numerical interest

Computationally speaking, resorting to quaternions is more efficient than resorting to rotation matrix or axis-angle representations [8].

A rotation can be expressed with 4 floats when using a quaternion while it would need 6 floats with the axis-angle representation and 9 floats with the rotation matrix representation. Moreover, the composition of two rotations can be done with 12 additions and 16 multiplications when using quaternions while it would need 18 additions and 27 multiplications when using rotation matrix. Composing rotations when using axis-angle representation is way harder since it would need to convert this representation to a rotation matrix or a quaternion, do the composition, and then extract the axis angle-pair.

However, when using quaternions, the rotation of n vectors needs – at least [8] – $12 + 6n$ additions and $12 + 9n$ multiplications and this result is achieved by converting the quaternion to a rotation matrix.

Quaternions are also more resistant to rounding errors. Indeed, while a slightly off quaternion still represents a rotation after being normalised, one may have a hard time to convert back a slightly off orthogonal matrix to a proper orthogonal matrix [9].

Furthermore, quaternions are used in many fields where it is essential to interpolate rotations smoothly – in video games for example, *Tomb Raider* (1996) being the first mass-market computer game to have used quaternions to achieve smooth 3D rotation [10], or aircraft kinematics [11] – something which is difficultly achievable with the means of rotation matrix or Euler angles.

1.2 Rotation of a rigid body

1.2.1 Equation of conservation of the angular momentum

Please find in appendix B the extensive demonstrations of the equations presented in this part.

Consider a body $\mathcal{O}$ of angular momentum $\vec{A} = \bar{\bar{I}}\vec{\omega}$, with $\bar{\bar{I}}$ its tensor of moments of inertia and $\vec{\omega}$ its rotation vector. If the total torque $\vec{M}$ is exerted on $\mathcal{O}$, then its angular momentum varies as

$$\boxed{\frac{d}{dt}\vec{A} = \frac{d}{dt}\bar{\bar{I}}\vec{\omega} = \vec{M}} \tag{1.2}$$

where both $\bar{\bar{I}}$ and $\vec{\omega}$ vary as a function of the time.

In the base $(\vec{u_i})_{i=1:3}$ formed by the axis of inertia of the body, the tensor of inertia is constant and diagonal, therefore

$$\vec{A} = \sum_{k=1}^{3} \underbrace{\bar{\bar{I}}\vec{u_k}}_{I_k} \underbrace{\vec{\omega} \cdot \vec{u_k}}_{\omega_k} \vec{u_k}$$

which allows us to write

$$\boxed{\forall k \in [\![1,3]\!],\ I_k\dot{\omega_k} + \varepsilon_{k,l,m}\omega_l I_m \omega_m = M_k} \tag{1.3}$$

1.2.2 Expression with quaternions

If $\vec{r}(t)$ denotes the orientation of the body in the world frame as a function of time then it can be obtained through a 3D rotation from $\vec{r}(0)$ [12]. This rotation can be expressed with an unit quaternion $q(t)$ such that

$$\boxed{\vec{r}(t) = q(t)\vec{r}(0)q^*(t)} \tag{1.4}$$

We have that $\vec{\omega}(t)$ satisfies $\dot{\vec{r}}(t) = \vec{\omega}(t) \times \vec{r}(t)$ and we can infer from equation 1.4 that

$$\begin{aligned}\dot{\vec{r}}(t) &= \dot{q}(t)\vec{r}(0)q^*(t) + q(t)\vec{r}(0)\dot{q}^*(t) \\ &= \dot{q}(t)q^*(t)\vec{r}(t)\cancel{q(t)q^*(t)} + \cancel{q(t)q^*(t)}\vec{r}(t)q(t)\dot{q}^*(t)\end{aligned}$$

We know that $\frac{d}{dt}qq^* = \frac{d}{dt}\underbrace{N^2(q)}_{=1} = 0 = \dot{q}q^* + q\dot{q}^*$ so $q\dot{q}^* = -\dot{q}q^*$ and then

$$\dot{\vec{r}}(t) = \underbrace{\dot{q}(t)q^*(t)}_{g(t)}\vec{r}(t) - \vec{r}(t)\underbrace{\dot{q}(t)q^*(t)}_{g(t)}$$

Moreover, the scalar part in the above equation equals to 0. We can then identify $g(t)$ to an $\mathbb{R}^3$ vector $\vec{g}(t)$ and write

$$\begin{aligned}\dot{\vec{r}}(t) &= \vec{g}(t) \times \vec{r}(t) - \vec{r}(t) \times \vec{g}(t) \\ &= 2\vec{g}(t) \times \vec{r}(t)\end{aligned}$$

By identification, it appears that $\vec{\omega}(t) = 2\vec{g}(t) = 2\dot{q}(t)q^*(t)$. We know that $\vec{\omega'}(t) = q^*(t)\vec{\omega}(t)q(t)$, therefore

$$\boxed{\vec{\omega'}(t) = 2q^*(t)\dot{q}(t)} \tag{1.5}$$

We now have an equation which links the rotation vector $\vec{\omega'}(t)$ and the rotation quaternion q [13]. Equation 1.3 showed that the first derivative of $\vec{\omega'}(t)$ is linked to the sum $\sum \vec{M'}$ of the moments exerted on the body and expressed in the body frame. We should then be able to have such a link between these moments and the quaternion q

$$\begin{aligned}\dot{\vec{\omega'}}(t) &= 2(\dot{q}^*(t)\dot{q}(t) + q^*(t)\ddot{q}(t)) \\ \Leftrightarrow \ddot{q}(t) &= \frac{1}{2}(q(t)\dot{\vec{\omega'}}(t) - 2q(t)\underbrace{\dot{q}^*(t)\dot{q}(t)}_{N^2(\dot{q}(t))}) \\ &= q(t)\left(\frac{1}{2}\dot{\vec{\omega'}} - N^2(\dot{q}(t))\right)\end{aligned}$$

Since that, according to equation 1.3, $\dot{\vec{\omega'}} = \bar{\bar{I}}^{-1}\left(\sum \vec{M'} - \vec{\omega'} \times (\bar{\bar{I}}\vec{\omega'})\right) = \bar{\bar{I}}^{-1}\left(\sum \vec{M'} - 2q^*\dot{q} \times (\bar{\bar{I}}2q^*\dot{q})\right)$ we can finally write

$$\boxed{\ddot{q}(t) = q(t)\left(\bar{\bar{I}}^{-1}\left(\frac{1}{2}\sum \vec{M'} - 2q^*(t)\dot{q}(t) \times \left(\bar{\bar{I}}q^*(t)\dot{q}(t)\right)\right) - N^2(\dot{q}(t))\right)} \tag{1.6}$$

For spherically symmetric bodies, a simpler equation can be derived from equation 1.2:

$$\boxed{\ddot{q}(t) = q(t)\left(\frac{1}{2I}\sum \vec{M'} - N^2(\dot{q}(t))\right)} \tag{1.7}$$

These equations are the quaternion expressions of the conservation of the angular momentum.

1.3 Numerical integration

1.3.1 Issue with the integration of quaternions

What we have to keep in mind is that the quaternion from equations 1.5 and 1.6 is an unit vector of $\mathbb{R}^4$. Therefore, this vector does not move in the whole $\mathbb{R}^4$ space but is **constrained to the 4D hypersphere of radius 1**.

The basic Euler method would guess from $q_0 \equiv q(t = t_0)$ and $\dot{q_0} \equiv \dot{q}(t = t_0)$ the value of the quaternion after an increment h of time, $q(t = t_0 + h) \equiv q_1 = q_0 + h\dot{q_0}$.

However, this new quaternion lies outside of the unit quaternion hypersphere and renormalisation is not enough. Indeed, if you consider the limit case of a body rotating infinitely fast, the Euler method followed by a renormalisation of the incremented quaternion would give a move of a quarter of the sphere instead of an infinite number of revolutions.

A better increment can be found through geometric considerations [14].

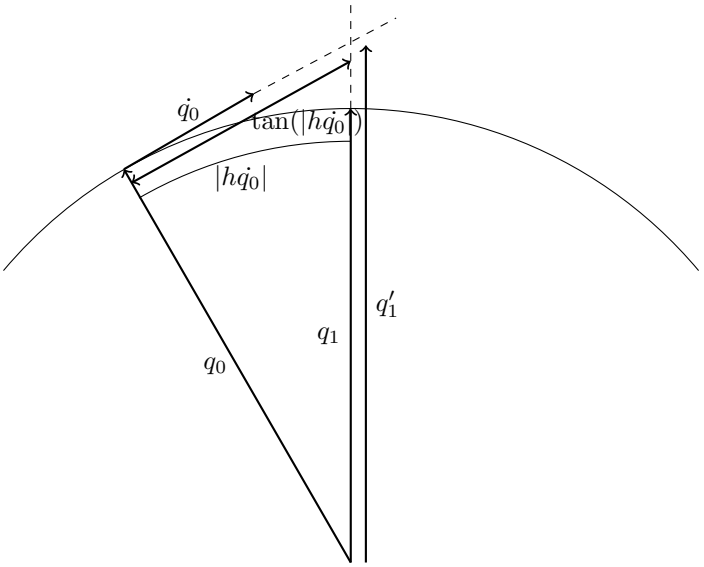

Figure 1.1: Scheme of the numerical integration

We can notice that $\forall t$, $\dot{q}(t) \cdot q(t) = \left(\frac{1}{2}q(t)\vec{\omega'}(t)\right) \cdot q(t)$ according to equation 1.5, then

$$\begin{aligned}
\dot{q}(t) \cdot q(t) &= \frac{1}{2}[\vec{q}(t) \times \vec{\omega'}(t) + q_0(t)\vec{\omega'}(t), -\vec{q(t)} \cdot \vec{\omega'}(t)] \cdot [\vec{q}(t), q_0(t)] \\
&= \underbrace{\cancel{\left(\vec{q}(t) \times \vec{\omega'}(t)\right) \cdot \vec{q}(t)}}_{=0} + \cancel{q_0(t)\vec{\omega'}(t) \cdot \vec{q}(t)} - \cancel{q_0(t)\vec{q}(t) \cdot \vec{\omega'}(t)} \\
&= 0
\end{aligned}$$

Therefore, since $q(t)$ is a radius of the hypersphere, $\dot{q}(t)$ is always tangent to the hypersphere.

In our integration, we want q_1 to have moved an arc of length $h\dot{q_0}$ on the hypersphere in the direction $\dot{q_0}$. From figure 1.1, we understand that we have to take q_1 in the direction of $q_1' \equiv q_0 + \tan(|h\dot{q_0}|)\frac{\dot{q_0}}{|\dot{q_0}|}$, so:

$$\boxed{q_1 = \frac{q_0 + \tan(|h\dot{q_0}|)\frac{\dot{q_0}}{|\dot{q_0}|}}{|q_0 + \tan(|h\dot{q_0}|)\frac{\dot{q_0}}{|\dot{q_0}|}|}} \tag{1.8}$$

1.3.2 Modified Verlet's method

A modified Verlet integration algorithm is proposed in [15].

Consider a quantity $\zeta(t)$ which is a function of time and whose derivatives are $\dot{\zeta}(t)$ and $\ddot{\zeta}(\zeta(t), \dot{\zeta}(t))$. Note $\zeta_0 \equiv \zeta(t = t_0)$ and $\dot{\zeta_0} \equiv \dot{\zeta}(t = t_0)$, then with

$$\begin{aligned}\dot{\tilde{\zeta}}_1 &= \dot{\zeta}_0 + h\ddot{\zeta}(\zeta_0, \dot{\zeta}_0)\\ \tilde{\zeta}_1 &= \zeta_0 + h\dot{\zeta}_0\end{aligned}$$

where h is the increment of time, we have

$$\begin{aligned}\dot{\zeta}_1 &= \dot{\zeta}_0 + \frac{h}{2}(\ddot{\zeta}(\zeta_0, \dot{\zeta}_0) + \ddot{\zeta}(\tilde{\zeta}_1, \dot{\tilde{\zeta}}_1))\\ \zeta_1 &= \zeta_0 + \frac{h}{2}(\dot{\zeta}_0 + \dot{\zeta}_1)\end{aligned}$$

where $\zeta_1 \equiv \zeta(t = t_0 + h)$ and $\dot{\zeta}_1 \equiv \dot{\zeta}(t = t_0 + h)$.

1.3.3 Quaternion direct integration

1.3.3.1 Principle

We have seen that the Euler's equation for the body's rotation vector $\vec{\omega}$ is equivalent to equation 1.6 expressed for the body's quaternion q, we can then solve this equation with the mean of the modified Verlet's method.

1.3.3.2 Initial conditions

The equation 1.6 is a second order differential equation, we then need initial conditions for both $q(t)$ and $\dot{q}(t)$.

There are 2 ways to initialise the quaternion:

- If we have already chosen the initial orientation $\vec{r}(0)$ of the body, then we must have $\boxed{q(0) = 1}$ according to equation 1.4 evaluated at $t = 0$.
- If we do not get to choose $\vec{r}(0)$, then we can obtain the initial orientation of the body through a rotation of angle 2θ around an axis $\vec{v}$ and we then have $\boxed{q(0) = [\vec{v}\sin\theta, \cos\theta]}$.

According to the equation 1.5 at $t = 0$ we have $\vec{\omega'}(0) = 2q^*(0)\dot{q}(0) \Rightarrow \boxed{\dot{q}(0) = \frac{1}{2}q(0)\vec{\omega'}(0)}$.

1.3.3.3 Integration scheme

We use the same notations as in part 1.3.2.

We have that $\dot{q}$ is not constrained to any particular space, therefore there is no particular precaution to take when integrating it with the modified Verlet's method. However, q is constrained to the 4D hypersphere. In

order to avoid errors, we have to use the technique developed in part 1.3.1 and calculate

$$\begin{aligned}
\tilde{q}_1 &= \frac{q_0 + \tan(|h\dot{q_0}|)\frac{\dot{q_0}}{|\dot{q_0}|}}{|q_0 + \tan(|h\dot{q_0}|)\frac{\dot{q_0}}{|\dot{q_0}|}|} \\
\dot{\tilde{q}}'_1 &= \frac{1}{2}(\dot{q}_0 + \dot{q}_1) \\
q_1 &= \frac{q_0 + \tan(|h\dot{\tilde{q}}'_1|)\frac{\dot{\tilde{q}}'_1}{|\tilde{q}'_1|}}{|q_0 + \tan(|h\dot{\tilde{q}}'_1|)\frac{\dot{\tilde{q}}'_1}{|\tilde{q}'_1|}|}
\end{aligned}$$

Higher order methods will then rely on the same trick.

1.3.4 Quaternion - rotation vector integration

1.3.4.1 Principle

Experimentally, we observe that the method described in part 1.3.3 is not numerically stable, and that the errors diverge exponentially over time in the case of torque-free precession.

A better method is to combine the solving of equation 1.3, which gives $\dot{\vec{\omega}}'(\vec{\omega}'(t), \vec{M}'(t))$, and equation 1.5, which can be rewritten as

$$\dot{q}(t) = \frac{1}{2}q(t)\vec{\omega}'(t)$$

and gives $\dot{q}(\vec{\omega}'(t), q(t))$.

1.3.4.2 Initial conditions

The equation 1.3 is a first order differential equation in $\vec{\omega}'$, therefore we only need an initial condition for the rotation vector of the body $\boxed{\vec{\omega}'(0) = \vec{\omega}'_0}$.

Equation 1.5 is a first order differential equation in q, therefore we only need an initial condition for the quaternion, for whcih we can refer to part 1.3.3.2.

1.3.4.3 Integration scheme

We use the same notations as in part 1.3.2. We will consider a body described by the position of its centre $\vec{r}$, its velocity $\vec{v}$, its quaternion q and its rotation vector $\vec{\omega}'$. We will denote $\vec{f}$ and $\vec{M}'$ the sum of the forces and the moments exerted on the body, in the reference and in the body frame respectively.

The first step is an Euler integration over the time step h

$$\begin{aligned}
\tilde{\vec{\omega}}'_1 &= \vec{\omega}'_0 + h\dot{\vec{\omega}}'_0(\vec{M}'(\vec{r_0}^{(i)}, \vec{v_0}^{(i)}, q_0^{(i)}, \vec{\omega}_0'^{(i)}), \vec{\omega}'_0) \\
\tilde{q}_1 &= \left\langle q_0 + \tan\left(|h\dot{q}_0(q_0, \vec{\omega}'_0)|\right)\frac{\dot{q}_0(q_0, \vec{\omega}'_0)}{|\dot{q}_0(q_0, \vec{\omega}'_0)|}\right\rangle \\
\tilde{\vec{v_1}} &= \vec{v_0} + \frac{h}{m}\vec{f}(\vec{r_0}^{(i)}, \vec{v_0}^{(i)}, q_0^{(i)}, \vec{\omega}_0'^{(i)}) \\
\tilde{\vec{r_1}} &= \vec{r_0} + h\vec{v_0}
\end{aligned}$$

where $\langle q \rangle = q/|q|$, from which we can calculate

$$\Delta q = \frac{h}{2}\left(\dot{q}_0(q_0, \vec{\omega}'_0) + \dot{q}_1(\tilde{q}_1, \tilde{\vec{\omega}}'_1)\right)$$

and finally do the integration

$$
\begin{aligned}
\vec{\omega_1'} &= \vec{\omega_0'} + \frac{h}{2}\left(\dot{\vec{\omega_0'}}(\vec{M'}(\vec{r_0}^{(i)}, \vec{v_0}^{(i)}, q_0^{(i)}, \vec{\omega_0'}^{(i)}), \vec{\omega_0'}) + \dot{\vec{\omega_1'}}(\vec{M'}(\tilde{\vec{r_1}}^{(i)}, \tilde{\vec{v_1}}^{(i)}, \tilde{q_1}^{(i)}, \tilde{\vec{\omega'}}_1^{(i)}), \tilde{\vec{\omega_1'}})\right) \\
q_1 &= \left\langle q_0 + \tan\left(|\Delta q|\right)\frac{\Delta q}{|\Delta q|}\right\rangle \\
\vec{v_1} &= \vec{v_0} + \frac{h}{2m}\Big(\underbrace{\vec{f}(\vec{r_0}^{(i)}, \vec{v_0}^{(i)}, q_0^{(i)}, \vec{\omega_0'}^{(i)})}_{m\frac{\tilde{\vec{v_1}}-\vec{v_0}}{h}} + \vec{f}(\tilde{\vec{r_1}}^{(i)}, \tilde{\vec{v_1}}^{(i)}, \tilde{q_1}^{(i)}, \tilde{\vec{\omega'}}_1^{(i)})\Big) \\
&= \frac{1}{2}\left(\tilde{\vec{v_1}} + \vec{v_0} + \frac{h}{m}\vec{f}(\tilde{\vec{r_1}}^{(i)}, \tilde{\vec{v_1}}^{(i)}, \tilde{q_1}^{(i)}, \tilde{\vec{\omega'}}_1^{(i)})\right) \\
\vec{r_1} &= \vec{r_0} + \frac{h}{2}\left(\vec{v_0} + \vec{v_1}\right)
\end{aligned}
$$

2 | Ellipsoids

Our goal here is to formalise the principle of belonging to an ellipsoid and show how this formalism can be exploited in numerical simulations to determine if and how ellipsoids are overlapping.

Please find in appendix C a complete presentation of ellipsoids.

2.1 Belonging matrix

Consider an ellipsoid $\mathcal{A}$ of centre $\vec{v}$, semi-axes $(R_i)_{i=1:3}$ and whose orientation is described by the quaternion q.

In the Euclidean 3D projective space, we can characterise the belonging to this ellipsoid with the mean of a matrix $B(\vec{v}, q, (R_i)_{i=1:3}) \in \mathcal{M}_4(\mathbb{R})$ with the following properties

$$\forall \vec{r} \in E^3, \begin{cases} \vec{r}^T B \vec{r} < 0 & \text{if } \vec{r} \in \mathcal{A} \setminus \bar{\mathcal{A}} \\ \vec{r}^T B \vec{r} = 0 & \text{if } \vec{r} \in \bar{\mathcal{A}} \\ \vec{r}^T B \vec{r} > 0 & \text{if } \vec{r} \notin \mathcal{A} \end{cases} \tag{2.1}$$

which we will call the *belonging matrix* of the ellipsoid $\mathcal{A}$.

Equivalently, we can define in $\mathbb{R}^3$ the matrix

$$\boxed{\bar{B}(q, (R_i)_{i=1:3}) \equiv \mathcal{Q}_q \text{diag}(R_i^{-2})_{i=1:3} \mathcal{Q}_q^T} \tag{2.2}$$

where $\mathcal{Q}_q$ is the rotation matrix associated with the quaternion q, with the following properties

$$\forall \vec{r} \in \mathbb{R}^3, \begin{cases} (\vec{r} - \vec{v})^T \bar{B} (\vec{r} - \vec{v}) < 1 & \text{if } \vec{r} \in \mathcal{A} \setminus \bar{\mathcal{A}} \\ (\vec{r} - \vec{v})^T \bar{B} (\vec{r} - \vec{v}) = 1 & \text{if } \vec{r} \in \bar{\mathcal{A}} \\ (\vec{r} - \vec{v})^T \bar{B} (\vec{r} - \vec{v}) > 1 & \text{if } \vec{r} \notin \mathcal{A} \end{cases} \tag{2.3}$$

which we will call the *reduced belonging matrix* of the ellipsoid $\mathcal{A}$.

From equation 2.3, we can define the function

$$\begin{aligned} \mathcal{F}_{\mathcal{A}} \colon \mathbb{R}^3 &\to \mathbb{R} \\ \vec{r} &\longmapsto (\vec{r} - \vec{v})^T \bar{B}(q, (R_i)_{i=1:3})(\vec{r} - \vec{v}) - 1 \end{aligned} \tag{2.4}$$

which we will call the *belonging function* of the ellipsoid $\mathcal{A}$. This function is linked $\forall \vec{r} \in \mathbb{R}^3$ to the rescaling factor $\mu(\vec{r})$ that has to be applied to $\mathcal{A}$ for $\vec{r}$ to be on its surface

$$\boxed{\mathcal{F}_{\mathcal{A}}(\vec{r}) = \mu^2(\vec{r}) - 1} \tag{2.5}$$

Therefore, we have that $\forall \vec{r_S} \in \bar{\mathcal{A}}$, the unit outward-facing normal vector to the ellipsoid in $\vec{r_S}$ is parallel to the gradient of $\mathcal{F}_{\mathcal{A}}(\vec{r_S})$ and has the same direction. We thus have

$$\boxed{\forall \vec{r_S} \in \bar{\mathcal{A}}, \vec{n}(\vec{r_S}) = \frac{\bar{B}(q, (R_i)_{i=1:3})(\vec{r_S} - \vec{v})}{|\bar{B}(q, (R_i)_{i=1:3})(\vec{r_S} - \vec{v})|}} \tag{2.6}$$

2.2 Separation of ellipsoids

In this section, we mean to present two methods of determining if two ellipsoids are overlapping. The Wang *et al.* described in part 2.2.2 was considered to be too much time-consuming to be able to implement it in our simulations.

We rather decided to implement the Perram and Wertheim method described in part 2.2.1.

2.2.1 Contact function condition

2.2.1.1 Principle

The following method was proposed by Perram and Wertheim [16] and was applied to the study of jammed packings of ellipsoidal particles [17]. It is extensively described in [18], however we will present here a slightly different version, which is closer the original.

Consider two ellipsoids $\mathcal{A}$ and $\mathcal{B}$ whose centers are located in $\vec{v}_\mathcal{A}$ and $\vec{v}_\mathcal{B}$ respectively, $\forall \vec{r} \in \mathbb{R}^3$ we introduce $\mu_\mathcal{A}(\vec{r})$ and $\mu_\mathcal{B}(\vec{r})$ the rescaling functions of the ellipsoids, *i.e.* the functions that associate to any point $\vec{r}$ the rescaling factor that has to be applied to the ellipsoid for $\vec{r}$ to be on its surface. We then define the *contact function* F such that

$$\forall \vec{r} \in \mathbb{R}^3, \forall \lambda \in [0,1], F(\vec{r},\lambda) = \lambda \mu^2_\mathcal{A}(\vec{r}) + (1-\lambda)\mu^2_\mathcal{B}(\vec{r}) \tag{2.7}$$

According to the authors of [16], $\forall \lambda \in [0,1]$, $\exists!\ \vec{r}(\lambda) \in \mathbb{R}^3$, $\vec{\nabla} F(\vec{r},\lambda) = 0$, where $\vec{r}(\lambda)$ corresponds to a minimum of the contact function. We can notice that $\vec{r}(\lambda=0) = \vec{v}_\mathcal{B}$, $\vec{r}(\lambda=1) = \vec{v}_\mathcal{A}$ and $\forall \lambda \in]0,1[$

$$\vec{\nabla} F(\vec{r}(\lambda),\lambda) = 0 \Leftrightarrow \lambda \vec{\nabla} \mu^2_\mathcal{A}(\vec{r}(\lambda)) = -(1-\lambda)\vec{\nabla}\mu^2_\mathcal{B}(\vec{r}(\lambda)) \tag{2.8}$$

which shows that if the ellipsoids $\mathcal{A}$ and $\mathcal{B}$ are rescaled with the rescaling factor $\mu_\mathcal{A}(\vec{r}(\lambda))$ and $\mu_\mathcal{B}(\vec{r}(\lambda))$ respectively, then the normal vectors to these ellipsoids in $\vec{r}(\lambda)$ are parallel with opposite directions.

The authors of [16] showed that $\frac{d^2F}{d\lambda^2}\Big|_{\vec{r}=\vec{r}(\lambda)}$ is negative definite, then $\exists!\ \lambda^*$, $\frac{dF}{d\lambda}\big|_{\vec{r}=\vec{r}(\lambda^*)} = 0$ and it corresponds to a maximum of $F(\vec{r}(\lambda),\lambda)$. We can notice that

$$\begin{aligned}
\frac{dF}{d\lambda}\bigg|_{\vec{r}=\vec{r}(\lambda^*)} = 0 \Leftrightarrow & \left[\frac{\partial F}{\partial \lambda}(\vec{r},\lambda) + \vec{r}'(\lambda)\cdot \underbrace{\cancel{\vec{\nabla} F(\vec{r},\lambda)}}_{\vec{\nabla}F(\vec{r}(\lambda),\lambda)=0}\right]_{\vec{r}=\vec{r}(\lambda^*)} = 0 \\
& \Leftrightarrow \mu^2_\mathcal{A}(\vec{r}(\lambda^*)) - \mu^2_\mathcal{B}(\vec{r}(\lambda^*)) = 0 \\
& \Leftrightarrow \mu^2_\mathcal{A}(\vec{r}(\lambda^*)) = \mu^2_\mathcal{A}(\vec{r}(\lambda^*))
\end{aligned}$$

Therefore, there exists a unique point $\vec{r_C} \equiv \vec{r}(\lambda^*)$ for which both ellipsoids $\mathcal{A}$ and $\mathcal{B}$ are externally tangent when rescaled with a common rescaling factor $\mu^2 \equiv \mu^2_\mathcal{A}(\vec{r}(\lambda^*)) = \mu^2_\mathcal{B}(\vec{r}(\lambda^*))$.

From the definition of F in equation 2.7 we can infer

$$\boxed{\mu^2 = \max_{0<\lambda<1} F(\vec{r}(\lambda),\lambda)} \tag{2.9}$$

This rescaling factor has to be greater than 1 if the ellipsoids are non-overlapping and lesser than 1 if they are overlapping. Therefore, the computation of μ tells us when $\mathcal{A}$ and $\mathcal{B}$ are overlapping.

2.2.1.2 Computation

According to equation 2.4 we can rewrite as a function of the reduced belonging matrix $\bar{B}_\mathcal{A}$ and $\bar{B}_\mathcal{B}$ and position $\vec{r_\mathcal{A}}$ and $\vec{r_\mathcal{B}}$ of ellipsoids $\mathcal{A}$ and $\mathcal{B}$ the equation 2.7

$$\forall \vec{r} \in \mathbb{R}^3, \forall \lambda \in [0,1], F(\vec{r},\lambda) = \lambda(\vec{r}-\vec{r_\mathcal{A}})^T \bar{B}_\mathcal{A}(\vec{r}-\vec{r_\mathcal{A}}) + (1-\lambda)(\vec{r}-\vec{r_\mathcal{B}})^T \bar{B}_\mathcal{B}(\vec{r}-\vec{r_\mathcal{B}}) \tag{2.10}$$

and the equation 2.8

$$\vec{\nabla} F(\vec{r}(\lambda),\lambda) = 0 \Leftrightarrow \lambda \bar{B}_\mathcal{A}(\vec{r}(\lambda)-\vec{r_\mathcal{A}}) = -(1-\lambda)\bar{B}_\mathcal{B}(\vec{r}(\lambda)-\vec{r_\mathcal{B}})$$

from which, if we denote

$$Y_{\mathcal{AB}} \equiv \lambda \bar{B}^{-1}_\mathcal{B} + (1-\lambda)\bar{B}^{-1}_\mathcal{A} \tag{2.11}$$

which is a polynomial of degree 3 easy to compute due to the definition of belonging matrix (equation 2.2), we can infer

$$\begin{aligned}
\vec{r}(\lambda) - \vec{r_\mathcal{A}} &= (1-\lambda)\bar{B}^{-1}_\mathcal{A} Y^{-1}_{\mathcal{AB}}(\vec{r_\mathcal{B}} - \vec{r_\mathcal{A}}) \\
\vec{r}(\lambda) - \vec{r_\mathcal{B}} &= -\lambda \bar{B}^{-1}_\mathcal{B} Y^{-1}_{\mathcal{AB}}(\vec{r_\mathcal{B}} - \vec{r_\mathcal{A}})
\end{aligned} \tag{2.12}$$

We can inject equations 2.12 in equation 2.10

$$\begin{aligned}\forall\lambda\in[0,1], F(\vec{r}(\lambda),\lambda) &= \lambda(1-\lambda)(\vec{r_{\mathcal{B}}}-\vec{r_{\mathcal{A}}})^T\left((1-\lambda)(\bar{B}_{\mathcal{A}}^{-1}Y_{\mathcal{AB}}^{-1})^T\cancel{\bar{B}_{\mathcal{A}}\bar{B}_{\mathcal{A}}^{-1}}+\lambda(\bar{B}_{\mathcal{B}}^{-1}Y_{\mathcal{AB}}^{-1})^T\cancel{\bar{B}_{\mathcal{B}}\bar{B}_{\mathcal{B}}^{-1}}\right)Y_{\mathcal{AB}}^{-1}(\vec{r_{\mathcal{B}}}-\vec{r_{\mathcal{A}}})\\ &= \lambda(1-\lambda)(\vec{r_{\mathcal{B}}}-\vec{r_{\mathcal{A}}})^T\Big(\underbrace{((1-\lambda)\bar{B}_{\mathcal{A}}^{-1}+\lambda\bar{B}_{\mathcal{B}}^{-1})\cancel{Y_{\mathcal{AB}}^{-1}}}_{\cancel{Y_{\mathcal{AB}}}}\Big)^T Y_{\mathcal{AB}}^{-1}(\vec{r_{\mathcal{B}}}-\vec{r_{\mathcal{A}}})\end{aligned}$$

which, by consideration that

$$\forall\lambda\in[0,1], Y_{\mathcal{AB}}^{-1}(\lambda)=\frac{\text{adj}\left(Y_{\mathcal{AB}}(\lambda)\right)}{\det\left(Y_{\mathcal{AB}}(\lambda)\right)}$$

leads to

$$\boxed{\forall\lambda\in[0,1], F(\vec{r}(\lambda),\lambda)=\frac{p_{\mathcal{AB}}(\lambda)}{q_{\mathcal{AB}}(\lambda)}\equiv\frac{\lambda(1-\lambda)(\vec{r_{\mathcal{B}}}-\vec{r_{\mathcal{A}}})^T\text{adj}\left(Y_{\mathcal{AB}}(\lambda)\right)(\vec{r_{\mathcal{B}}}-\vec{r_{\mathcal{A}}})}{\det\left(Y_{\mathcal{AB}}(\lambda)\right)}} \tag{2.13}$$

where adj designates the adjugate matrix – *i.e.* the transpose of the cofactor matrix –, det the determinant and where $p_{\mathcal{AB}}$ and $q_{\mathcal{AB}}$ are polynomials of degree 4 and 3 respectively.

Therefore, the parameter λ^* for which $F(\vec{r}(\lambda),\lambda)$ is maximum is the unique root of the polynomial

$$h_{\mathcal{AB}}=p'_{\mathcal{AB}}q_{\mathcal{AB}}-p_{\mathcal{AB}}q'_{\mathcal{AB}} \tag{2.14}$$

in the interval]0,1[, where $h_{\mathcal{AB}}$ is a polynomial of degree 6.

2.2.1.3 Root finding

We want to find the unique root of the polynomial $h_{\mathcal{AB}}$ (equation 2.14) in the interval $]0,1[$.

To do so, we can use an Householder's method – in particular the Newton's method or the Halley's method – for which we will provide a precision ε such that the root λ^* found by the algorithm verifies $|h_{\mathcal{AB}}(\lambda^*)|\leq\varepsilon$.

These methods find a root close to an initial guess. We will choose the root of F we would be looking for if $\mathcal{A}$ and $\mathcal{B}$ were spheres, *i.e.*

$$\Lambda=\frac{R_{\mathcal{A}}}{R_{\mathcal{A}}+R_{\mathcal{B}}}$$

with $R_{\mathcal{A}}$ and $R_{\mathcal{B}}$ the longest semi-axes of ellipsoids $\mathcal{A}$ and $\mathcal{B}$, as suggested by Donev [18].

For an integer $d>1$, the Householder's method of order d applied to $h_{\mathcal{AB}}$ has a rate of convergence of $d+1$ and is defined by the sequence $(\lambda_n)_n\in\mathbb{R}^{\mathbb{N}}$ such that

$$\lambda_0=\Lambda \text{ and } \forall n\in\mathbb{N}, \lambda_{n+1}=\lambda_n+\frac{(1/h_{\mathcal{AB}})^{(d-1)}(\lambda_n)}{(1/h_{\mathcal{AB}})^{(d)}(\lambda_n)} \tag{2.15}$$

from which we infer

$$\lambda^*=\lambda_N, \text{ where } N=\min(n\in\mathbb{N}, |h_{\mathcal{AB}}(\lambda_n)|\leq\varepsilon) \tag{2.16}$$

Newton's method

It corresponds to the Householder's method of order 1, therefore

$$\lambda_0=\Lambda \text{ and } \forall n\in\mathbb{N}, \lambda_{n+1}=\lambda_n-\frac{h_{\mathcal{AB}}(\lambda_n)}{h'_{\mathcal{AB}}(\lambda_n)} \tag{2.17}$$

Haley's method

This method has a greater rate of convergence than the Newton's method, however it needs to compute the second derivative of $h_{\mathcal{AB}}$ in addition to the first derivative.

It corresponds to the Householder's method of order 2, therefore

$$\lambda_0=\Lambda \text{ and } \forall n\in\mathbb{N}, \lambda_{n+1}=\lambda_n-\frac{h_{\mathcal{AB}}(\lambda_n)}{h'_{\mathcal{AB}}(\lambda_n)}\left(1-\frac{h_{\mathcal{AB}}(\lambda_n)}{h'_{\mathcal{AB}}(\lambda_n)}\cdot\frac{h''_{\mathcal{AB}}(\lambda_n)}{2h'_{\mathcal{AB}}(\lambda_n)}\right)^{-1} \tag{2.18}$$

Error

These methods return, for a given $\varepsilon > 0$, $\lambda^* \in]0,1[$ such that $|h_{\mathcal{AB}}(\lambda^*)| \leq \varepsilon$, therefore we can geometrically determine an approximate interval of certainty err of the position of this root

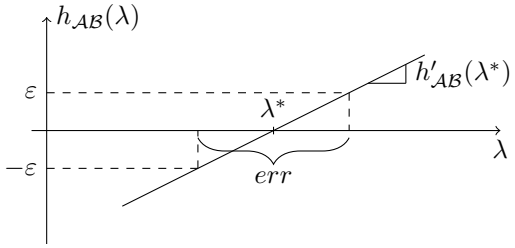

which is given by

$$\boxed{err = \frac{2\varepsilon}{h'_{\mathcal{AB}}(\lambda^*)}} \tag{2.19}$$

2.2.1.4 Polynomial computation

We will use Horner's rule for polynomial computation, which reduces the number of necessary multiplications and results in less numerical instability due to potential substraction of one large number from another [19].

For a given polynomial $p(x) = \sum_{i=0}^{n} a_i x^i$, we define $\forall\ x_0$ the sequence $(b_n, \ldots, b_0)$ such that

$$\begin{aligned} b_n &\coloneqq a_n \\ b_{n-1} &\coloneqq a_{n-1} + b_n x_0 \\ &\vdots \\ b_0 &\coloneqq a_0 + b_1 x_0 \end{aligned} \tag{2.20}$$

then, $\boxed{b_0 = p(x_0)}$.

2.2.2 Algebraic condition

The following method is extensively described in [20]. Contrarily to the method described in part 2.2.1 which is essentially numerical, the following method provides a more simple and accurate condition to determine if two ellipsoids are overlapping, according to the authors. This method was used for continuous collision detection between two moving ellipsoids [21].

2.2.2.1 Principle

Consider two ellipsoids $\mathcal{A}$ and $\mathcal{B}$ whose centers are located in $\vec{v_{\mathcal{A}}}$ and $\vec{v_{\mathcal{B}}}$, whose orientations are described by the unit quaternions q_A and q_B and whose semi-axes are $(R_i^{(\mathcal{A})})_{i=1:3}$ and $(R_i^{(\mathcal{B})})_{i=1:3}$. We then define the *characteristic polynomial* f such that

$$\forall \lambda \in \mathbb{R}, f(\lambda) = \det\left(\lambda B(\vec{v_A}, q_A, (R_i^{(\mathcal{A})})_{i=1:3}) + B(\vec{v_B}, q_B, (R_i^{(\mathcal{B})})_{i=1:3})\right) \tag{2.21}$$

The authors of [20] showed that

(i) The *characteristic equation* $f(\lambda) = 0$ always has at least two negative roots.

(ii) The two ellipsoids are non-overlapping if and only if $f(\lambda) = 0$ has two distinct positive roots.

(iii) The two ellipsoids touch other externally if and only if $f(\lambda) = 0$ has a positive dooble root.

Note that if $f(\lambda) = 0$ has a positive double root λ_0, then $\text{rank}(\lambda_0 A + B) = 3$ and the homogeneous coordinates of the contact point X_0 are given by the unique non-trivial solution of $(\lambda_0 A + B)X = 0$ [21].

The key to this method is then to determine the sign of the roots of the characteristic equation. This can be easily computed thanks to Sturm's theorem, presented in part 2.2.2.2.

2.2.2.2 Sturm's theorem

Sturm's theorem expresses the number of distinct real roots of a polynomial $p \in \mathbb{R}[x]$ located in an interval in terms of the number of changes of signs of the *Sturm's sequence* at the bounds of the interval [22].

The Sturm's sequence of the polynomial p is constructed as following

$$\begin{aligned} p_0(x) &\coloneqq p(x) \\ p_1(x) &\coloneqq p'(x) \\ p_2(x) &\coloneqq -\text{rem}(p_0, p_1) \\ &\vdots \\ 0 &= -\text{rem}(p_{m-1}, p_m) \end{aligned} \tag{2.22}$$

where $\text{rem}(p_i, p_j)$ denotes the remainder of the Euclidean division of p_i by p_j.

Given that sequence, we will note $\forall \xi \in \bar{\mathbb{R}}$, $\sigma(\xi)$ the number of sign changes (ignoring zeroes) in the sequence $p_0(\xi), \dots, p_m(\xi)$. Sturm's theorem then states that $\forall a, b \in \mathbb{R}$, $a \neq b$, the number of distinct roots of p in $(a, b]$ is $\sigma(a) - \sigma(b)$ if a nor b is a multiple root of p.

2.2.2.3 Lagrange polynomial

We want to use Sturm's theorem presented in part 2.2.2.2 on the characteristic polynomial p of equation 2.21. However, it is easier to construct the Sturm's sequence of equation 2.22 if we know the coefficients of p. We can choose between these two options to do so:

(i) Formally calculate the p according to equation 2.21 for a symbolic λ.

(ii) Determine a Lagrange polynomial [23] which is equal to p.

We will show how to use the latter option.

Since any belonging matrix $B \in \mathcal{M}_4(\mathbb{R})$, we have $p \in \mathbb{R}_4[x]$. We choose $\lambda_1, \lambda_2, \lambda_3, \lambda_4, \lambda_5 \in \mathbb{R}$ such that $i \neq j \Leftrightarrow \lambda_i \neq \lambda_j$, then

$$\begin{aligned} p(x) = p_l(x) &\equiv \sum_{i=1}^{5} p(\lambda_i) \prod_{\substack{j=1 \\ j \neq i}}^{5} \frac{x - \lambda_j}{\lambda_i - \lambda_j} \\ &= \sum_{i=1}^{5} \left(\frac{P(\lambda_i)}{\prod_{\substack{j=1 \\ j \neq i}}^{5} (\lambda_i - \lambda_j)} \right) \underbrace{\prod_{\substack{j=1 \\ j \neq i}}^{5} (x - \lambda_j)}_{\pi_i} \end{aligned}$$

Indeed, since $p - p_l \in \mathbb{R}_4[x]$ and $(p - p_l)(\lambda_i) = 0 \ \forall i \in [\![1, 5]\!]$ then $p - p_l = 0 \Leftrightarrow p = p_l$.

We can expanse π_i $\forall i \in [\![1, 5]\!]$ with Viète theorem [24]:

$$\pi_i = \prod_{\substack{j=1 \\ j \neq i}}^{5} (x - \lambda_j) = x^4 - x^3 \sum_{\substack{j=1 \\ j \neq i}}^{5} \lambda_j + x^2 \sum_{\substack{j=1 \\ j \neq i}}^{5} \sum_{\substack{k>j \\ k \neq i}} \lambda_j \lambda_k - x \sum_{\substack{j=1 \\ j \neq i}}^{5} \sum_{\substack{k>j \\ k \neq i}} \sum_{\substack{l>k \\ l \neq i}} \lambda_j \lambda_k \lambda_l + \prod_{\substack{j=1 \\ j \neq i}}^{5} \lambda_j$$

and then write

$$
\begin{aligned}
p(x) = p_l(x) = x^4 \left(\sum_{i=1}^{5} \frac{P(\lambda_i)}{\prod_{\substack{j=1 \\ j\neq i}}^{5} (\lambda_i - \lambda_j)} \right) - x^3 \left(\sum_{i=1}^{5} \frac{P(\lambda_i)}{\prod_{\substack{j=1 \\ j\neq i}}^{5} (\lambda_i - \lambda_j)} \sum_{\substack{j=1 \\ j\neq i}}^{5} \lambda_j \right) \\
+ x^2 \left(\sum_{i=1}^{5} \frac{P(\lambda_i)}{\prod_{\substack{j=1 \\ j\neq i}}^{5} (\lambda_i - \lambda_j)} \sum_{\substack{j=1 \\ j\neq i}}^{5} \sum_{\substack{k>j \\ k\neq i}} \lambda_j \lambda_k \right) - x \left(\sum_{i=1}^{5} \frac{P(\lambda_i)}{\prod_{\substack{j=1 \\ j\neq i}}^{5} (\lambda_i - \lambda_j)} \sum_{\substack{j=1 \\ j\neq i}}^{5} \sum_{\substack{k>j \\ k\neq i}} \sum_{\substack{l>k \\ l\neq i}} \lambda_j \lambda_k \lambda_l \right) \\
+ \sum_{i=1}^{5} \frac{P(\lambda_i)}{\prod_{\substack{j=1 \\ j\neq i}}^{5} (\lambda_i - \lambda_j)} \prod_{\substack{j=1 \\ j\neq i}}^{5} \lambda_j
\end{aligned}
\tag{2.23}
$$

2.3 Distance between two ellipsoids

2.3.1 Presentation of the problem

Consider two ellipsoids $\mathcal{A}$ and $\mathcal{B}$, the distance between these ellipsoids is the positive real number $d(\mathcal{A}, \mathcal{B})$ defined as

$$
d(\mathcal{A}, \mathcal{B}) = \begin{cases} \min_{\vec{r_A} \in \mathcal{A}, \vec{r_B} \in \mathcal{B}} ||\vec{r_A} - \vec{r_B}|| & \text{if } \mathcal{A} \cap \mathcal{B} = \emptyset \\ 0 & \text{if } \mathcal{A} \cap \mathcal{B} \neq \emptyset \end{cases} \tag{2.24}
$$

An algorithm to determine this distance was developed by Lin and Han [25]. We will present in part 2.3.2 our version of this algorithm, however the interested reader must refer to the original paper in order to find a demonstration of its convergence and an analysis of its efficiency.

2.3.2 Algorithm

2.3.2.1 Principle

Consider two ellipsoids $\mathcal{A}$ and $\mathcal{B}$ of belonging matrix $B_{\mathcal{A}}$ and $B_{\mathcal{B}}$ respectively.

The algorithm generates two sequences of points $\{x_k\}$ and $\{y_k\}$ which belong to $\bar{\mathcal{A}}$ and $\bar{\mathcal{B}}$ respectively which satisfy $\lim_{k\to\infty} ||x_k - y_k|| = d(\mathcal{A}, \mathcal{B})$.

At the k$^{\text{th}}$ iteration, from the two points $x_k \in \mathcal{A}$ and $y_k \in \mathcal{B}$, we construct the balls $B(c_1, r_1) \subseteq \mathcal{A}$ and $B(c_2, r_2) \subseteq \mathcal{B}$ which are tangent to their belonging ellipsoids at x_k and y_k respectively (figure 2.1).

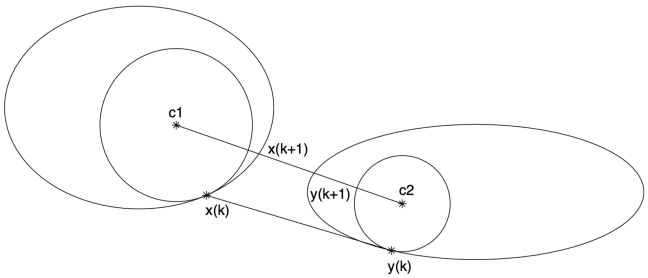

Figure 2.1: *source:* [25]

We then check that the line segment $[c_1, c_2]$ is entirely contained in $\mathcal{A} \cup \mathcal{B}$:

- if it is, then $\mathcal{A}$ and $\mathcal{B}$ are overlapping and therefore $d(\mathcal{A}, \mathcal{B}) = 0$ according to its definition in equation 2.24,
- if it is not, we continue and compute the new points x_{k+1} and y_{k+1} which are the intersections of the segment line $[c_1, c_2]$ with $\mathcal{A}$ and $\mathcal{B}$ respectively.

The authors of [25] have shown that

$$\theta_1 \equiv (y_{k+1} - x_{k+1}; B_{\mathcal{A}} x_{k+1}) = \theta_2 \equiv (x_{k+1} - y_{k+1}; B_{\mathcal{B}} y_{k+1}) = 0 \Leftrightarrow d(\mathcal{A}, \mathcal{B}) = ||x_{k+1} - y_{k+1}|| \tag{2.25}$$

We then have to check for that condition by computing θ_1 and θ_2.

2.3.2.2 Construction of the balls

We need to determine the aforementioned radii and centres of the balls, r_1, c_1 and r_2, c_2.

Since the balls have to be tangent to their belonging matrix, we must have that at the k^{th} iteration $c_1 = x_k - r_1 \vec{n_{\mathcal{A}}}(x_k)$ and $c_2 = y_k - r_2 \vec{n_{\mathcal{B}}}(y_k)$. Our problem is then to find, for a given ellipsoid $\mathcal{E}$ of reduced belonging matrix $\bar{B}_{\mathcal{E}}$, centre $\vec{v}$ and semi-axes $(R_i^{(\mathcal{E})})_{i=1:3}$, a positive real r which satisfies $\forall \vec{r} \in \bar{\mathcal{E}}$, $B(\vec{r} - r\vec{n_{\mathcal{E}}}(\vec{r}), r) \subseteq \mathcal{E}$.

We can show that

$$\boxed{\forall \gamma \in \mathbb{R}, 0 < \gamma \leq \frac{1}{\rho(\bar{B}_{\mathcal{E}})}, \forall \vec{r} \in \bar{\mathcal{E}},\ B(\vec{r} - \gamma \bar{B}_{\mathcal{E}}(\vec{r} - \vec{v}), \gamma ||\bar{B}_{\mathcal{E}}(\vec{r} - \vec{v})||) \subseteq \mathcal{E}} \tag{2.26}$$

with $\rho(\bar{B}_{\mathcal{E}})$ the spectral radius [26] of $\bar{B}_{\mathcal{E}}$. According to equation 2.2, we have that $\mathrm{sp}(\bar{B}_{\mathcal{E}}) = ((R_i^{(\mathcal{E})})^{-2})_{i=1:3}$ therefore $\boxed{\rho(\bar{B}_{\mathcal{E}}) = \max((R_i^{(\mathcal{E})})^{-2})_{i=1:3}}$.

To do so, we have to show that $\forall \vec{r} \in \bar{\mathcal{E}}, \forall \vec{u} \in B(\vec{r} - \gamma \bar{B}_{\mathcal{E}}(\vec{r} - \vec{v}), \gamma ||\bar{B}_{\mathcal{E}}(\vec{r} - \vec{v})||), \vec{u} \in \mathcal{E} \Leftrightarrow (\vec{u} - \vec{v})^T \bar{B}_{\mathcal{E}}(\vec{u} - \vec{v}) \leq 1$ according to equation 2.3.

First, we can notice that $\forall \vec{r} \in \bar{\mathcal{E}}, \forall \vec{u} \in B(\vec{r} - \gamma \bar{B}_{\mathcal{E}}(\vec{r} - \vec{v}), \gamma ||\bar{B}_{\mathcal{E}}(\vec{r} - \vec{v})||)$,

$$\begin{aligned}
(\vec{u} - \vec{r})^T \bar{B}_{\mathcal{E}}(\vec{u} - \vec{r}) =& ((\vec{u} - \vec{v}) - (\vec{r} - \vec{v}))^T \bar{B}_{\mathcal{E}}((\vec{u} - \vec{v}) - (\vec{r} - \vec{v})) \\
=& (\vec{u} - \vec{v})^T \bar{B}_{\mathcal{E}}(\vec{u} - \vec{v}) \underbrace{-(\vec{u} - \vec{v})^T \bar{B}_{\mathcal{E}}(\vec{r} - \vec{v}) - (\vec{r} - \vec{v})^T \bar{B}_{\mathcal{E}}(\vec{u} - \vec{v})}_{-2(\vec{u}-\vec{v})^T \bar{B}_{\mathcal{E}}(\vec{r}-\vec{v})} + \cancelto{1}{(\vec{r} - \vec{v})^T \bar{B}_{\mathcal{E}}(\vec{r} - \vec{v})} \\
\Leftrightarrow (\vec{u} - \vec{v})^T \bar{B}_{\mathcal{E}}(\vec{u} - \vec{v}) =& (\vec{u} - \vec{r})^T \bar{B}_{\mathcal{E}}(\vec{u} - \vec{r}) + 2\underbrace{(\vec{u} - \vec{v})}_{(\vec{u}-\vec{r})+(\vec{r}-\vec{v})}{}^T \bar{B}_{\mathcal{E}}(\vec{r} - \vec{v}) - 1 \\
=& (\vec{u} - \vec{r})^T \bar{B}_{\mathcal{E}}(\vec{u} - \vec{r}) + 2(\vec{u} - \vec{r})^T \bar{B}_{\mathbb{E}}(\vec{r} - \vec{v}) + \cancelto{1}{2(\vec{r} - \vec{v})^T \bar{B}(\vec{r} - \vec{v})} - 1 \\
=& (\vec{u} - \vec{r})^T \bar{B}_{\mathcal{E}}(\vec{u} - \vec{r}) + 2(\vec{u} - \vec{r})^T \bar{B}_{\mathbb{E}}(\vec{r} - \vec{v}) + 1
\end{aligned}$$

From Cauchy-Schwarz inequality we can infer

$$|(\vec{u} - \vec{r})^T \bar{B}_{\mathcal{E}}(\vec{u} - \vec{r})| = |(\vec{u} - \vec{r}) \cdot \bar{B}_{\mathcal{E}}(\vec{u} - \vec{r})| \leq ||(\vec{u} - \vec{r})||\ ||\bar{B}_{\mathcal{E}}(\vec{u} - \vec{r})||$$

Let $(\vec{f_i})_{i=1:3}$ be the eigenvectors of $\bar{B}_{\mathcal{E}}$ and $(\lambda_i)_{i=1:3}$ the associated eigenvalues, then

$$\exists (\mu_i)_{i=1:3} \in \mathbb{R}^3, \vec{u} - \vec{r} = \sum_{i=1}^{3} \mu_i \vec{f_i}$$

and

$$\bar{B}_{\mathcal{E}}(\vec{u} - \vec{r}) = \sum_{i=1}^{3} \lambda_i \mu_i \vec{f_i}$$

From the definition of the spectral radius [26], we have that $\forall i \in [\![1, 3]\!], \lambda_i \leq \rho(\bar{B}_{\mathcal{E}})$ so

$$\begin{aligned}
||\bar{B}_{\mathcal{E}}(\vec{u} - \vec{r})|| &= ||\sum_{i=1}^{3} \lambda_i \mu_i \vec{f_i}|| \\
&\leq \rho(\bar{B}_{\mathcal{E}}) \underbrace{||\sum_{i=1}^{3} \mu_i \vec{f_i}||}_{||\vec{u}-\vec{r}||}
\end{aligned}$$

therfore

$$\begin{aligned}|(\vec{u}-\vec{r})^T\bar{B}_{\mathcal{E}}(\vec{u}-\vec{r})| &\leq ||(\vec{u}-\vec{r})||\ ||\bar{B}_{\mathcal{E}}(\vec{u}-\vec{r})|| \\ &\leq \rho(\bar{B}_{\mathcal{E}})||\vec{u}-\vec{r}||^2 \\ \Rightarrow (\vec{u}-\vec{r})^T\bar{B}_{\mathcal{E}}(\vec{u}-\vec{r}) &\leq \rho(\bar{B}_{\mathcal{E}})||\vec{u}-\vec{r}||^2\end{aligned}$$

Moreover, since that $\vec{u} \in B(\vec{r}-\gamma\bar{B}_{\mathcal{E}}(\vec{r}-\vec{v}), \gamma||\bar{B}_{\mathcal{E}}(\vec{r}-\vec{v})||)$, we can write

$$\begin{aligned}&||\vec{u}-\vec{r}+\gamma\bar{B}_{\mathcal{E}}(\vec{r}-\vec{v})||^2 \leq \gamma^2||\bar{B}_{\mathcal{E}}(\vec{r}-\vec{v})||^2 \\ \Leftrightarrow &||\vec{u}-\vec{r}||^2 + 2(\vec{u}-\vec{r})^T\gamma\bar{B}_{\mathcal{E}}(\vec{r}-\vec{v}) + \cancel{\gamma^2||\bar{B}_{\mathcal{E}}(\vec{r}-\vec{v})||^2} \leq \cancel{\gamma^2||\bar{B}_{\mathcal{E}}(\vec{r}-\vec{v})||^2} \\ \Leftrightarrow &(\vec{u}-\vec{r})^T\bar{B}_{\mathcal{E}}(\vec{r}-\vec{v}) \leq -\frac{1}{2\gamma}||\vec{u}-\vec{r}||^2\end{aligned}$$

Finally, we then have that

$$\begin{aligned}(\vec{u}-\vec{v})^T\bar{B}_{\mathcal{E}}(\vec{u}-\vec{v}) &= (\vec{u}-\vec{r})^T\bar{B}_{\mathcal{E}}(\vec{u}-\vec{r}) + 2(\vec{u}-\vec{r})^T\bar{B}_{\mathcal{E}}(\vec{r}-\vec{v}) + 1 \\ &\leq \rho(\bar{B}_{\mathcal{E}})||\vec{u}-\vec{r}||^2 - \cancel{2}\frac{1}{\cancel{2}\gamma}||\vec{u}-\vec{r}||^2 + 1 \\ &\leq ||\vec{u}-\vec{r}||^2\left(\rho(\bar{B}_{\mathcal{E}}) - \frac{1}{\gamma}\right) + 1\end{aligned}$$

We chose γ such that $\gamma \leq \frac{1}{\rho(\bar{B}_{\mathcal{E}})} \Leftrightarrow \rho(\bar{B}_{\mathcal{E}}) \leq \frac{1}{\gamma} \Leftrightarrow \rho(\bar{B}_{\mathcal{E}}) - \frac{1}{\gamma} \leq 0$, therefore $(\vec{u}-\vec{v})^T\bar{B}_{\mathcal{E}}(\vec{u}-\vec{v}) \leq 1 \Leftrightarrow \vec{u} \in \mathcal{E}$.

We now have a condition to chose the radius of the balls that have to be constructed in the algorithm. One can notice that this condition is independent of the iteration, therefore we can construct balls that will always be the same size.

2.3.2.3 Intersection of the line segment with the ellipsoids

Authors' method

We need to check if the line segment $[c_1, c_2]$ is entirely contained in $\mathcal{A} \cup \mathcal{B}$ and if so, determine the intersections of this segment with both ellipsoids.

To do so, the authors of [25] compute t_1 and t_2 defined as

$$\begin{aligned}t_1 &= \max\{t \in [0,1], (1-t)c_1 + tc_2 \in \mathcal{A} \Leftrightarrow \mathcal{F}_{\mathcal{A}}((1-t)c_1 + tc_2) \leq 0\} \\ t_2 &= \min\{t \in [0,1], (1-t)c_1 + tc_2 \in \mathcal{B} \Leftrightarrow \mathcal{F}_{\mathcal{B}}((1-t)c_1 + tc_2) \leq 0\}\end{aligned} \tag{2.27}$$

- if $t_2 \leq t_1$, the intersection of $\mathcal{A}$ and $\mathcal{B}$ is non-empty and therefore $d(\mathcal{A}, \mathcal{B}) = 0$,
- if $t_2 > t_1$, we have $\bar{x} = (1-t_1)c_1 + t_1c_2$ and $\bar{y} = (1-t_2)c_1 + t_2c_2$ the intersections of the line segments with ellipsoids $\mathcal{A}$ and $\mathcal{B}$ respectively.

Polynomial method

The authors' method is essentially numerical, furthermore it makes no use of the information that provides the values of the belonging functions. The following method gives the exact value of the coefficients t_1 and t_2 introduced in equation 2.27.

We want to determine the intersections r_1 and r_2 of the line segment $[c_1, c_2]$ with ellipsoids $\mathcal{A}$ and $\mathcal{B}$ respectively, whose centres are located in v_1 and v_2 and whose reduced belonging matrix are $\bar{B}_1$ and $\bar{B}_2$.

We will introduce $\alpha_i > 0$ such that

$$\begin{aligned}&r_i = c_i + \alpha_i(c_j - c_i) \\ \Leftrightarrow\ &r_i - v_i = c_i - v_i + \alpha_i(c_j - c_i)\end{aligned}$$

then, according to equation 2.3,

$$\begin{aligned}(r_i - v_i)^T \bar{B}_i (r_i - v_i) &= 1 \\ &= (c_i - v_i + \alpha_i(c_j - c_i))^T \bar{B}_i (c_i - v_i + \alpha_i(c_j - c_i)) \\ &= \underbrace{(c_i - v_i)^T \bar{B}_i (c_i - v_i)}_{\mathcal{F}_i(c_i)+1} + 2\alpha_i (c_i - v_i)^T \bar{B}_i (c_j - c_i) + \alpha_i^2 (c_j - c_i)^T \bar{B}_i (c_j - c_i) \\ \Leftrightarrow 0 &= \alpha_i^2 \underbrace{(c_j - c_i)}_{\vec{a_i}}^T \bar{B}_i \underbrace{(c_j - c_i)}_{\vec{a_i}} + 2\alpha_i \underbrace{(c_i - v_i)}_{\vec{b_i}}^T \bar{B}_i \underbrace{(c_j - c_i)}_{\vec{a_i}} + \mathcal{F}_i(c_i)\end{aligned}$$

therefore, α_i is a root of the polynomial

$$p_i(x) = x^2 \vec{a_i}^T \bar{B}_i \vec{a_i} + 2x \vec{b_i}^T \bar{B}_i \vec{a_i} + \mathcal{F}_i(c_i)$$

We can calculate the discriminant Δ_i of p_i

$$\Delta_i = (2\vec{b_i}^T \bar{B}_i \vec{a_i})^2 - 4\vec{a_i}^T \bar{B}_i \vec{a_i} \mathcal{F}_i(c_i)$$

where $\bar{B}_i$ is positive definite matrix according to equation 2.2, therefore $\vec{a_i} \bar{B}_i \vec{a_i} \geq 0$, and c_i is in the corresponding ellispoids, therefore $\mathcal{F}_i(c_i) \leq 0$, which finally leads to

$$\Delta_i \geq (2\vec{b_i}^T \bar{B}_i \vec{a_i})^2 \geq 0$$

so p_i has two real roots

$$x_\pm = \frac{-2\vec{b_i}^T \bar{B}_i \vec{a_i} \pm \sqrt{\Delta_i}}{2\vec{a_i}^T \bar{B}_i \vec{a_i}}$$

of which only x_+ is positive, therefore

$$\boxed{\alpha_i = \frac{-2\vec{b_i}^T \bar{B}_i \vec{a_i} + \sqrt{(2\vec{b_i}^T \bar{B}_i \vec{a_i})^2 - 4\vec{a_i}^T \bar{B}_i \vec{a_i} \mathcal{F}_i(c_i)}}{2\vec{a_i}^T \bar{B}_i \vec{a_i}}} \tag{2.28}$$

We have that α_i is maximum when $\mathcal{F}_i(c_i)$ is minimum, which is when

$$\mathcal{F}_i(c_i) = -1 \Rightarrow c_i = v_i \Rightarrow \begin{cases} \vec{b_i} = \vec{0} \\ \vec{a_i} = c_j - v_i \end{cases}$$

where c_j is not in the ellipsoid of centre v_i, therefore $\vec{a_i} \bar{B}_i \vec{a_i} \geq 1$, which leads to

$$\alpha_{i,\max} = \frac{\sqrt{\vec{a_i}^T \bar{B}_i \vec{a_i}}}{\vec{a_i}^T \bar{B}_i \vec{a_i}} \leq 1$$

therefore

$$0 \leq \alpha_i \leq 1 \tag{2.29}$$

According to equation 2.27, we have that

$$\begin{aligned}(1 - t_1)c_1 + t_1 c_2 = r_1 = c_1 + \alpha_1(c_2 - c_1) &\Leftrightarrow t_1(c_2 - c_1) = \alpha_1(c_2 - c_1) \\ (1 - t_2)c_1 + t_2 c_2 = r_2 = c_2 + \alpha_2(c_1 - c_2) &\Leftrightarrow t_2(c_2 - c_1) = (1 - \alpha_2)(c_2 - c_1)\end{aligned}$$

where $c_2 - c_1 \neq \vec{0}$, therefore

$$\boxed{\begin{array}{ll} t_1 = \alpha_1 & \in [0, 1] \\ t_2 = 1 - \alpha_2 & \in [0, 1] \end{array}} \tag{2.30}$$

2.3.3 Overlapping condition

Since we have the equivalence $\mathcal{A} \cap \mathcal{B} \neq \emptyset \Leftrightarrow d(\mathcal{A}, \mathcal{B}) = 0$ according to equation 2.24, we can check if two ellipsoids are overlapping by computing their distance.

3 | Jamming

Many recent works have studied the properties of the jamming transition for packings of 2D and 3D soft- and hard-core spherical particles. Our goal here is to investigate how these properties are affected when considering spheroids.

We will first introduce the jamming transition and the models and methods that have been involved to study this transition for spheres and then present the modifications we have brought to these in order to study rotating spheroids, based on the theoretical knowledge and numerical methods we have summarised on quaternions and ellipsoids.

3.1 Jamming transition

3.1.1 Phenomenon

A few decades ago, little was still known about granular materials. According to Pierre-Gilles de Gennes, "granular matter in 1998 [was] at the level of solid state physics in 1930." [27] Yet, these materials are of great theoretical interest in the domain of statistical physics [28].

What has been observed is that granular materials develop a yield stress in a disordered state [29] – or a stress relaxation time which exceeds a reasonable experimental time – upon increasing the packing fraction ϕ above a critical value ϕ_J. At low ϕ, each particle can move independently of its neighbours while at high ϕ the particles can not avoid each other, resulting in a bulk modulus since the pressure increases upon compression. This phenomenon is called jamming and corresponds to a transition from a flowing liquid-like state to an amorphous rigid solid state.

Jamming is encountered everywhere, whether it is unintended – *e.g.*, grains and beans jam in hoppers [30–32], cars jam on the highway [33] – or purposefully put into practice in engineering applications – *e.g.*, to easily, efficiently and reliably hold objects [34, 35].

The phenomenon is also present in other systems with other control parameters [36]. Foams jam upon decreasing the applied shear stress and supercooled liquids jam upon decreasing the temperature – the latter phenomenon being already known as the glass transition from a flowing liquid to a frozen glass.

These observations led Liu and Nagel to hypothesise that they are controlled by the same mechanisms [3], and thus to summarise them in a phase diagram [29] which axis are the aforementioned parameters: temperature T, shear stress σ and packing fraction ϕ (figure 3.1). The surface below which states are jammed corresponds to the points for which the system behaves like a solid on any experimental time scale and the point J is meant to correspond to the packing fraction ϕ_J at which the system at $T = 0$ and $\sigma = 0$ jam in the thermodynamic limit (infinite system, *i.e.*, $N \to +\infty$).

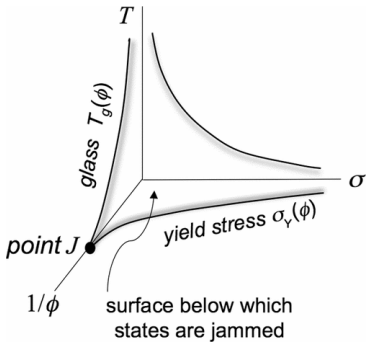

Figure 3.1: *source:* [5]

Defining what is exactly a "jammed system" is a problem of great mathematical and physical interest [37, 38], in particular it has finally allowed physicists to replace the concept of random close packing (RCP) with the more rigorous and precise concept of maximally random jammed (MRJ) state [39]. We will however set aside these considerations to rather focus on the critical behaviours (parts 3.1.2, 3.1.3 and 3.1.4) observed at the transition to such a state.

3.1.2 Critical behaviour

In the vicinity of J, we have that the shear viscosity $\eta \equiv \sigma/\dot{\gamma}$ – with σ the shear stress and $\dot{\gamma}$ the shear strain rate, – or equivalently the pressure viscosity $\eta_p \equiv p/\dot{\gamma}$ – with p the pressure, – and a correlation length scale ξ diverge as

$$\begin{aligned} \eta, \eta_p &\underset{\phi \to \phi_J}{\sim} (\phi_J - \phi)^{-\beta} \\ \xi &\underset{\phi \to \phi_J}{\sim} (\phi_J - \phi)^{-\nu} \end{aligned} \tag{3.1}$$

for soft-core particles in the limit $\dot{\gamma} \to 0$ [4, 40] and for hard-core particles [41].

Using η_p rather than η has been proven to reduce errors due to necessary corrections to scaling [40]. Moreover, we have to keep in mind that equation 3.1 holds only very close to ϕ_J. Since the macroscopic friction coefficient $\mu \equiv \eta/\eta_p$ has a strong ϕ-dependence, corrections may have to be added to the scaling for larger packing fractions intervals [40, 42]. Please refer to part 3.3 for more details on the scaling methods.

This power-law divergence of the transport coefficient and of a correlation length scale are reminiscent of the behaviour near a critical point [40, 43, 44] of a second-order continuous phase transition.

For frictional particles, it has been shown that the jamming transition was discontinuous [45]. However, equation 3.1, which has been well demonstrated for frictionless particles, can also be applied to frictional particles by introducing a fictitious critical density, somewhat higher than the density at which the system develops a yield stress.

The original conjecture of the authors of [29] was that J was indeed a critical point which "may control the region around it and thereby govern the nature of the entire jamming surface in the phase diagram." This point would then be the athermal jamming point corresponding to the $T \to 0$ limit of the equilibrium glass transition curve in the $(1/\phi, T)$ plane. However, it was later suggested that the equilibrium glass transition would be governed by a critical point distinct from J [5].

3.1.3 Relaxation time

For a packing of soft-core particles at a density $\phi < \phi_J$ in the thermodynamic limit $N \to +\infty$, the state of minimum energy will always be a state where the particles do not overlap, therefore a state of zero energy and zero pressure. When one applies a constant shear strain rate to such a system, the particles overlap and the energy becomes non-zero. One can then be interested in the decay of the energy and the pressure when the shearing ceases.

Authors of [42] studied this decay for systems of soft-core disks with harmonic elastic interactions (see part 3.4) at constant shear strain rate. What they have observed is that after a short transient time, the pressure decays exponentially to zero with a characteristic time scale $\tau(\phi, \dot{\gamma})$

$$\boxed{p(t) \sim \exp\left(-t/\tau(\phi, \dot{\gamma})\right)} \tag{3.2}$$

which they called the *relaxation time*. This relaxation time increases with increasing initial shear strain rate $ga\dot{m}ma$ for a given ϕ and diverges as ϕ approaches ϕ_J from below.

Another relevant time scale presented by the authors is the *dissipation time* $\tau_{\text{diss}}(\phi, \dot{\gamma})$, which represents the initial decay rate of the energy. It is obtained by taking the ratio of the energy E by the dissipated power P_{diss}. If the system is steadily sheared, then P_{diss} equals the input power $P_{\text{in}} \sim \sigma\dot{\gamma}$ with σ the shear stress. Therefore, $\tau_{\text{diss}}(\phi, \dot{\gamma}) \sim E/\sigma\dot{\gamma}$.

Since that, for harmonic elastic interactions, we have $p \sim \delta$ and $E \sim \delta^2$ with δ the overlap, we then expect the energy to decay exponentially with a characteristic time scale $\tau(\phi, \dot{\gamma})/2$. In consequence, the authors chose

$$\boxed{\tau_{\text{diss}}(\phi, \dot{\gamma}) = 2\frac{E}{\sigma\dot{\gamma}}} \tag{3.3}$$

for this time scale to be compared with $\tau(\phi, \dot{\gamma})$. Contrarily to the relaxation time, the dissipation time decreases with increasing initial shear strain rate $\dot{\gamma}$, but also diverges as ϕ approaches ϕ_J from below.

Indeed, if we notice that

$$\tau_{\text{diss}} = 2\frac{E}{\sigma\dot{\gamma}} \sim \frac{E/\dot{\gamma}^2}{\sigma/\dot{\gamma}} \sim \frac{(p/\dot{\gamma})^2}{\sigma/\dot{\gamma}} \sim \frac{\eta_p^2}{\eta}$$

we can directly infer from equation 3.1 that

$$\boxed{\tau_{\text{diss}} \underset{\phi\to\phi_J}{\sim} (\phi_J - \phi)^{-\beta}} \tag{3.4}$$

therefore, the dissipation time diverges with the same exponent as the viscosity and its pressure equivalent.

Authors of [42] finally showed that in the limit of low initial shear strain rate $\dot{\gamma} \to 0$, the relaxation time and the dissipation time behave essentially the same close to ϕ_J

$$\tau \underset{\substack{\dot{\gamma}\to 0\\ \phi\to\phi_J}}{\sim} \tau_{\text{diss}} \tag{3.5}$$

therefore the relaxation time also diverges with the critical exponent β.

We emphasise that equations 3.4 and 3.5 give, in addition to the study of the quantities in equation 3.1, a way to determine the critical exponent associated with the divergence of the viscosity at the jamming transition.

It was then suggested that τ may be a fundamental quantity which controls the overlap $\delta/\dot{\gamma}$ and thus would be behind the divergence of the transport coefficients.

3.1.4 Contact number

Many works have focused on determining the coordination number z – *i.e.*, the number of contacts per particle – for static packings near the jamming transition.

An important result is that disordered packings of disks and spheres are *isostatic* at jamming [29, 42, 46], meaning that the total number of contacts is equal to the total number of degrees of freedom [47], then leading to a completely statically defined system – however, one has to remove rattlers, *i.e.* particles with less than 3 contacts which are then not locked up at a fixed position, from the calculation. With d_f the number of degrees of freedom, we then have the isostatic contact number, $z_{\text{iso}} = 2d_f$, where d_f equals to 2 for disks and 3 for spheres (translational degrees of freedom). This *isostatic conjecture* relies on two assumptions[48]:

(i) as many constraints as degrees of freedom are needed to fix the positions and orientations,

(ii) disordered packings will have the minimal number of contacts necessary since additional contacts implies additional correlations.

Moreover, the difference of the contact number to its isostatic value $\delta z \equiv z_{\text{iso}} - z$ vanishes algebrically when the packing fraction approaches its jamming value ϕ_J from below

$$\delta z \underset{\phi\to\phi_J}{\sim} (\phi_J - \phi)^{u_z} \tag{3.6}$$

which with equations 3.4 and 3.5 leads to

$$\tau \underset{\substack{\dot{\gamma}\to 0\\ \phi\to\phi_J}}{\sim} \delta z^{-\beta/u_z} \tag{3.7}$$

for soft-core particles near the hard-core limit, according to [42].

Authors of [42], whose method is described in part 3.2.2, emphasised the following results from their study of the relaxation of sheared packings of soft-core frictionless disks:

- the contact number always decreases in the relaxation process,
- this change is bigger when increasing the initial shear rate,
- the contact number after relaxation decreases slowly with decreasing initial shear rate,
- the contact number in sheared packings can be above isostaticity while the contact number after relaxation is always below.

It has been suggested that packings of non-spherical particles do not satisfy this isostaticity property [17] and in particular that jammed packings of frictionless ellipsoids are hypostatic [49], *i.e.* exhibit a contact number at jamming lesser than its isostatic value.

The contact number and especially its critical value at jamming, alongside with the jamming packing fraction, are thought to be at the origin of the critical behaviours of the mechanical properties of frictionless packings of spherical and ellipsoidal particles [50].

3.1.5 Orientational ordering

Considering non-spherical particles breaks down the isotropy of the rotation phase space. Therefore one can expect that, near the jamming transition, a system of ellipsoidal particles would develop a significant orientational ordering.

Nonetheless, it has been suggested that packings of ellipsoidal particles showed no such ordering at jamming in static simulations [49] but, since shearing breaks the isotropy of space, one can still hypothesise that such a phenomenon is to be expected in shearing simulations.

3.1.6 Universality

A frequent question in statistical physics is whether different critical phenomena – observed in identical or different systems – behave similarly, which is characterised by them having the same critical exponents. Such similar phenomena are said to belong to an unique *universality class*. It was empirically found that the elements of an universality class were linked by their spatial dimensionality and the symmetry of their ordered phase [43].

It was showed that different models for the dissipation of the energy in packings of soft-core spheres did not influence the critical exponents characterising the jamming transition [42, 51], while different models for the elastic interaction between particles did [29]. Moreover, it was suggested that the critical exponent characterising the vanishing of the excess contact number to isostaticity was independent of both the spatial dimensionality of the packing and the elastic interaction considered for soft-core spheres [29].

When considering ellipsoidal particles, it would be interesting to determine how the asphericity of the particles influences the critical exponents of the jamming transition and whether systems of oblate and prolate spheroids behave the same.

3.1.7 Finite-size effects

For a finite number N of particles, the system will jam at a packing fraction ϕ somewhat below ϕ_J because there is always a finite probability to find a configuration with a force chain spanning the width of the system, causing the system to jam.

When shearing a packing of particles the system explores an increasing region of configuration space, it will thus eventually find a configuration causing it to jam. The statistical weight of these configurations, associated with the time required for the system to jam, decreases as one decreases the packing fraction ϕ or increases the number of particle N. Therefore, in the limit of a infinite system $N \to +\infty$, it is expected that the system jam in a finite time only for $\phi \geq \phi_J$ [4].

3.2 Methods

3.2.1 Jamming transition

Many numerical methods have been used to study the jamming of a system of spherical particles:

- Most of them consist of evaluating and studying the proportion of jammed states as a function of the density and infer from these data the jamming packing fraction. What distinguishes the methods is then the way the system is prepared:
  - Relaxation from initially random states simulations [5, 44]. A system corresponding to a completely random state ($T = +\infty$) is cooled by using energy minimisation techniques.
  - Quasistatic shearing [44]. A system of which the energy has been initially minimised is gradually sheared, with energy minimisation steps between each increment of the shear strain.
  - Compression [52].
- Other methods are based on the shearing at constant shear rate of a given system [4], which can be performed using Lees-Edwards periodic boundary conditions [53, 54]. From the assumption of a critical behaviour of the mechanical properties (*e.g.*, pressure, shear modulus) near the jamming point J, the scaling analysis of the behaviour of the system enables one to infer the jamming packing fraction and the critical exponents.

However, there appears to have little agreement in the values for the jamming density and of the critical exponents found in the literature. This is thought to be caused by the neglect of corrections to scaling in these papers [40]. Moreover, in relaxation and compression protocols, particles tend to order themselves into clusters. This leads to values of the jamming density which are dependent of the way the samples were prepared and treated – a dependence which is often to be expected when studying granular materials [55, 56]. Some authors suggested that, since ϕ_J was history-dependent, the point J may be ill-defined, even when clustering plays no role [52].

We can note that, to avoid crystallisation, most simulations involve polydispersity [52].

On the contrary, the process of shearing – no matter how slow – breaks the clustering at the origin of varying and higher than expected values of ϕ_J. It has then been showed that quasistatic shearing protocols lead to an unique – well-defined – value of the jamming density ϕ_J, corresponding to the jamming density for shearing simulations in the limit of vanishing shear strain rate, which does not depend on the initial configuration or the details of the shearing protocol [5].

It has then been proposed to study jamming in the $(1/\phi, T, \dot{\gamma})$ phase space – where $\dot{\gamma}$ is the shear strain rate – where J would be unique. In such a phase space, the $(1/\phi, T)$ plane at $\dot{\gamma} \to 0$ corresponds to the plane of quasistatically sheared steady states.

3.2.2 Relaxation time

To study the relaxation time $\tau(\phi, \dot{\gamma})$ of a system of soft-core particles, the authors of [42] made use of a 2-stage process. First, the system is driven at steady shear with the constant shear strain rate $\dot{\gamma}$. Then, the shearing is stopped but the dynamics is continued until the system relaxes down to a minimum energy.

3.2.3 Soft- to hard-core mapping

Shearing simulations are more or less easily conducted with soft-core particles. We can be interested to know how the data from these simulation can be used to study the rheological behaviour of packings of hard-core particles near the jamming transition.

We can find in [41] a method to map soft-core particles at a given packing fraction ϕ and shear strain rate $\dot{\gamma}$ to equivalent hard-core particles at a lesser packing fraction ϕ_{eff} such as

$$\begin{aligned} \eta_p^s(\phi, \dot{\gamma}) &= \eta_p^s(\phi_{\text{eff}}, \dot{\gamma} \to 0) \\ \eta_p^h(\phi_{\text{eff}}) \equiv \eta_p^s(\phi_{\text{eff}}, \dot{\gamma} \to 0) &\underset{\phi_{\text{eff}} \to \phi_J}{\sim} (\phi_J - \phi_{\text{eff}})^{-\beta} \end{aligned} \tag{3.8}$$

according to equation 3.1. We denoted η_s and η_p are the pressure equivalents of viscosity for packings of soft- and hard-core particles respectively.

This mapping is done by assuming that ϕ_{eff} is determined by the extent of particle overlaps, measured by the average energy per particle $E(\phi, \dot{\gamma})$. Authors of [41] then proposed the following relation

$$\phi_{\text{eff}}(\phi, \dot{\gamma}) = \phi - h(E(\phi, \dot{\gamma})) \tag{3.9}$$

where h can be determined asymptotically close to ϕ_J.

We can first notice that there is no distinction between soft-core and hard-core particles in a system where the particles do not overlap. In such a system, the average energy per particle equals to 0, therefore we must have

$$h(0) = 0 \tag{3.10}$$

In a jammed system – *i.e.*, $\phi \geq \phi_J$ – of soft-core particles, particles have no choice but to overlap leading to $p > 0$ even as $\dot{\gamma} \to 0$, and then $\eta_p^s(\phi \geq \phi_J, \dot{\gamma} \to 0) \to +\infty$. In consequence, according to equation 3.8, we must have $\eta_p^h(\phi_{\text{eff}}) \to +\infty$, which is only achieved for a system of hard-core particles at $\phi_{\text{eff}} = \phi_J$, therefore

$$\phi_{\text{eff}}(\phi \geq \phi_J, \dot{\gamma} \to 0) = \phi_J \tag{3.11}$$

From equations 3.9 and 3.11, we have that

$$\phi_{\text{eff}}(\phi \geq \phi_J, \dot{\gamma} \to 0) = \phi - h(E(\phi, \dot{\gamma} \to 0)) = \phi_J \Rightarrow h(E(\phi, \dot{\gamma} \to 0)) = \phi - \phi_J$$

and, since $E(\phi, \dot{\gamma} \to 0)$ vanishes algebraically close to ϕ_J, we can write

$$\begin{aligned} E(\phi, \dot{\gamma} \to 0) \underset{\phi \to \phi_J}{\sim} (\phi - \phi_J)^{y_E} &\Leftrightarrow E(\phi, \dot{\gamma} \to 0)^{1/y_E} \underset{\phi \to \phi_J}{\sim} \phi - \phi_J \\ &\Rightarrow E(\phi, \dot{\gamma} \to 0)^{1/y_E} \underset{\phi \to \phi_J}{\sim} h(E(\phi, \dot{\gamma} \to 0)) \\ &\Rightarrow X^{1/y_E} \underset{X \to 0}{\sim} h(X) \end{aligned}$$

where the latter equivalence can be applied to $E(\phi, \dot{\gamma})$ in the vicinity of ϕ_J, therefore

$$\boxed{\phi_{\text{eff}}(\phi, \dot{\gamma}) \underset{\phi \to \phi_J}{=} \phi - cE(\phi, \dot{\gamma})^{1/y_E}} \tag{3.12}$$

with c a constant.

3.3 Scaling analysis

3.3.1 Scaling assumption

3.3.1.1 Principle

Please find in appendix D a presentation of renomalisation group theory.

According to the discussions of parts 3.1.1 and 3.2.1, we can describe an athermal system of particles with the variables $\delta\phi = \phi - \phi_J$ and $\dot{\gamma}$. We will always assume that our system is in the thermodynamic limit $N \to +\infty \Leftrightarrow 1/L \to 0$, where L is the characteristic length and then neglect any finite-size effect arising from the finite number of particles N composing the system.

Renormalisation group theory suggests that close to the jamming point, *i.e.* $(\delta\phi \to 0, \dot{\gamma} \to 0)$, there exists $y_{\delta\phi}$ and $y_{\dot{\gamma}}$ such that the correlation length transforms under a change of length scale with a factor l as

$$\xi(\delta\phi, \dot{\gamma}) = l\xi(\delta\phi l^{y_{\delta\phi}}, \dot{\gamma} l^{y_{\dot{\gamma}}})$$

which, when choosing l such that $\delta\phi l^{y_{\delta\phi}} = -b \Leftrightarrow l = \left(-\frac{\delta\phi}{b}\right)^{-1/y_{\delta\phi}} \geq 1$, gives

$$\xi(\delta\phi, \dot{\gamma}) = \left(-\frac{\delta\phi}{b}\right)^{-1/y_{\delta\phi}} \xi\left(-b, \dot{\gamma}\left(-\frac{\delta\phi}{b}\right)^{-y_{\dot{\gamma}}/y_{\delta\phi}}\right) \underset{\delta\phi \to 0}{\sim} (-\delta\phi)^{-1/y_{\delta\phi}}$$

where we recognise $\nu = 1/y_{\delta\phi} > 0$ according to equation 3.1.

We will assume that variables which vanish at jamming are somehow linked to the free energy density of the system. Therefore, in accordance with renormalisation group theory, we here suggest the following assumption on the scaling of a vanishing variable $\mathcal{O}$ close to the jamming point for a change of length scale with a factor l

$$\mathcal{O}(\delta\phi, \dot{\gamma}) \sim l^{-y_{\mathcal{O}}/\nu} g_{\mathcal{O}}(\delta\phi l^{1/\nu}, \dot{\gamma} l^z) \tag{3.13}$$

where we can choose $\delta\phi l^{1/\nu} = -b \Leftrightarrow l = \left(-\frac{\delta\phi}{b}\right)^{-\nu} \geq 1$ and deduce

$$p(\delta\phi, \dot{\gamma}) \sim \left(\frac{\delta\phi}{b}\right)^{y_{\mathcal{O}}} g_{\mathcal{O}}\left(-b, \dot{\gamma}\left(\frac{\delta\phi}{b}\right)^{-\nu z}\right)$$

where we take the $\delta\phi \to 0$ limit, which gives

$$\mathcal{O}(\delta\phi, \dot{\gamma}) \underset{\delta\phi \to 0}{\sim} (-\delta\phi)^{y_{\mathcal{O}}} \tag{3.14}$$

with $y_{\mathcal{O}} > 0$ thus being the critical exponent associated to the vanishing of the variable $\mathcal{O}$ at jamming.

3.3.1.2 Pressure

We introduce the function $\tilde{g}_p$ such that equation 3.13 applied to the pressure p can be written

$$p(\delta\phi, \dot{\gamma}) \sim \dot{\gamma} l^z l^{-y_p/\nu} \tilde{g}_p(\delta\phi l^{1/\nu}, \dot{\gamma} l^z)$$

and then choose l such that $\delta\phi l^{1/\nu} = -b \Leftrightarrow l = \left(-\frac{\delta\phi}{b}\right)^{-\nu} \geq 1$, which leads to

$$p(\delta\phi, \dot{\gamma}) \sim \dot{\gamma}\left(-\frac{\delta\phi}{b}\right)^{-(\nu z - y)} \tilde{g}_p\left(-b, \dot{\gamma}\left(-\frac{\delta\phi}{b}\right)^{-\nu z}\right)$$

and therefore

$$\eta_p(\delta\phi, \dot{\gamma}) \equiv p(\delta\phi, \dot{\gamma})/\dot{\gamma} \underset{\delta\phi \to 0}{\sim} (-\delta\phi)^{-(\nu z - y)} \tag{3.15}$$

where we recognise $\beta = \nu z - y$ according to equation 3.1.

We now choose l such that $\dot{\gamma} l^z = b \Leftrightarrow l = \left(\frac{\dot{\gamma}}{b}\right)^{-1/z} \geq 1$, which put in equation 3.13 for p leads to

$$p(\delta\phi, \dot{\gamma}) \sim \dot{\gamma}^{y_p/\nu z} g_p\left(\delta\phi\left(\frac{\dot{\gamma}}{b}\right)^{-1/\nu z}, b\right)$$

and finally introduce the function $g_p^{(\mathrm{fit})}$ in order to ignore the constant b in this last equation, which becomes

$$p(\delta\phi, \dot{\gamma}) \sim \dot{\gamma}^{y_p/\nu z} g_p^{(\mathrm{fit})}(\delta\phi \dot{\gamma}^{-1/\nu z}) \tag{3.16}$$

and in which we will denote $q_p \equiv y_p/\nu z$ and $h_p \equiv -1/\nu z$, thus leading to $\beta = (q_p - 1)/h_p$, in addition to $Y_p \equiv p(\delta\phi, \dot{\gamma})\dot{\gamma}^{-q_p}$ and $X_p \equiv \delta\phi\dot{\gamma}^{h_p}$.

A graphical method to determine the values of ϕ_J and q_p, based on the study of equation 3.16, is described in [40], we will however use a different method that allows us to determine these parameters and h_p, and therefore find the critical exponent β.

3.3.1.3 Contact number

We have that the difference of the contact number to its isostatic value vanishes when the packing fraction approaches its jamming value ϕ_J for packings of 2D and 3D spherical particles, according to equation 3.6.

We will assume that, in the general case, it is the difference of the contact number and a critical value of this variable z_c that vanishes at the jamming transition

$$\delta z \equiv z_c - z \underset{\phi \to \phi_J}{\sim} (\phi_J - \phi)^{u_z} \tag{3.17}$$

with $z_c = z_{\text{iso}}$ for spherical particles then.

Following equation 3.13, we formulate the following assumption on the scaling of the δz close to the jamming point for a change of length scale with a factor l

$$\delta z(\delta\phi, \dot{\gamma}) \sim l^{-u_z/\nu} g_{\delta z}(\delta\phi l^{1/\nu}, \dot{\gamma} l^z) \tag{3.18}$$

where ν and z are identical to equation 3.13.

We can choose l such that $\delta\phi l^{1/\nu} = -b \Leftrightarrow l = \left(-\frac{\delta\phi}{b}\right)^{-\nu} \geq 1$, which leads to

$$\delta z(\delta\phi, \dot{\gamma}) \sim \left(-\frac{\delta\phi}{b}\right)^{u_z} g_{\delta z}\left(-b, \dot{\gamma}\left(-\frac{\delta\phi}{b}\right)^{-\nu z}\right)$$

and introduce the function $g_{\delta z}^{(\text{fit})}$ such that

$$\delta z(\delta\phi, \dot{\gamma}) \sim (-\delta\phi)^{u_z} g_{\delta z}^{(\text{fit})}\left(\dot{\gamma}(-\delta\phi)^{-\nu z}\right) \tag{3.19}$$

in which we will denote $q_{\delta z} \equiv u_z$ and $h_{\delta z} \equiv -\nu z$, in addition to $Y_{\delta z} \equiv \delta z(\delta\phi, \dot{\gamma})(-\delta\phi)^{-q_{\delta z}}$ and $X_{\delta_z} \equiv \dot{\gamma}(-\delta\phi)^{h_{\delta z}}$.

3.3.2 Method

3.3.2.1 Fitting

Equation 3.16 and 3.19 suggest that it is possible to collapse the data from simulations at different packing fractions and shear strain rates on a single curve in the ($X_{\mathcal{O}}$,$Y_{\mathcal{O}}$) plane. To perform this fitting, we choose arbitrarily the expression of $g_{\mathcal{O}}^{(\text{fit})}$

$$g_{\mathcal{O}}^{(\text{fit})} : X_{\mathcal{O}} \mapsto \exp\left(\sum_{i=0}^{5} a_{\mathcal{O},i} X_{\mathcal{O}}^i\right)$$

and use the Levenberg-Marquardt algorithm [57, 58] with ϕ_J, z_c, $q_{\mathcal{O}}$, $h_{\mathcal{O}}$ and $a_{\mathcal{O},0}$ through $a_{\mathcal{O},5}$ as free parameters to the corresponding variable fitting. The goal of this algorithm is to minimise the deviation of the experimental data from the fitted curve with respect to the standard deviation for each experimental point. This is equivalent to the minimisation of the chi-square function, introduced in equation 3.21.

This then allows us to determine the relevant critical parameters at the jamming transition.

We thus have shown that z_c may be determined both by the observation of the relaxation process according to equation 3.7 and by the analysis of shearing simulations according to equation 3.19. However, the latter method is not as efficient as the former. Indeed, in shearing simulations involving soft-core particles, the contact number is not as relevant as the way particles overlap because all overlapping particles do not contribute to the stability of the system at the same level, contrarily to hard-core particles. Therefore, this method was not used to study the number of contacts.

3.3.2.2 Evaluation of errors

Measurements

Variables can be measured for each choice of external parameters by averaging their values over the configurations of the system during a single shearing simulation. However, for a given variable x, we have that its values are not exactly independent from configuration to configuration.

Therefore one has to separate the different configurations of the system into blocks to which are associated an unique value of the variable x denoted X_j, indexed over th blocks of configurations. We can then calculate the standard deviation σ_x of the variable x with

$$\sigma_x^2 = \sum_{j=1}^{N_b} \frac{\langle X_j^2 \rangle - \langle X_j \rangle^2}{N_b - 1} \tag{3.20}$$

where N_b is the number of blocks, determined empirically according to the shear rate.

Fitting parameters

Errors on the parameters returned by the Levenberg-Marquardt algorithm are determined by observing how these parameters vary when including noise in the input parameters.

Quality of the fitting

Consider n experimental points (x_i, y_i), each associated with a standard deviation σ_i, which we fit with a function $y(x, a_1, \dots, a_m)$ where $p_1, \dots, p_m$ are free parameters. We define the *chi-square* function

$$\chi^2 \equiv \sum_{i=1}^{n} \left(\frac{y_i - y(x_i, a_1, \dots, a_m)}{\sigma_i} \right)^2 \tag{3.21}$$

whose value should ideally be close to the number of degrees of freedom $n - m$ [59].

To check the quality of the fit obtained with the Levenberg-Marquardt algorithm, we will be very mindful to the following conditions as suggested by [40]:

(i) The agreement between data and the fitting model, as measured by the value of the quotient of the chi-square by the degrees of freedom χ^2/DOF, is good, *i.e.* χ^2/DOF is close to unity.

(ii) The fitting parameters are reasonably independent of the precise range of the data included in the fit.

Multi-variable functions

Consider a function f of the experimental variables $X_1, \dots, X_m$. We will either assume that the correlations between the $(X_i)_{1:m}$ are negligible or that these variables are independent – both assumptions imply that the covariances between the $(X_i)_{1:m}$ are negligible. Then, at a given experimental point $(X_1 = x_1, \dots, X_m = x_m)$, where each x_i is associated to a standard deviation σ_i, we can write the standard deviation of f at this point, $\sigma_f(x_i, \dots, x_m)$, as a function of the $(\sigma_i)_{1:m}$ [60]

$$\sigma_f(x_1, \dots, x_m) = \sqrt{\sum_{i=1}^{m} \left(\frac{\partial f}{\partial X_i}\bigg|_{X_i = x_i} \right)^2 \sigma_i^2} \tag{3.22}$$

3.3.3 Complement on soft- to hard-core mapping

We can make use of our scaling assumption for the pressure to determine the coefficient y_E in equation 3.12.

We can fist notice that in our model of harmonic elastic interactions, the pressure and the energy scale as $E \sim p^2$ as it has already been pointed out in part 3.1.3. Therefore, we have that y_E satifies the following relation

$$y_E = 2y_p \Leftrightarrow y_E = -2q_p/h_p \tag{3.23}$$

where q_p and h_p are the exponents introduced in equation 3.16.

Therefore, considering that q_p and h_p have been determined, c remains the only unknown variable in equation 3.12. We then have a quick way to check the efficiency of this method.

Equations 3.8 and 3.12 can be rewritten as

$$\eta_p^s(\phi, \dot{\gamma}) = A \left(\phi_J - \phi + cE(\phi, \dot{\gamma})^{-h_p/2q_p} \right)^{-\beta} \tag{3.24}$$

where A is an additional parameter which can be determined if we take two points $\eta_{p,1} \equiv \eta_p(\phi_1, \dot{\gamma}_1)$ and $\eta_{p,2} \equiv \eta_p(\phi_2, \dot{\gamma}_2)$, whose corresponding energies are $E_1 \equiv E(\phi_1, \dot{\gamma}_1)$ and $E_2 \equiv E(\phi_2, \dot{\gamma}_2)$, which we hypothesise satisfy equation 3.24.

We can isolate c in equation 3.24, giving

$$c = E(\phi, \dot{\gamma})^{h_p/2q_p} \left(A^{1/\beta} \eta_p(\phi, \dot{\gamma})^{-1/\beta} - \phi_J + \phi \right)$$

which has to be satisfied by the two aforementioned points, therefore

$$E_1^{h_p/2q_p}\left(A^{1/\beta}\eta_{p,1}^{-1/\beta}-\phi_J+\phi_1\right)=E_2^{h_p/2q_p}\left(A^{1/\beta}\eta_{p,2}^{-1/\beta}-\phi_J+\phi_2\right)$$
$$\Leftrightarrow A=\left(\left(\eta_{p,1}^{-1/\beta}E_1^{h_p/2q_p}-\eta_{p,2}^{-1/\beta}E_2^{h_p/2q_p}\right)^{-1}\left(E_1^{h_p/2q_p}(\phi_J-\phi_1)+E_2^{h_p/2q_p}(\phi_2-\phi_J)\right)\right)^{\beta}$$

which can be re-injected in the expression of c evaluated in either point.

We can thus graphically evaluate the efficiency of the mapping in a log-log plot of $\eta_p(\phi,\dot{\gamma})$ vs. $\phi_J-\phi_{\text{eff}}$.

Another, more time-consuming, solution is of course to apply the Levenberg-Marquardt algorithm (part 3.3.2) on equation 3.24 with A and c as free parameters.

3.4 Model of frictionless soft-core particles

3.4.1 Interactions between spherical particles

Much work on jamming has focused on a model of athermal, frictionless – *i.e.*, with no inter-particle Coulombic friction – and spherical soft-core particles with repulsive contact interaction proposed by D. J. Durian to describe foam mechanics [61], in which the rotational motion of the particles does not play any role. For two spheres $\mathcal{S}_i$ and $\mathcal{S}_j$, this model gives the following elastic potential of interaction

$$\boxed{\mathcal{V}_{ij}(r_{ij})=\begin{cases}\frac{1}{2}k_e(1-r_{ij}/d_{ij})^2 & \text{if } r_{ij}\leq d_{ij}\Leftrightarrow \mathcal{S}_i\cap\mathcal{S}_j\neq\emptyset\\ 0 & \text{if } r_{ij}>d_{ij}\Leftrightarrow \mathcal{S}_i\cap\mathcal{S}_j=\emptyset\end{cases}} \tag{3.25}$$

where $\vec{r_{i/j}}$ and $R_{i/j}$ are the positions and the radii of $\mathcal{S}_i$ and $\mathcal{S}_j$, $r_{ij}=||\vec{r_i}-\vec{r_j}||$ and $d_{ij}=R_i+R_j$.

This potential of interaction thus leads to the following force exterted on $\mathcal{S}_i$ by $\mathcal{S}_j$

$$\boxed{\vec{f}_i^{\text{el}}(r_{ij})=\begin{cases}-\frac{k_e}{d_{ij}}(1-r_{ij}/d_{ij})\,\hat{r_{ij}} & \text{if } \mathcal{S}_i\cap\mathcal{S}_j\neq\emptyset\\ 0 & \text{if } \mathcal{S}_i\cap\mathcal{S}_j=\emptyset\end{cases}} \tag{3.26}$$

where $\hat{r_{ij}}=(\vec{r_i}-\vec{r_j})/||\vec{r_i}-\vec{r_j}||$.

The original idea of Durian was to model the interaction between two bubbles in contact by the compression of two springs in series which constants would scale with the Laplace pressures, *i.e.* inversely proportionnal to the bubbles' radii, hence the harmonic potential.

Because of the finite range of the interactions, the potential energies vanish at a fixed finite radius, therefore this system is a good starting point to study macroscopic granular or colloidal systems, suspensions, foams, emulsions and liquids [29, 51].

When simulating the shearing dynamics of such a system, one has to introduce a way to dissipate the energy. This can be done with either one of these two manners, also proposed by Durian [51, 61] :

- A contact dissipation (CD) which is a pairwise interaction, additive and proportional to the difference of the velocities of the moving particles in contact,

$$\boxed{\vec{f}_{\text{CD},i}^{\text{dis}}=-k_d\sum_{j\text{ neighbours}}(\vec{v_i}-\vec{v_j})} \tag{3.27}$$

  where $\vec{v_i}$ denotes the velocity of the particle i. This was originally meant to model the dissipation in the liquid between moving bubbles.

- A reservoir dissipation (RD), which is a mean-field approximation of CD where the pairwise difference of the velocities is replaced for each particle by a dissipation with respect to the average shear flow of the background reservoir,

$$\boxed{\vec{f}_{\text{RD},i}^{\text{dis}}=-k_d\,(\vec{v_i}-\dot{\gamma}y_i\vec{e_x})} \tag{3.28}$$

where $\vec{v_i}$ and y_i denote the velocity and ordinate of the particle i, and $\dot{\gamma}$ and $\vec{e_x}$ denote the shearing strain rate and direction.

Therefore the translational motion of the particles is described by

$$m_i\dot{\vec{v_i}} = \vec{f_i^{\text{el}}} + \vec{f_i^{\text{dis}}} \tag{3.29}$$

To neglect the effects of inertia, we have to consider the overdamped limit $m_i \to 0$, which is easily done in the RD model. For the CD model, it is numerically necessary to take a finite value of the mass, therefore the overdamped limit has to be verified *a posteriori* [51]. However, it has been verified for sheared disks that the effect of finite mass were negligible in the CD model for shear rates $\dot{\gamma} \leq 10^{-3}$ [62].

3.4.2 Elastic force between ellipsoids

3.4.2.1 Reformulation of the elastic potential of interaction for spheres

The distance between the centres of two ellipsoids is not directly relevant to the intensity of their interactions. We need to reformulate equation 3.25 with parameters which would be relevant for ellipsoids. In [17], the overlap potential of two ellipsoids is a function of μ the rescaling factor by which the particles need to be resized in order to be externally tangent. We can investigate whether the equation 3.25 can be reformulate as a function of such a number.

First of all, we can show that if two spheres $\mathcal{A}$ and $\mathcal{B}$, of centres $A \equiv \vec{r_A}$ and $B \equiv \vec{r_B}$ and of radii R_A and R_B respectively, are externally tangent and that none of these spheres is entirely contained in the other, then their point of contact is located on the $[AB]$ line segment. Indeed, if we denote C their point of contact and assume it is not on the $[AB]$ line segment, then

$$||AB|| < ||AC|| + ||BC||$$

If we denote U and V the intersection of the $[AB]$ line segment with $\mathcal{A}$ and $\mathcal{B}$ respectively, then

$$||AB|| = ||AU|| + ||UV|| + ||VB|| < ||AC|| + ||BC||$$

Since $U, C \in \mathcal{A}$ and $V, C \in \mathcal{B}$, then

$$||AU|| = ||AC|| \text{ and } ||VB|| = ||BC|| \Rightarrow ||UV|| < 0$$

which is not possible, therefore their point of contact C have to be on the $[AB]$ line segment.

We we will denote $\forall \vec{r} \in [AB]$, $\mu_A(\vec{r})$ and $\mu_B(\vec{r})$ the rescaling factor that has to be applied to $\mathcal{A}$ and $\mathcal{B}$ respectively for $\vec{r}$ to be on their surface. Then

$$\begin{aligned} 1 = \frac{||\vec{r} - \vec{r_A}||}{\mu_A(\vec{r})R_A} &\Leftrightarrow \mu_A(\vec{r}) = \frac{||\vec{r} - \vec{r_A}||}{R_A} \\ 1 = \frac{||\vec{r} - \vec{r_B}||}{\mu_B(\vec{r})R_B} &\Leftrightarrow \mu_B(\vec{r}) = \frac{||\vec{r} - \vec{r_B}||}{R_B} \end{aligned}$$

Moreover, since $\vec{r} \in [AB]$ we have

$$\begin{aligned} \vec{r} &= \vec{r_A} + \mu_A(\vec{r})R_A\frac{\vec{r_B} - \vec{r_A}}{||\vec{r_B} - \vec{r_A}||} \\ \vec{r} &= \vec{r_B} + \mu_B(\vec{r})R_B\frac{\vec{r_A} - \vec{r_B}}{||\vec{r_A} - \vec{r_B}||} \end{aligned} \tag{3.30}$$

We are now looking for the point $\vec{r_C} \in [AB]$ which satisfies $\mu_A(\vec{r_C}) = \mu_B(\vec{r_C}) = \mu(\vec{r_\mathcal{A}}, \vec{r_\mathcal{B}})$. For such a point we have

$$\begin{aligned} \vec{r_C} = \vec{r_C} \Leftrightarrow &\vec{r_A} + \underbrace{\mu_A(\vec{r_C})}_{\mu(\vec{r_\mathcal{A}}, \vec{r_\mathcal{B}})}R_A\frac{\vec{r_B} - \vec{r_A}}{||\vec{r_B} - \vec{r_A}||} = \vec{r_B} + \underbrace{\mu_B(\vec{r_C})}_{\mu(\vec{r_\mathcal{A}}, \vec{r_\mathcal{B}})}R_B\frac{\vec{r_A} - \vec{r_B}}{||\vec{r_A} - \vec{r_B}||} \\ \Leftrightarrow &(\vec{r_A} - \vec{r_B})||\vec{r_A} - \vec{r_B}|| = \mu(\vec{r_\mathcal{A}}, \vec{r_\mathcal{B}})(\vec{r_A} - \vec{r_B})(R_A + R_B) \\ \xRightarrow[\vec{r_A} \neq \vec{r_B}]{} &\mu(\vec{r_\mathcal{A}}, \vec{r_\mathcal{B}}) = \frac{||\vec{r_A} - \vec{r_B}||}{R_A + R_B} \end{aligned} \tag{3.31}$$

What we have just showed is that for two spheres $\mathcal{S}_i$ and $\mathcal{S}_j$ there exists a point $\vec{r_C}$ on the segment connecting their centres for which $\mu_i(\vec{r_C}) = \mu_j(\vec{r_C}) = \mu(\vec{r_C}) = r_{ij}/d_{ij}$. Therefore, we can reformulate equation 3.25

$$\boxed{\mathcal{V}_{ij}(\vec{r_i}, \vec{r_j}) = \begin{cases} \frac{1}{2}k_e(1 - \mu(\vec{r_i}, \vec{r_j}))^2 & \text{if } \mathcal{S}_i \cap \mathcal{S}_j \neq \emptyset \\ 0 & \text{if } \mathcal{S}_i \cap \mathcal{S}_j = \emptyset \end{cases}} \tag{3.32}$$

We can verify that this new formulation leads to the same elastic force that in equation 3.26. If we denote $\vec{f}^{\text{el}}_{ij}$ the elastic force exerted on $\mathcal{S}_i$ by $\mathcal{S}_j$, then we should have

$$\vec{f}^{\text{el}}_{ij} = -\frac{d\mathcal{V}_{ij}}{d\vec{r_i}}(\vec{r_i}, \vec{r_j}) = k_e(1 - \mu(\vec{r_i}, \vec{r_j}))\frac{d\mu}{d\vec{r_i}}(\vec{r_i}, \vec{r_j})$$

From equation 3.30 we can infer

$$\frac{d\mu_i}{d\vec{r_i}}(\vec{r_i}, \vec{r_j}) = -\frac{1}{R_i}\frac{\vec{r_j} - \vec{r_i}}{||\vec{r_j} - \vec{r_i}||}$$

and from equation 3.31

$$\begin{aligned} \vec{r_C} &= \vec{r_i} + \mu R_i \frac{\vec{r_j} - \vec{r_i}}{||\vec{r_j} - \vec{r_i}||} \\ &= \vec{r_i} + \frac{\cancel{||\vec{r_j} - \vec{r_i}||}}{R_i + R_j} R_i \frac{\vec{r_j} - \vec{r_i}}{\cancel{||\vec{r_j} - \vec{r_i}||}} \\ &= \vec{r_i} + R_i \frac{\vec{r_j} - \vec{r_i}}{R_i + R_j} \end{aligned}$$

therefore $\frac{d\mu}{d\vec{r_i}}(\vec{r_C}) = \frac{1}{R_i+R_j}\frac{\vec{r_i}-\vec{r_j}}{||\vec{r_i}-\vec{r_j}||} = \frac{1}{d_{ij}}\frac{\vec{r_i}-\vec{r_j}}{||\vec{r_i}-\vec{r_j}||}$. Finally, we have the correct expression for the elastic force

$$\vec{f}^{\text{el}}_{ij} = \frac{k_e}{d_{ij}}\left(1 - \frac{r_{ij}}{d_{ij}}\right)\frac{\vec{r_i} - \vec{r_j}}{||\vec{r_i} - \vec{r_j}||} \tag{3.33}$$

corresponding to equation 3.26.

3.4.2.2 Elastic force between ellipsoids

We will assume that the equation 3.32 remains valid for two ellipsoids $\mathcal{A}$ and $\mathcal{B}$.

$$\boxed{\mathcal{V}_{\mathcal{AB}}(\vec{r_\mathcal{A}}, \vec{r_\mathcal{B}}) = \begin{cases} \frac{1}{2}k_e(1 - \mu(\vec{r_\mathcal{A}}, \vec{r_\mathcal{B}}))^2 & \text{if } \mathcal{A} \cap \mathcal{B} \neq \emptyset \\ 0 & \text{if } \mathcal{A} \cap \mathcal{B} = \emptyset \end{cases}} \tag{3.34}$$

Let $\bar{B}_\mathcal{A}$ be the reduced belonging matrix of $\mathcal{A}$, $\vec{r_\mathcal{A}}$ its centre and $\vec{r_C}$ the point of external tangency of ellipsoids $\mathcal{A}$ and $\mathcal{B}$ when rescaled by a common rescaling factor $\mu(\vec{r_\mathcal{A}}, \vec{r_\mathcal{B}})$, then

$$\mu^2(\vec{r_\mathcal{A}}, \vec{r_\mathcal{B}}) = (\vec{r_C} - \vec{r_\mathcal{A}})^T \bar{B}_\mathcal{A}(\vec{r_C} - \vec{r_\mathcal{A}}) \tag{3.35}$$

according to equation C.13.

According to equation 3.34, the force exerted on $\mathcal{A}$ by $\mathcal{B}$ is

$$\begin{aligned} \vec{f}^{\text{el}}_{\mathcal{AB}}(\vec{r_\mathcal{A}}, \vec{r_\mathcal{B}}) &= -\frac{d\mathcal{V}_{\mathcal{AB}}}{d\vec{r_A}}(\vec{r_\mathcal{A}}, \vec{r_\mathcal{B}}) \\ &= k_e(1 - \mu(\vec{r_\mathcal{A}}, \vec{r_\mathcal{B}}))\frac{d\mu}{d\vec{r_\mathcal{A}}}(\vec{r_\mathcal{A}}, \vec{r_\mathcal{B}}) \end{aligned} \tag{3.36}$$

Equation 3.35 shows that, contrarily to the case of spheres (equation 3.31), for ellipsoids the rescaling factor $\mu(\vec{r_\mathcal{A}}, \vec{r_\mathcal{B}})$ is not uniquely determined by the positions of their centres. Indeed, if we were to add $d\vec{r_\mathcal{A}}$ to the position $\vec{r_\mathcal{A}}$ of the centre of ellipsoid $\mathcal{A}$, the contact point $\vec{r_C}$ with ellipsoid $\mathcal{B}$ would move as well.

Since we are looking for the first derivative of the quantity $\mu(\vec{r_\mathcal{A}}, \vec{r_\mathcal{B}})$, we will approximate rescaled ellipsoids by their respective tangent planes at $\vec{r_C}$ as suggested by [18].

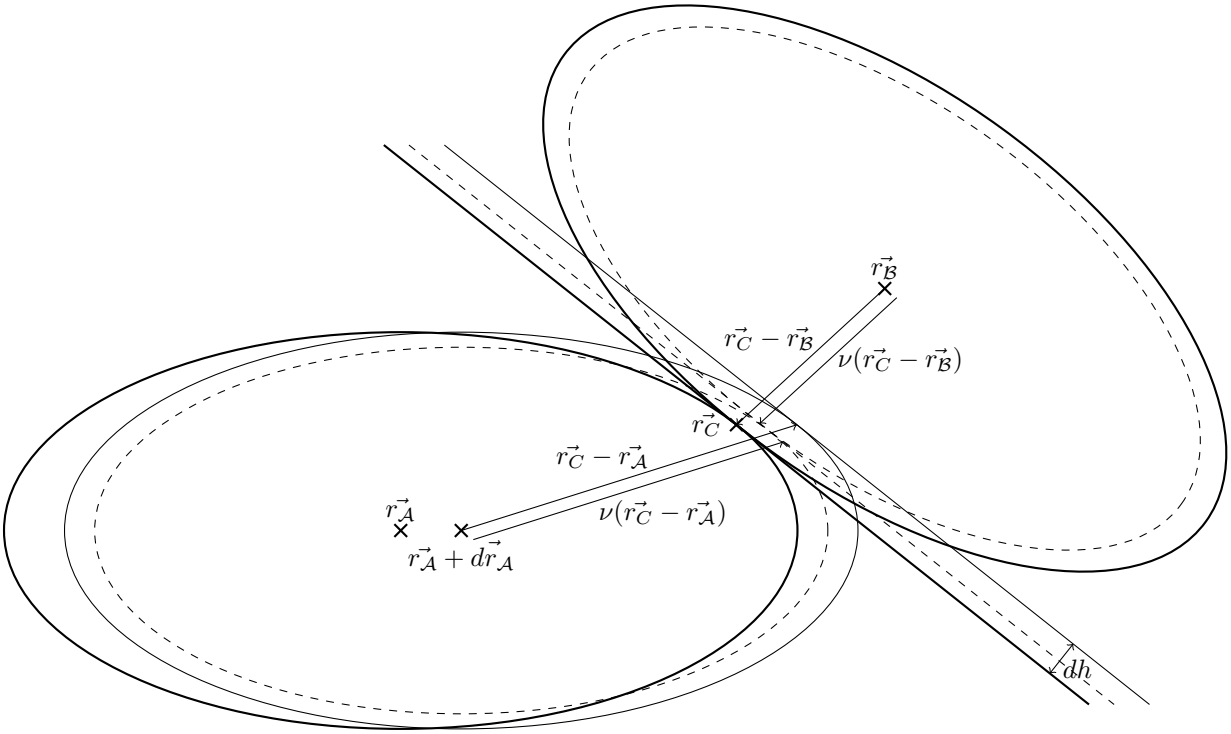

Figure 3.2: Ellipsoids rescaled with rescaling factor $\mu(\vec{r_{\mathcal{A}}}, \vec{r_{\mathcal{B}}})$ and their contact plane in plain thick trait. Ellipsoids rescaled with rescaling factor $\mu(\vec{r_{\mathcal{A}}} + \vec{dr_{\mathcal{A}}}, \vec{r_{\mathcal{B}}})$ and their contact plane in dashed trait.

If ellipsoid $\mathcal{A}$ is moved by $\vec{dr_{\mathcal{A}}}$, there appears a gap dh between the tangent planes of the rescaled ellipsoids with

$$dh = \vec{dr_{\mathcal{A}}} \cdot \vec{n}_{\mathcal{A}}(\vec{r_C}) \tag{3.37}$$

where $\vec{n}_{\mathcal{A}}(\vec{r_C})$ is the outward-facing unitary surface vector of ellipsoid $\mathcal{A}$ in $\vec{r_C}$.

To close this gap, we have to rescale the – yet rescaled – ellipsoids with a factor ν so that

$$((\vec{r_C} - \vec{r_{\mathcal{A}}}) - \nu(\vec{r_C} - \vec{r_{\mathcal{A}}})) \cdot \vec{n}_{\mathcal{A}}(\vec{r_C}) - ((\vec{r_C} - \vec{r_{\mathcal{B}}}) - \nu(\vec{r_C} - \vec{r_{\mathcal{B}}})) \cdot \vec{n}_{\mathcal{A}}(\vec{r_C}) = dh \Rightarrow 1 - \nu = \frac{dh}{(\vec{r_{\mathcal{B}}} - \vec{r_{\mathcal{A}}}) \cdot \vec{n}_{\mathcal{A}}(\vec{r_C})}$$

and

$$\mu(\vec{r_{\mathcal{A}}} + \vec{dr_{\mathcal{A}}}, \vec{r_{\mathcal{B}}}) = \nu\mu(\vec{r_{\mathcal{A}}}, \vec{r_{\mathcal{B}}}) \Rightarrow \vec{dr_{\mathcal{A}}} \cdot \frac{d\mu}{\vec{dr_{\mathcal{A}}}}(\vec{r_{\mathcal{A}}}, \vec{r_{\mathcal{B}}}) = -\mu(\vec{r_{\mathcal{A}}}, \vec{r_{\mathcal{B}}})(1 - \nu)$$

which, with equation 3.37, leads to

$$\frac{d\mu}{\vec{dr_{\mathcal{A}}}}(\vec{r_{\mathcal{A}}}, \vec{r_{\mathcal{B}}}) = -\mu(\vec{r_{\mathcal{A}}}, \vec{r_{\mathcal{B}}}) \frac{\vec{n}_{\mathcal{A}}(\vec{r_C})}{(\vec{r_{\mathcal{B}}} - \vec{r_{\mathcal{A}}}) \cdot \vec{n}_{\mathcal{A}}(\vec{r_C})}$$

We can then conclude, with equation C.15, that

$$\frac{d\mu}{\vec{dr_{\mathcal{A}}}}(\vec{r_{\mathcal{A}}}, \vec{r_{\mathcal{B}}}) = -\frac{\mu(\vec{r_{\mathcal{A}}}, \vec{r_{\mathcal{B}}})}{(\vec{r_{\mathcal{B}}} - \vec{r_{\mathcal{A}}})^T \bar{B}_{\mathcal{A}}(\vec{r_C} - \vec{r_{\mathcal{A}}})} \bar{B}_{\mathcal{A}}(\vec{r_C} - \vec{r_{\mathcal{A}}}) \tag{3.38}$$

Therefore, with equation 3.36, we finally have that

$$\boxed{\vec{f}^{\text{el}}_{\mathcal{AB}}(\vec{r_{\mathcal{A}}}, \vec{r_{\mathcal{B}}}) = -k_e \frac{\mu(\vec{r_{\mathcal{A}}}, \vec{r_{\mathcal{B}}})\,(1 - \mu(\vec{r_{\mathcal{A}}}, \vec{r_{\mathcal{B}}}))}{(\vec{r_{\mathcal{B}}} - \vec{r_{\mathcal{A}}})^T \bar{B}_{\mathcal{A}}(\vec{r_C} - \vec{r_{\mathcal{A}}})} \bar{B}_{\mathcal{A}}(\vec{r_C} - \vec{r_{\mathcal{A}}})} \tag{3.39}$$

We can verify once again that this new formulation leads to the same elastic force that in equation 3.26. With the notations of this equation, we have that if $\mathcal{A}$ and $\mathcal{B}$ are spheres, then

$$\mu(\vec{r_{\mathcal{A}}}, \vec{r_{\mathcal{B}}}) = \frac{r_{\mathcal{AB}}}{d_{\mathcal{AB}}}, \text{ and } \frac{\bar{B}_{\mathcal{A}}(\vec{r_C} - \vec{r_{\mathcal{A}}})}{||\bar{B}_{\mathcal{A}}(\vec{r_C} - \vec{r_{\mathcal{A}}})||} = r_{\hat{\mathcal{AB}}}$$

therefore

$$\begin{aligned}\vec{f}^{\text{el}}_{\mathcal{AB}}(\vec{r_{\mathcal{A}}}, \vec{r_{\mathcal{B}}}) &= -k_e \frac{\cancel{r_{\mathcal{AB}}}}{d_{\mathcal{AB}}} \frac{1 - \frac{r_{\mathcal{AB}}}{d_{\mathcal{AB}}}}{\cancel{(\vec{r_{\mathcal{B}}} - \vec{r_{\mathcal{A}}}) \cdot \hat{r_{\mathcal{AB}}}}} \hat{r_{\mathcal{AB}}} \\ &= -\frac{k_e}{d_{\mathcal{AB}}} \left(1 - \frac{r_{\mathcal{AB}}}{d_{\mathcal{AB}}}\right) \hat{r_{\mathcal{AB}}}\end{aligned}$$

which is correct.

3.4.3 Dissipative force between ellipsoids

The expressions proposed for the dissipative force exerted on a particle i by a particle j in equations 3.27 and 3.28 remain relevant for ellipsoids.

However, we now have that the elastic force exerted by an ellipsoid on another (equation 3.39) can induce a rotational motion of both particles. Authors of [15] had already proposed for spheres to couple rotational and translational motion by taking into account the rotation velocities of the particles in the contact dissipation model of the dissipative force

$$\boxed{\vec{f}^{\text{dis}}_{ij} = -k_d(\vec{v_i}^{C_j} - \vec{v_j}^{C_i})} \tag{3.40}$$

where $\vec{v_i}^{C_j}$ is the local velocity of particle i at its point of contact with particle j.

Consider two ellipsoids $\mathcal{A}$ and $\mathcal{B}$, whose centres are located in $\vec{r_{\mathcal{A}}}$ and $\vec{r_{\mathcal{B}}}$, whose orientations are described by $q_{\mathcal{A}}$ and $q_{\mathcal{B}}$ and whose velocities are $\vec{v_{\mathcal{A}}}$ and $\vec{v_{\mathcal{B}}}$. We assume their points of contacts are $r_{\vec{C,\mathcal{A}}}$ and $r_{\vec{C,\mathcal{B}}}$ respectively, with the expressions given in equation 3.49. Then, we can calculate the local velocity of the ellipsoids at their points of contact

$$\boxed{\begin{aligned}\vec{v_{\mathcal{A}}}^{C_{\mathcal{A}}} &= \vec{v_{\mathcal{A}}} + \vec{\omega_{\mathcal{A}}} \times (r_{\vec{C,\mathcal{A}}} - \vec{r_{\mathcal{A}}}) \\ \vec{v_{\mathcal{B}}}^{C_{\mathcal{B}}} &= \vec{v_{\mathcal{B}}} + \vec{\omega_{\mathcal{B}}} \times (r_{\vec{C,\mathcal{B}}} - \vec{r_{\mathcal{B}}})\end{aligned}} \tag{3.41}$$

where $\vec{\omega}$ is the rotation vector.

According to equation 1.5, we have $\vec{\omega} = 2\dot{q}q^*$, therefore we can reformulate the equation 3.41 with the quaternions of the ellipsoids

$$\begin{aligned}\vec{v_{\mathcal{A}}}^{C_{\mathcal{B}}} &= \vec{v_{\mathcal{A}}} + 2\dot{q}_{\mathcal{A}} q^*_{\mathcal{A}} \times (r_{\vec{C,\mathcal{A}}} - \vec{r_{\mathcal{A}}}) \\ \vec{v_{\mathcal{B}}}^{C_{\mathcal{A}}} &= \vec{v_{\mathcal{B}}} + 2\dot{q}_{\mathcal{B}} q^*_{\mathcal{B}} \times (r_{\vec{C,\mathcal{B}}} - \vec{r_{\mathcal{B}}})\end{aligned} \tag{3.42}$$

Nonetheless, we finally decided to take $r_{\vec{C,\mathcal{A}}} = r_{\vec{C,\mathcal{B}}} = \vec{r_C}$ for the computation of the dissipative force.

3.4.4 Pressure in a sheared packing of ellipsoids

To determine the pressure in the system, we have to determine its pressure tensor P which consists of three pieces [15, 63]

(i) the kinetic part

$$P_{\text{kin}} = \frac{1}{L^2} \sum_{i<j} m_i \delta\vec{v_i} \delta\vec{v_i}^T \tag{3.43}$$

with m_i the mass of particle i and $\delta\vec{v_i}$ the fluctuation of the velocity of particl i away from the average velocity profile which caracterises the flow,

(ii) the dissipative part

$$P_{\text{dis}} = \frac{1}{L^2} \sum_{i<j} \left(\vec{f}^{\text{dis}}_{ij} (r_{\vec{C,i}} - \vec{r_i})^T + \vec{f}^{\text{dis}}_{ji} (r_{\vec{C,j}} - \vec{r_j})^T \right) \tag{3.44}$$

with $\vec{f}^{\text{dis}}_{ij}$ the dissipative force exerted on particle i by particle j (equation 3.40), $r_{\vec{C,i}}$ the point of contact on particle i and $\vec{r_i}$ the centre of particle i,

(iii) and the elastic part [63]

$$P_{\text{el}} = \frac{1}{L^2} \sum_{i<j} \left(\vec{f}_{ij}^{\text{el}} \left(r\vec{C},i - \vec{r_i} \right)^T + \vec{f}_{ji}^{\text{el}} \left(r\vec{C},j - \vec{r_j} \right)^T \right) \tag{3.45}$$

with $\vec{f}_{ij}^{\text{dis}}$ the dissipative force exerted on particle i by particle j (equation 3.39), leading to

$$P = P_{\text{kin}} + P_{\text{dis}} + P_{\text{el}} \tag{3.46}$$

from which we define the average pressure of the system as

$$p = \frac{1}{D} \text{Tr}(P) \tag{3.47}$$

where $D = 3$ is the dimension of the system.

Most often in shearing simulations, for small enough shear strain rates $\dot{\gamma}$, the elastic part of the pressure

$$p_{\text{el}} = \frac{1}{D} \text{Tr}(P_{\text{el}}) \tag{3.48}$$

dominates over the kinetic and dissipative parts [64]. We will then identify the pressure and its elastic part without further notice.

3.4.5 Points of contact

3.4.5.1 Determination

Consider two ellipsoids $\mathcal{A}$ and $\mathcal{B}$, whose centres are located in $\vec{r_A}$ and $\vec{r_B}$. The determination of their points of contact is determinant to the calculation of the dissipative force between them (equation 3.40).

We have defined our elastic potential of interaction with the rescaling factor $\mu(\vec{r_\mathcal{A}}, \vec{r_\mathcal{B}}) = \mu_\mathcal{A}(\vec{r_C}) = \mu_\mathcal{B}(\vec{r_C})$ that have to be applied to both ellipsoids for them to be externally tangent in $\vec{r_C}$.

The logical choice for the points of contact is then the equivalents of the point $\vec{r_C}$ on the original ellipsoids. These points are located on the lines passing by $\vec{r_C}$ and the centres of the respective ellipsoids.

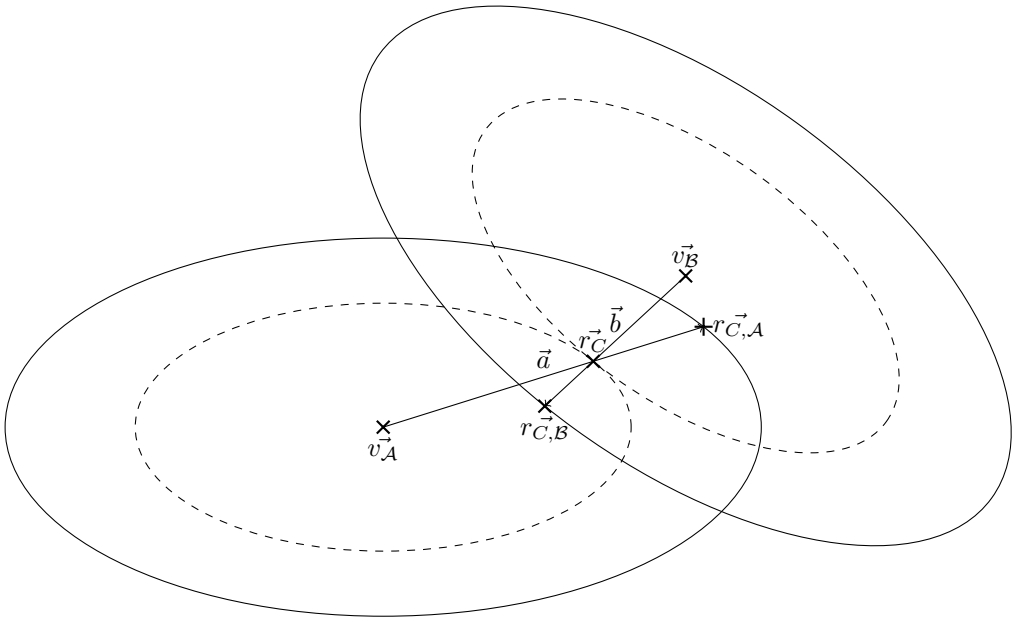

Figure 3.3: Original ellipsoids in plain and rescaled ellipsoids in dashed.

Therefore, we can find such equivalents by translating the centres of the ellipsoids to the origin, dilating the ellipsoids, and translating them back

$$\boxed{\begin{aligned} r_{\vec{C},\mathcal{A}} &= r_{\mathcal{A}} + \underbrace{\nu(r_{\mathcal{A}}, r_{\mathcal{B}})(r_{\vec{C}} - r_{\mathcal{A}})}_{\vec{a}} &&= \nu(r_{\mathcal{A}}, r_{\mathcal{B}})r_{\vec{C}} + (1 - \nu(r_{\mathcal{A}}, r_{\mathcal{B}}))r_{\mathcal{A}} \\ r_{\vec{C},\mathcal{B}} &= r_{\mathcal{B}} + \underbrace{\nu(r_{\mathcal{A}}, r_{\mathcal{B}})(r_{\vec{C}} - r_{\mathcal{B}})}_{\vec{b}} &&= \nu(r_{\mathcal{A}}, r_{\mathcal{B}})r_{\vec{C}} + (1 - \nu(r_{\mathcal{A}}, r_{\mathcal{B}}))r_{\mathcal{B}} \end{aligned}} \tag{3.49}$$

with $\nu(r_{\mathcal{A}}, r_{\mathcal{B}}) \equiv 1/\mu(r_{\mathcal{A}}, r_{\mathcal{B}})$.

We can notice that since

$$\begin{aligned} r_{\vec{C},\mathcal{A}} - r_{\mathcal{A}} &= \nu(r_{\mathcal{A}}, r_{\mathcal{B}})(r_{\vec{C}} - r_{\mathcal{A}}) \\ r_{\vec{C},\mathcal{B}} - r_{\mathcal{B}} &= \nu(r_{\mathcal{A}}, r_{\mathcal{B}})(r_{\vec{C}} - r_{\mathcal{B}}) \end{aligned}$$

we have

$$\boxed{\begin{aligned} \vec{n}_{\mathcal{A}}(r_{\vec{C}}) &= \vec{n}_{\mathcal{A}}(r_{\vec{C},\mathcal{A}}) \\ \vec{n}_{\mathcal{B}}(r_{\vec{C}}) &= \vec{n}_{\mathcal{B}}(r_{\vec{C},\mathcal{B}}) \end{aligned}} \tag{3.50}$$

according to equation C.15. Therefore, according to equation 3.39, we have that the elastic force exerted by an ellipsoid on the other is orthogonal to its surface.

3.4.5.2 Relative positions

In order to evaluate if ellipsoidal particles are more often in contact in a certain configuration, we need to have coordinates of the points of contact which are relative to the position, the orientation and the semi-axes of the corresponding ellipsoids.

Consider an ellipsoid $\mathcal{A}$, of semi-axes $(R_i)_{i=1:3}$, whose centre is located in $r_{\mathcal{A}}$ and whose orientation is described by the quaternion $q_{\mathcal{A}}$, then we will denote

$$\boxed{\tilde{r_{\vec{C},\mathcal{A}}} \equiv \mathrm{diag}(R_i^{-1})_{i=1:3}\mathcal{Q}_{q_{\mathcal{A}}}^T(r_{\vec{C},\mathcal{A}} - r_{\mathcal{A}})} \tag{3.51}$$

the positions of the contact point on ellipsoid $\mathcal{A}$ relative to ellipsoid $\mathcal{A}$.

We can take the absolute value of all the coordinates of $\tilde{r_{\vec{C},\mathcal{A}}}$ since two points on an ellipsoid which are symmetric to each other with respect to a principal plane of this ellipsoid are equivalent.

3.4.6 Computation of the interactions

To compute the forces and the points of contact between two ellipsoids, we need to know if ellipsoids are overlapping and, if so, the rescaling factor for ellipsoids to be tangent and the contact point of these rescaled ellipsoids.

All this information can be accessed by using the Perram and Wertheim method described in part 2.2.1.

3.4.7 Dispersity

As we have pointed out in part 3.2.1, polydispersity is necessary to prevent crystallisation. In our simulations we use two sizes of ellipsoids in equal number, with a corresponding axis ratio of 1.4 between these sizes. We chose the masses of the ellipsoids to be $m = 1$ and $m = 1.4^3$ to ensure that ellipsoids of both sizes have the same density.

3.5 Rheology

The shearing rheology of athermal frictionless soft-core disks has been thoroughly studied in [15, 64] and gives hints on what to expect of the shearing rheology of spheroids in our model near the jamming transition. Authors of these papers stressed that the model chosen for the dissipation was determinant to the behaviours observed. In this part we will only focus on the contact dissipation model which takes into account the rotation of the

particles (equation 3.40).

Vågberg *et al.* showed that upon increasing the packing fraction, disks sharply transitioned from Bagnoldian rheology

$$\sigma, p \sim \dot{\gamma}^2 \Leftrightarrow \frac{\partial}{\partial \dot{\gamma}} B_{\sigma,p} = 0, \;\; B_{\sigma,p} \equiv \sigma, p/\dot{\gamma}^2 \tag{3.52}$$

to Newtonian rheology

$$\sigma, p \sim \dot{\gamma} \Leftrightarrow \frac{\partial}{\partial \dot{\gamma}^2} \eta_{\sigma,p} = 0, \;\; \eta_{\sigma,p} \equiv \sigma, p/\dot{\gamma} \tag{3.53}$$

at a precise packing fraction which depended on the inelasticity of collisions between particles, as measured by the parameter $Q \propto \sqrt{mk_e/k_d^2}$ with m, k_e and k_d introduced in equations 3.25, 3.27 and 3.28.

We will call $B_{\sigma,p}$ the *Bagnoldian transport coefficient* associated to shear strain or pressure and $\eta_{\sigma,p}$ the *Newtonian transport coefficient* associated to shear strain or pressure.

At low packing fractions, *i.e.* for dilute systems, particles separate if the contact velocity is not damped to zero during the collision, which is possible for elastic enough interactions. Particles in such systems have few instantaneous contacts; In this case, the system is in an "inertial" regime: the dissipation term in equation 3.29 is negligible and the trajectories are determined by the balance of elastic and kinetic terms, hence the Bagnoldian rheology at small $\dot{\gamma}$ [64]. Shearing simulations showed that disks are able to adjust their rotation to cancel out the relative motion of particles, so that the tangential component of the contact velocity difference is as small as the normal component, hence the small dissipative force [15].

At high packing fractions, *i.e.* for dense systems, compressive motion which would induce particle overlaps is energetically prohibitive. Normally directed relative motion is thus greatly suppressed and the collisions are primarily tangential. Shearing simulations have showed that, in this case, disks fluctuate in their rotational motion but that these fluctuations are uncorrelated with the tangential component of the velocity difference, thus leading to a large tangential component of the dissipative force compared to its normal component. This lack of correlations of the rotation is thought to result from the increasing constraint on rotational motion due to the higher number of contacts at higher densities [15]. The system is then in an "overdamped" regime: the kinetic term in equation 3.29 is negligible and the trajectories are determined by the balance of elastic and dissipative terms, hence the Newtonian rheology at small $\dot{\gamma}$ [64]. Because of the tangential dissipation, particles tend to cluster together, with force chains percolationg throughout the systems, and have more instantaneous contacts.

Furthermore, authors showed that η_p was independent of Q in the Newtonian regime and that their system was always Newtonian at jamming. Therefore, they concluded that the value of ϕ_J as well as the exponent characterising the divergence of η_p should be independent of the inelasticity of collisions, *i.e.* of the parameters m, k_e and k_d [15].

4 | Results and discussion

4.1 Preliminary results

Preliminary simulations were performed with only 64 particles, first to ensure that our models and methods were effective and gave realistic results, then to determine what phenomena were different with ellipsoids than with spheres. Simulations performed with this few particles have the advantage to quickly give results to analyse, however finite-size effects are not negligible and can affect the jamming transition (see part 3.1.7).

4.1.1 Rheological transition

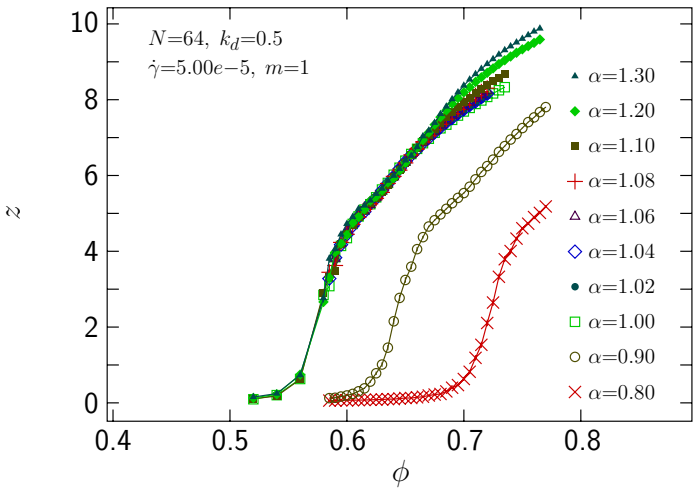

Figure 4.1: Average contact number per particle as a function of the packing fraction for aspect ratios $0.8 \leq \alpha \leq 1.3$. $N = 64,\ k_d = 0.5,\ \dot{\gamma} = 5e-5,\ m = 1$.

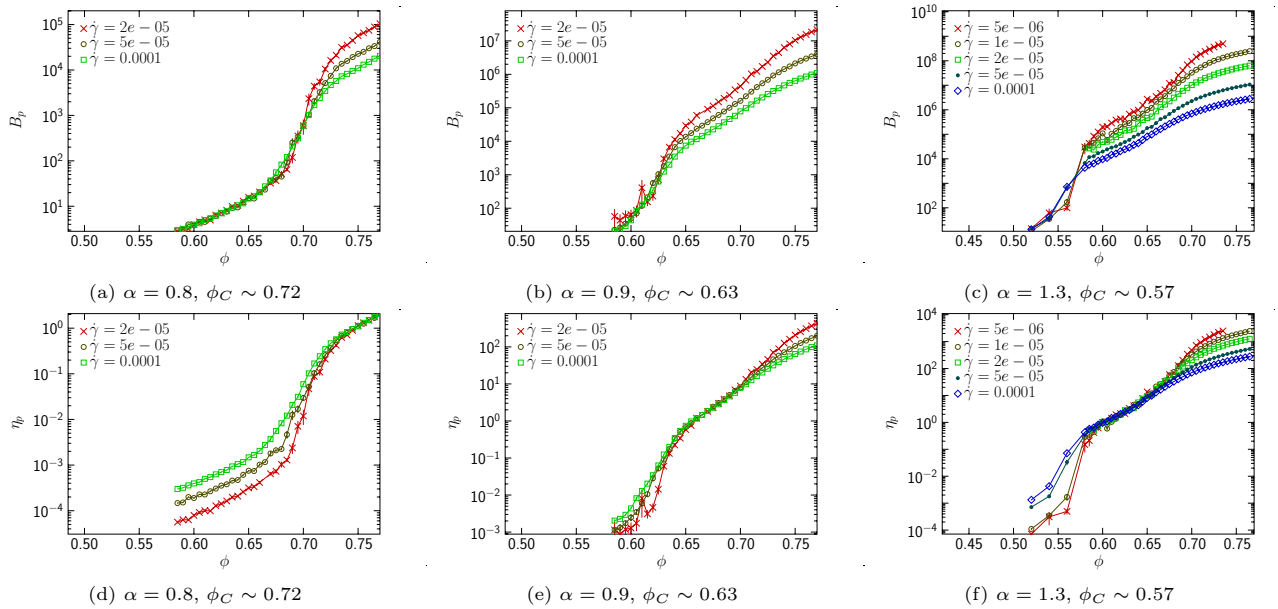

(a) $\alpha = 0.8,\ \phi_C \sim 0.72$ (b) $\alpha = 0.9,\ \phi_C \sim 0.63$ (c) $\alpha = 1.3,\ \phi_C \sim 0.57$

(d) $\alpha = 0.8,\ \phi_C \sim 0.72$ (e) $\alpha = 0.9,\ \phi_C \sim 0.63$ (f) $\alpha = 1.3,\ \phi_C \sim 0.57$

Figure 4.2: Bagnoldian (figures 4.2a, 4.2b and 4.2c) and Newtonian (figures 4.2d, 4.2e and 4.2f) transport coefficients associated to pressure. $N = 64,\ k_d = 0.5,\ m = 1$. We denote ϕ_C the transition packing fraction.

We observe in figure 4.1 a sharp increase in the average contact number per particle upon increasing the packing fraction. According to the development of part 3.5, this increase is the sign of a transition from Bagnoldian rheology to Newtonian rheology. We confirm this by determining the Bagnoldian and Newtonian transport coefficients associated to pressure as functions of the packing fraction, and verifying the transitions from a regime to the other occurs at the same packing fractions as the increase of contact number (figure 4.2).

We also observe that the Newtonian transport coefficients become $\dot{\gamma}$-dependent for high enough packing fractions, we will see in part 4.1.2.1 that this is due to a deviation from the hard-core limit near the jamming transition.

Moreover, we can notice that for $1 \leq \alpha < 1.3$ (sphere and prolate spheroids) the transition from the Bagnoldian to the Newtonian regime occurs approximately at the same packing fraction, while for $\alpha = 0.8, 0.9$ (oblate spheroids) the transition packing fraction ϕ_C varies with the aspect ratio and is higher than the value obtained for the former particles.

4.1.2 Critical behaviour

4.1.2.1 Deviation from the hard-core limit close to jamming

We expect from the development of part 3.5 that the system would display Newtonian rheology sufficiently close to the jamming transition, *i.e.* the Newtonian transport coefficients would be independent of the shear rates at which they are determined. However, this holds only in the hard-core limit.

Close to the jamming transition, the overlapping of the particles is non-negligible, hence the deviation from the hard-core limit. This deviation being even more important for higher shear strain rates (figure 4.3).

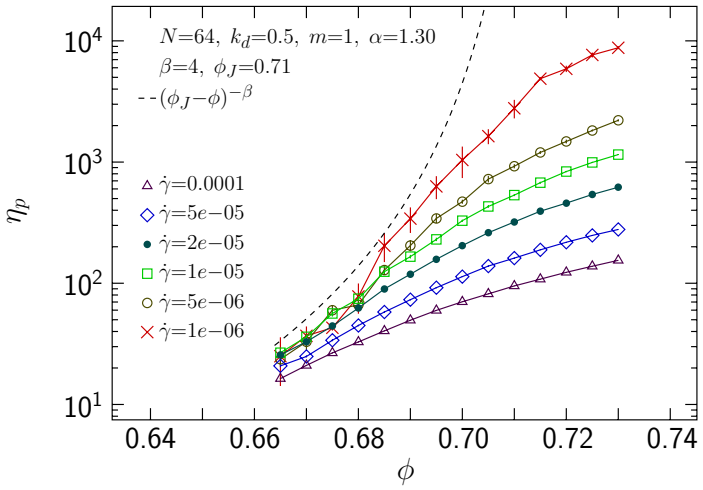

Figure 4.3: Newtonian coefficient of transport associated to pressure as a function of the packing fraction for $\alpha = 1.3$.

4.1.2.2 Effectiveness of scaling

Figure 4.4a shows that we have successfully made experimental data from simulations at different density and shear strain rates collapse on a single curve with the method described in part 3.3, thus confirming its effectiveness. Scaling exponents from this graph then allowed us to make Newtonian transport coefficients associated to pressure inferred from simulations at different shear rates collapse on a single straight line characterising the critical behaviour described by equation 3.1 for hard-core particles with satisfactory visual precision in figure 4.4b.

Moreover, we can notice that the mapping parameters determined graphically in figure 4.4b ($A = 1.9$, $c = 0.48$) are close to the values found in [41] for disks ($A = 1.53$, $c = 0.458$).

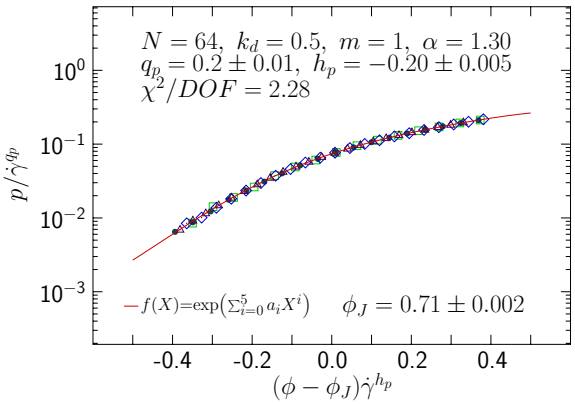

(a) Pressure scaling plot, as described in part 3.3.1.2.

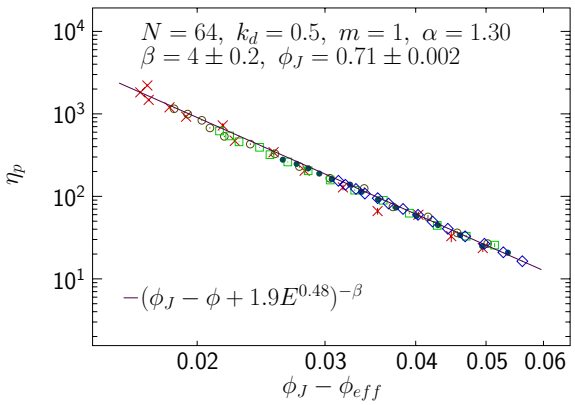

(b) Newtonian transport coefficient associated to pressure scaling plot, obtained with the soft- to hard-core mapping method described in parts 3.2.3 and 3.3.3. We privileged here the graphical determination of the mapping parameters.

Figure 4.4: Scaling plots for $\alpha = 1.3$.

4.1.2.3 Jamming density and critical exponent

From plots such as figure 4.4a we were able to determine the jamming density and critical exponents for different aspect ratios (see figure 4.5).

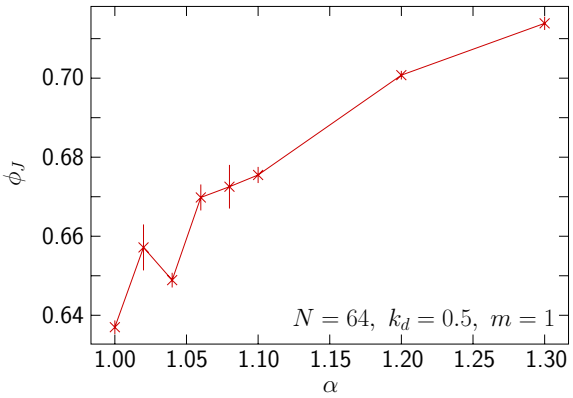

(a) Jamming packing fraction as a function of the aspect ratio.

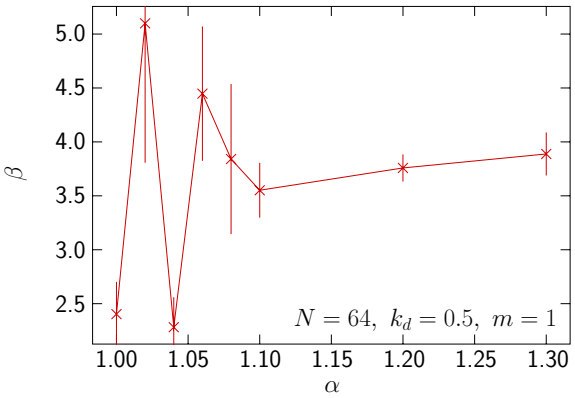

(b) Critical exponent associated to the divergence of the Newtonian transport coefficients as a function of the aspect ratio.

Figure 4.5: Jamming parameters for spheres and prolate spheroids.

We can first notice that for $\alpha = 1$, *i.e.* for spheres, we have $\beta \sim 2.5$ which is close to the result of [41] for disks ($\beta = 2.58$). Moreover, we have the jamming packing fraction $\phi_J \sim 0.64$ close to the random close packing fraction for spheres [49].

For the set of aspect ratios considered ($1 \leq \alpha \leq 1.3$), we have that the jamming packing fraction is an increasing function of the aspect ratio (figure 4.5a) – if we exclude $\alpha = 1.04$. This is in accordance with [49] which found that ϕ_J was an increasing function of the aspect ratio for $1 \leq \alpha \lesssim 1.6$. It is intuitive from the iscostatic conjecture (part 3.1.4) that close-to-spherical ellipsoids should pack more densely than spheres: if the number of degrees of freedom increases by introducing rotations then the number of contacts should also increase, resulting in denser packings [48].

Simulations with 64 particles were performed for oblate particles but not close enough to the jamming transition to give ϕ_J and β with good precision. Nonetheless, we also observed for these particles that the jamming packing fraction would be greater than its value for packings of spheres. More specifically, we estimated $0.7 < \phi_J(\alpha = 0.9) < \phi_J(\alpha = 0.8)$.

It is more difficult to predict the behaviour of the critical exponent β from figure 4.5b. However – if we exclude $\alpha = 1.04$ once again – we can assume that the critical exponent associated to the divergence of the Newtonian

transport coefficients is higher, and has a value close to ~ 4, for prolate spheroids than for spheres.

4.1.3 Orientation

Following the claim that shearing breaks the isotropy of space in part 3.1.5, we wished to check if

(i) spheroids tend to angle themselves in a particular direction,

(ii) the orientation of the spheroids is correlated.

4.1.3.1 Direction of orientation

We denote O_i the mean over configurations of the system of the square of the projection of the axis of symmetry of the spheroid on the i^{th} axis, with then $\sum_{i=1}^{3} O_i^2 = 1$ and the 0^{th} and 1^{st} axis corresponding the directions of the shear and the gradient of shear velocity respectively.

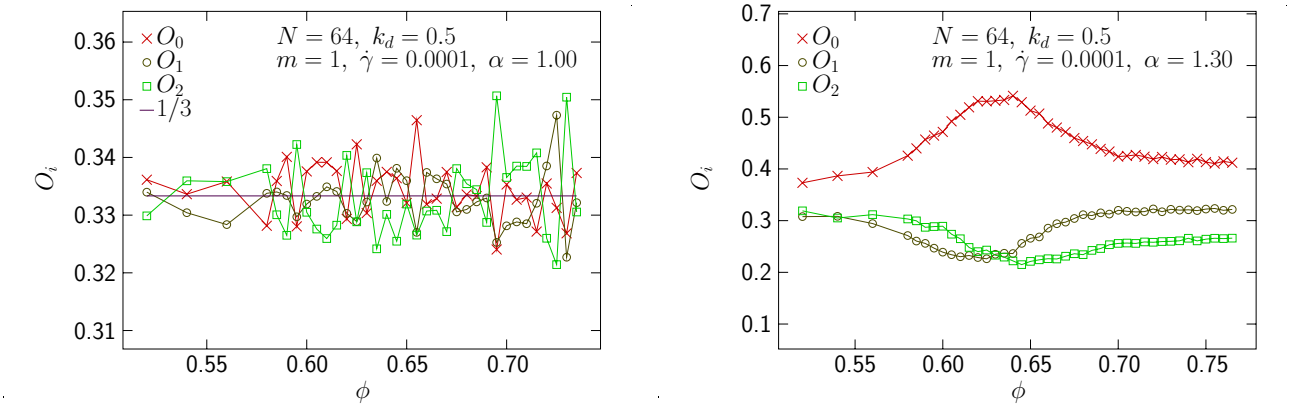

(a) $\alpha = 1$. Straight line corresponds to $O_i = 1/3$.

(b) $\alpha = 1.3$

Figure 4.6: Mean squared orientation of the axis of symmetry of the particles.

We expect that all orientations are equivalent for spheres, which is confirmed by figure 4.6a in which the projections do not show any particular behaviours.

For spheroids we see that the 0^{th} direction may be privileged since the mean squared projection of the axis of symmetry on this direction describes a well-defined peak around a given packing fraction while the projections on the other directions reach their minimum around this same packing fraction but both at different densities though (figure 4.6b).

Moreover, since the projection curves on the 1^{st} and 2^{nd} directions are well-defined – contrarily to the curves in figure 4.6a – we cannot say that the shear direction is the only relevant direction in our system.

Prolate spheroids

For all the aspect ratios greater than one we have tested, the mean projection of the axis of symmetry of the particles on the shear direction reaches a well-defined peak (figure 4.7a). We have that the height of this peak is approximately proportional to the aspect ratio α (figure 4.7b).

We can notice that the packing fractions at which these peaks appear are somewhat lower than the jamming densities corresponding to the aspect ratios. Indeed, we can read $\phi_J(\alpha > 1) \gtrsim 0.65$ from figure 4.5a. They are also undoubtedly higher than the rheological transition packing fractions (figure 4.1) and therefore these peaks do not correspond to any transition or phenomenon we have already described or expected.

Furthermore, what figure 4.7b also shows is that the position of the peak is much less dependent of the aspect ratio than the jamming density, and even seems not to vary at all – if we exclude $\alpha = 1.02$. However, it should be delicate to extrapolate such a result to hard-core particles since the overlaps are not negligible this close to the jamming transition, which suggests that we should rather be attentive to these variables as functions of the effective packing fraction (figure 4.8).

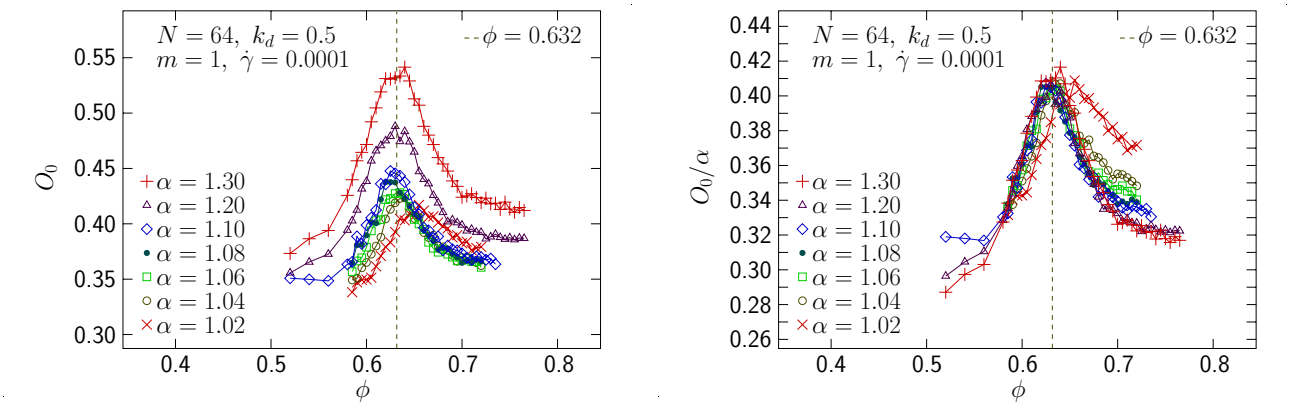

(a) Raw projections.

(b) Projections ratioed with the aspect ratio.

Figure 4.7: Mean of the squared projection of the axis of symmetry of the particles on shear direction as a function of the packing fraction.

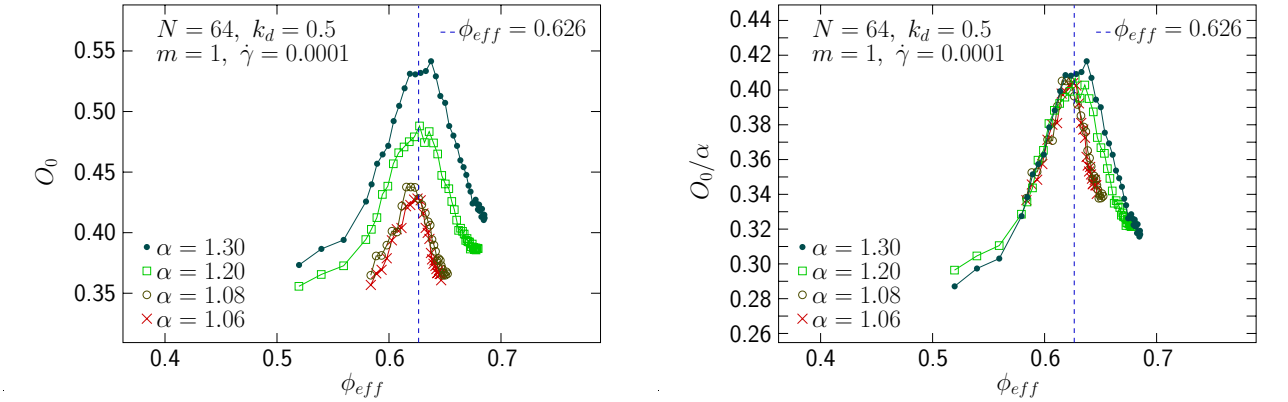

(a) Raw projections.

(b) Projections ratioed with the aspect ratio.

Figure 4.8: Mean projection of the axis of symmetry of the particles on the direction of the shear rate as a function of the effective packing fraction. We only show the aspect ratios for which the soft- to hard-core mapping gives a satisfactory visual precision.

A quick visual analysis of figure 4.8 shows that the effective packing fraction at which the projection of the axis of symmetry of prolate spheroids on the shear direction reaches its peak is also much less dependent of the aspect ratio than the jamming packing fraction is.

We can also be interested in knowing if the observations on the projection of the axis of symmetry on the shear direction (figure 4.7) hold for the two other projections (figure 4.9).
As expected from figure 4.6b, both projections reach a minimum which position, for a given aspect ratio, depends on the axis of projection. Visually, we can claim that the packing fraction at which O_0 reaches its maximum (see figure 4.7) is higher than the packing fraction at which O_1 reaches its minimum and lower than than the packing fraction at which O_2 reaches its minimum, in accordance with figure 4.6b.

There is no relation of proportionality between the depths of the minimums and the aspect ratio for these projections, contrarily to what we would have expected from figure 4.7b. Moreover, we observe that for $1 < \alpha < 1.3$, *i.e.* for not too elongated prolate spheroids, the minimum reached by O_1 is lower than the minimum reached by O_2.

We still observe that the positions of the minimums are much less dependent of the aspect ratio than the jamming density, as we observed for the projection on the shear direction.

Oblate spheroids

We do not have data at sufficiently high packing fraction to observe the peak of the projection of the axis of symmetry on the shear direction for $\alpha = 0.8$, however the data presented in figure 4.10 clearly shows that

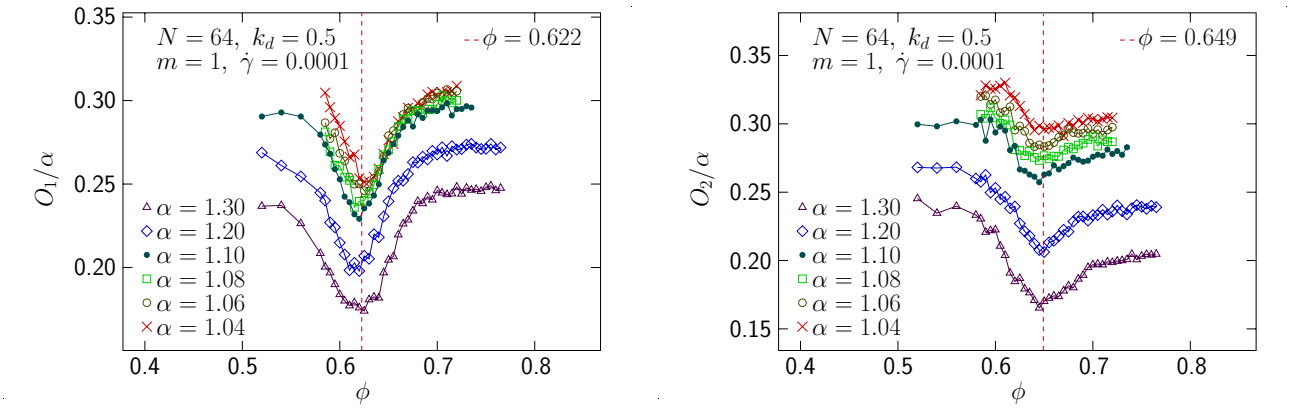

(a) Projection on the direction of the gradient of shear rate.

(b) Projection on the 2nd direction.

Figure 4.9: Mean of the squared projections of the axis of symmetry of the particles as functions of the packing fraction.

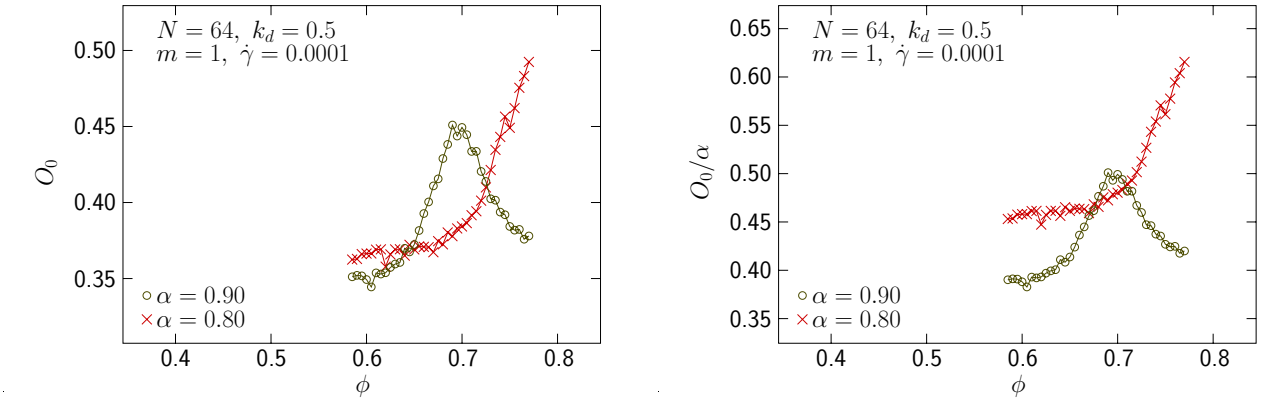

(a) Raw projections.

(b) Projections ratioed with the aspect ratio.

Figure 4.10: Mean projection of the axis of symmetry of the particles on the direction of the shear rate as a function of the packing fraction.

we should expect for oblate spheroids that the position of the peak strongly depends on the aspect ratio and moreover that its height is not proportional to the aspect ratio, contrarily to prolate spheroids.

This, in addition to the fact that the rheological transition also does not appear at the same packing fractions for oblate spheroids contrarily to prolate spheroids (part 4.1.1), shows that the behaviour of packings of prolate and oblate spheroids is very different, and suggest we may expect the mechanisms governing the jamming transition for these types of particles to be different.
Otherwise, we expect the observations we have made about the projections on all axis as functions of the packing fraction for a given aspect ration (see figure 4.6b) to remain valid for oblate spheroids (see figure 4.11).

4.1.3.2 Correlation

$\mathcal{C}_{ij}$ is a function which increases with increasing correlation between the orientations of the spheroids.

Prolate spheroids

As the mean squared projection of the axis of symmetry on the shear direction (see figure 4.7), the correlation function $\mathcal{C}_{ij}$ reaches a peak which height is proportional to the aspect ratio if we let aside $\alpha = 1.3$, *i.e.* if we only consider not too elongated prolate spheroids. Moreover, the position of this peak is much less dependent of the aspect ratio than the jamming density (see figure 4.12).

However, despite the striking resemblance of the aforementioned figures, we have that $\mathcal{C}_{ij}$ reaches its maximum at a packing fraction slightly higher than the packing fraction at which O_0 reaches its. Indeed, it rather seems to correspond to the packing fraction at which O_2 reaches its minimum (see figure 4.9b).

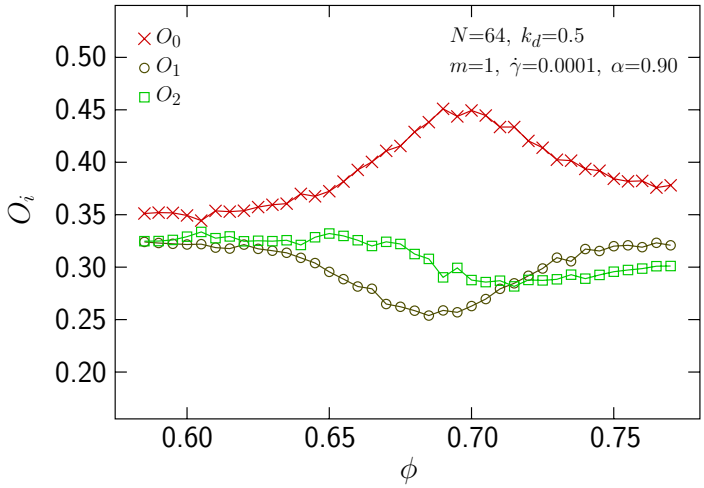

Figure 4.11: Mean squared orientation of the axis of symmetry of the particles for $\alpha = 0.8$.

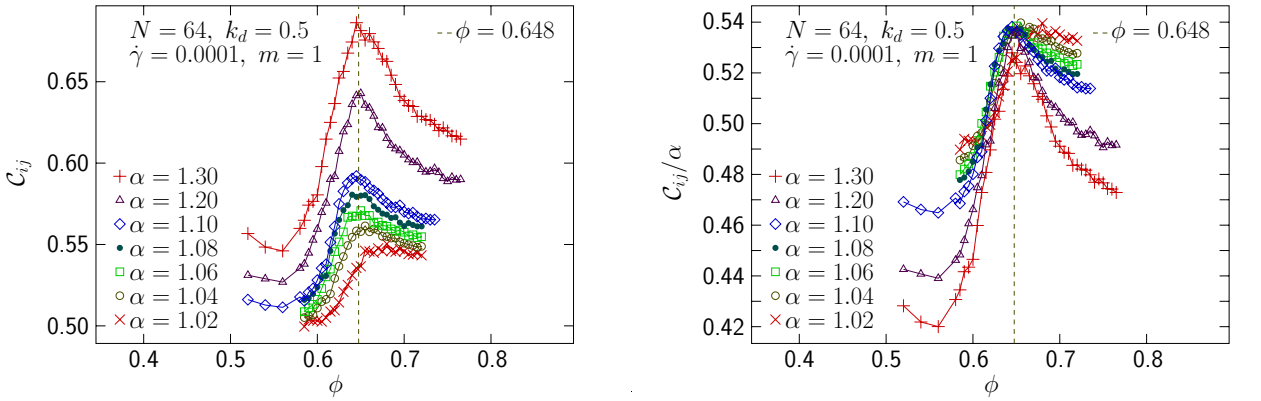

(a) Raw correlation function.

(b) Correlation function ratioed with the aspect ratio.

Figure 4.12: Orientation correlation as a function of the packing fraction.

Oblate spheroids

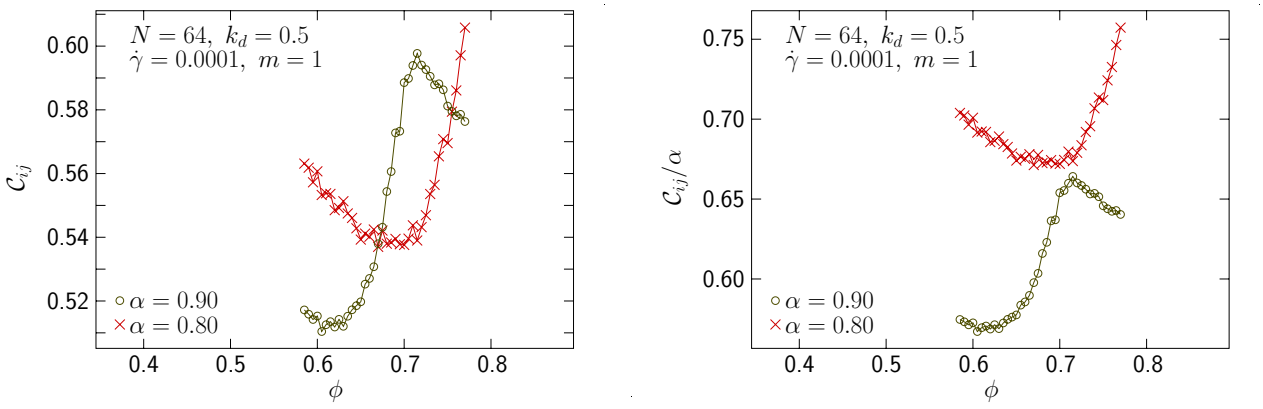

(a) Raw correlation function.

(b) Correlation function ratioed with the aspect ratio.

Figure 4.13: Orientation correlation as a function of the packing fraction.

As for the projection of the axis of symmetry on the shear direction for oblate particles (see figure 4.10), we observe here that the position of the peak of correlation function strongly depends on the aspect ratio for oblate particles (see figure 4.13), contrarily to prolate particles (see figure 4.12) – even though data at higher packing fractions and for more aspect ratios would be needed.

Moreover, and still in accordance to what we have observed for the aforementioned projection, there is a relation of proportionality between the value of the maximum of the correlation function and the aspect ratio for oblate particles.

4.2 Dominance of the elastic pressure

We claimed in part 3.4.4 that the elastic part of the pressure, p_{el}, was the main contribution to the total pressure, p.

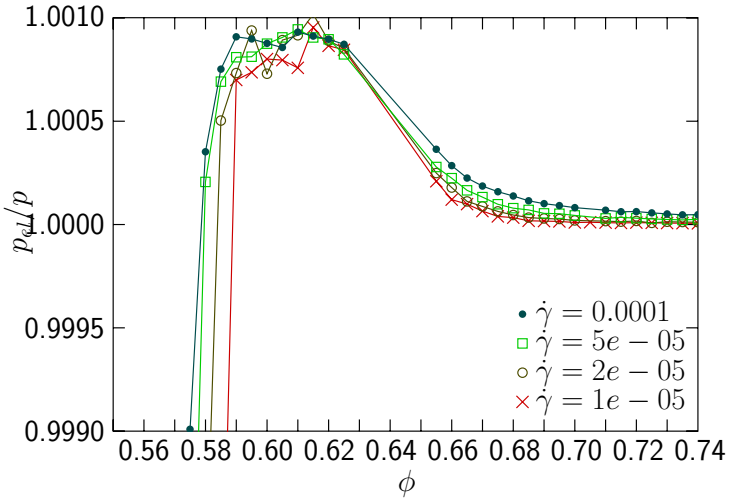

Figure 4.14: Ratio of the elastic pressure p_{el} and the total pressure p.

Figure 4.14 shows that, for $0.59 \leq \phi \leq 0.74$, approximating the total pressure by its elastic part gives an error lesser than 0.01%, thus justifying our claim. We will then use the notation p to designate p_{el}.

4.3 Relaxation time

Relaxation simulations, of which the method is described in part 3.2.2, were performed with 16384 particles.

4.3.1 Exponential decay of the pressure

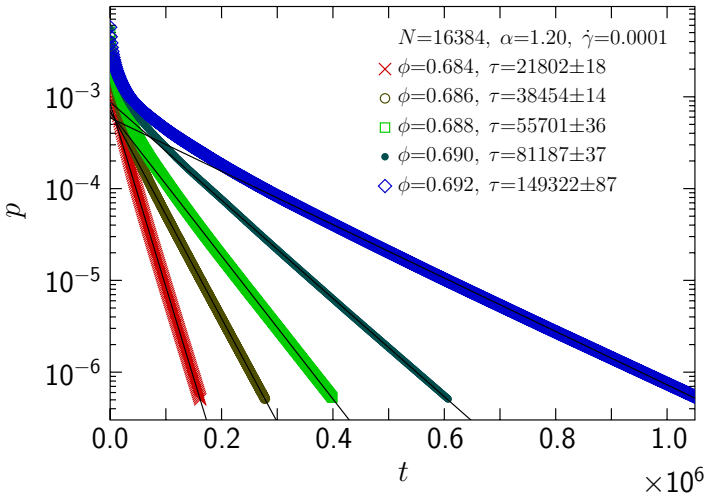

Figure 4.15: Semi-log plot of the pressure versus the time, where $t = 0$ corresponds to the time the shearing stopped.

We predicted that after a short transient time, the pressure would decay exponentially to zero with a characteristic time scale $\tau(\phi, \dot{\gamma})$ – named the relaxation time – where ϕ is the packing fraction and $\dot{\gamma}$ the shear strain

rate before the relaxation phase (see part 3.1.3, and especially equation 3.2). We confirm these predictions with figure 4.15.

4.3.2 Scaling of the relaxation time with the packing fraction

Figure 4.15 indicates that the relaxation time would increase with increasing packing fractions for systems below jamming, which is what suggested equations 3.4 and 3.5. By plotting the relaxation time versus the difference to the jamming packing fraction in a log-log plot, we should then be graphically able to determine both the critical exponent β and the jamming transition ϕ_J (see figure 4.16).

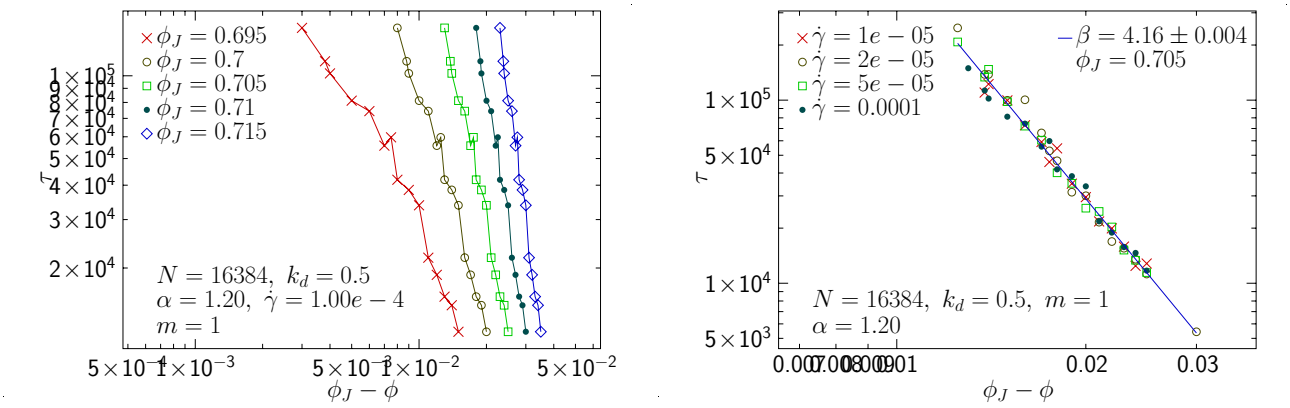

(a) Graphical determination of ϕ_J.

(b) Linear regression to determine β.

Figure 4.16: Graphical determination of the critical exponent β and the jamming packing fraction ϕ_J.

From figure 4.16a we can visually determine that the jamming packing fraction is $\phi_J \sim 0.705$. We then plot the relaxation time τ versus $\phi_J - \phi$ to determine from the slope the critical exponent $\beta \sim 4.16$. These results are consistent with those obtained from the shearing method with 64 particles (see figure 4.5).

Simulations for densities closer to the jamming packing fraction and for other aspect rations have not been performed yet, the relaxation process being too long to have precise enough data within a month. Still, figure 4.16 shows the efficiency of our method.

4.4 Contact number

4.5 Critical behaviour

**** MAYBE TELL HOW THE OBSERVATIONS FOR THE RHEOLOGICAL TRANSITION GIVE HINTS ON WHAT'S HAPPENING AT JAMMING (ESPECIALLY WHY JAMMING MIGHT BE GOVERNED BY DIFFERENT MECHANISMS FOR OBLATE AND PROLATE SPHEROIDS) ****

4.6 Orientation

**** PRECISE THAT IT WOULD BE INTERESTING TO CHECK FOR PERIODICITY IN THE ORIENTATION ****

4.7 Rotation velocity

References

[1] Richard Patrick, Mario Nicodemi, Renaud Delannay, Philippe Ribiere, and Daniel Bideau. Slow relaxation and compaction of granular systems. *Nature materials*, 4(2):121, 2005.

[2] National Science Foundation. Granular materials – YouTube. https://www.youtube.com/watch?v=R7g6wdmYB78. [Online; accessed 13-July-2017].

[3] Andrea J Liu and Sidney R Nagel. Nonlinear dynamics: Jamming is not just cool any more. *Nature*, 396 (6706):21–22, 1998.

[4] Peter Olsson and Stephen Teitel. Critical scaling of shear viscosity at the jamming transition. *Physical review letters*, 99(17):178001, 2007.

[5] Daniel Vågberg, Peter Olsson, and Stephen Teitel. Glassiness, rigidity, and jamming of frictionless soft core disks. *Physical Review E*, 83(3):031307, 2011.

[6] Ken Shoemake. Animating rotation with quaternion curves. In *ACM SIGGRAPH computer graphics*, volume 19, pages 245–254. ACM, 1985.

[7] Antonio Munjiza, Scott M Johnson, John R Williams, and Benjamin K Cook. On the application of quaternion-based approaches in discrete element methods. *Engineering Computations*, 26(6):610–620, 2009.

[8] David Eberly. Rotation representations and performance issues. *Magic Software, Inc., Chapel Hill, NC*, 2002.

[9] Wikipedia. Quaternions and spatial rotation — Wikipedia, the free encyclopedia. https://en.wikipedia.org/wiki/Quaternions_and_spatial_rotation#Comparison_with_other_representations_of_rotations, 2017. [Online; accessed 24-May-2017].

[10] Nick Bobick. Rotating objects using quaternions. *Game Developer*, 2(26):21–31, 1998.

[11] WF Phillips, CE Hailey, and GA Gebert. Review of attitude representations used for aircraft kinematics. *Journal of aircraft*, 38(4):718–737, 2001.

[12] DC Rapaport. Molecular dynamics simulation using quaternions. *Journal of Computational Physics*, 60 (2):306–314, 1985.

[13] Indrek Mandre. Rigid body dynamics using euler's equations, runge-kutta and quaternions. www.mare.ee/indrek/varphi/vardyn.pdf.

[14] Martin Kleppmann. Simulation of colliding constrained rigid bodies. Technical report, University of Cambridge, Computer Laboratory, 2007.

[15] Daniel Vågberg, Peter Olsson, and S Teitel. Shear banding, discontinuous shear thickening, and rheological phase transitions in athermally sheared frictionless disks. *Physical Review E*, 95(5):052903, 2017.

[16] John W Perram and MS Wertheim. Statistical mechanics of hard ellipsoids. i. overlap algorithm and the contact function. *Journal of Computational Physics*, 58(3):409–416, 1985.

[17] Aleksandar Donev, Robert Connelly, Frank H Stillinger, and Salvatore Torquato. Underconstrained jammed packings of nonspherical hard particles: Ellipses and ellipsoids. *Physical Review E*, 75(5):051304, 2007.

[18] Aleksandar Donev. *Jammed Packings of Hard Particles*. PhD thesis, Princeton University, September 2006. http://cims.nyu.edu/~donev/Thesis.pdf.

[19] Eric W. Weisstein. Horner's Rule. From MathWorld–A Wolfram Web Resource. http://mathworld.wolfram.com/HornersRule.html. [Online; accessed 12-June-2017].

[20] Wenping Wang, Jiaye Wang, and Myung-Soo Kim. An algebraic condition for the separation of two ellipsoids. *Computer aided geometric design*, 18(6):531–539, 2001.

[21] Yi-King Choi, Jung-Woo Chang, Wenping Wang, Myung-Soo Kim, and Gershon Elber. Continuous collision detection for ellipsoids. *IEEE Transactions on visualization and Computer Graphics*, 15(2):311–325, 2009.

[22] Wikipedia. Sturm's theorem — Wikipedia, the free encyclopedia. https://en.wikipedia.org/wiki/Sturm's_theorem, 2017. [Online; accessed 13-May-2017].

[23] Wikipedia. Lagrange polynomial — Wikipedia, the free encyclopedia. https://en.wikipedia.org/wiki/Lagrange_polynomial, 2017. [Online; accessed 13-May-2017].

[24] Encyclopedia of Mathematics. Viète theorem. https://www.encyclopediaofmath.org/index.php/Vi%E8te_theorem, 2012. [Online; accessed 13-May-2017].

[25] Anhua Lin and Shih-Ping Han. On the distance between two ellipsoids. *SIAM Journal on Optimization*, 13(1):298–308, 2002.

[26] Wikipedia. Spectral radius — Wikipedia, the free encyclopedia. https://en.wikipedia.org/wiki/Spectral_radius, 2017. [Online; accessed 13-May-2017].

[27] Pierre-Gilles de Gennes. Granular matter: a tentative view. *Reviews of modern physics*, 71(2):S374, 1999.

[28] Leo P Kadanoff. Built upon sand: Theoretical ideas inspired by granular flows. *Reviews of Modern Physics*, 71(1):435, 1999.

[29] Corey S O'hern, Leonardo E Silbert, Andrea J Liu, and Sidney R Nagel. Jamming at zero temperature and zero applied stress: The epitome of disorder. *Physical Review E*, 68(1):011306, 2003.

[30] Junyao Tang and R.P. Behringer. How granular materials jam in a hopper (processed) – YouTube. https://www.youtube.com/watch?v=lWSJwZhqoQw. [Online; accessed 29-June-2017].

[31] Junyao Tang. Ellptical particles flowing in a hopper – YouTube. https://www.youtube.com/watch?v=p3lwWfF2dTI. [Online; accessed 29-June-2017].

[32] Kiwing To, Pik-Yin Lai, and HK Pak. Jamming of granular flow in a two-dimensional hopper. *Physical review letters*, 86(1):71, 2001.

[33] B Eisenblätter, L Santen, A Schadschneider, and M Schreckenberg. Jamming transition in a cellular automaton model for traffic flow. *Physical Review E*, 57(2):1309, 1998.

[34] Cornell CCSL. Universal robotic gripper based on the jamming of granular material playing at original volume. – YouTube. https://www.youtube.com/watch?v=bFW7VQpY-Ik. [Online; accessed 29-June-2017].

[35] Eric Brown, Nicholas Rodenberg, John Amend, Annan Mozeika, Erik Steltz, Mitchell R Zakin, Hod Lipson, and Heinrich M Jaeger. Universal robotic gripper based on the jamming of granular material. *Proceedings of the National Academy of Sciences*, 107(44):18809–18814, 2010.

[36] Gianfranco D'Anna and Gerard Grémaud. The jamming route to the glass state in weakly perturbed granular media. *Nature*, 413(6854):407, 2001.

[37] Salvatore Torquato and Frank H Stillinger. Multiplicity of generation, selection, and classification procedures for jammed hard-particle packings. *The Journal of Physical Chemistry B*, 105(47):11849–11853, 2001.

[38] Aleksandar Donev, Frank H Stillinger, PM Chaikin, and Salvatore Torquato. Unusually dense crystal packings of ellipsoids. *Physical review letters*, 92(25):255506, 2004.

[39] Salvatore Torquato, Thomas M Truskett, and Pablo G Debenedetti. Is random close packing of spheres well defined? *Physical review letters*, 84(10):2064, 2000.

[40] Peter Olsson and S Teitel. Critical scaling of shearing rheology at the jamming transition of soft-core frictionless disks. *Physical Review E*, 83(3):030302, 2011.

[41] Peter Olsson and S Teitel. Herschel-bulkley shearing rheology near the athermal jamming transition. *Physical review letters*, 109(10):108001, 2012.

[42] Peter Olsson. Relaxation times and rheology in dense athermal suspensions. *Physical Review E*, 91(6): 062209, 2015.

[43] Michael Plischke and Birger Bergersen. *Equilibrium statistical physics*. World Scientific Publishing Co Inc, 1994.

[44] Daniel Vågberg, Daniel Valdez-Balderas, MA Moore, Peter Olsson, and Stephen Teitel. Finite-size scaling at the jamming transition: Corrections to scaling and the correlation-length critical exponent. *Physical Review E*, 83(3):030303, 2011.

[45] Michio Otsuki and Hisao Hayakawa. Critical scaling near jamming transition for frictional granular particles. *Physical Review E*, 83(5):051301, 2011.

[46] Corey S O'Hern, Stephen A Langer, Andrea J Liu, and Sidney R Nagel. Random packings of frictionless particles. *Physical Review Letters*, 88(7):075507, 2002.

[47] Shlomo Alexander. Amorphous solids: their structure, lattice dynamics and elasticity. *Physics reports*, 296 (2-4):65–236, 1998.

[48] PM Chaikin, Aleksandar Donev, Weining Man, Frank H Stillinger, and Salvatore Torquato. Some observations on the random packing of hard ellipsoids. *Industrial & engineering chemistry research*, 45(21): 6960–6965, 2006.

[49] Aleksandar Donev, Ibrahim Cisse, David Sachs, Evan A Variano, Frank H Stillinger, Robert Connelly, Salvatore Torquato, and Paul M Chaikin. Improving the density of jammed disordered packings using ellipsoids. *Science*, 303(5660):990–993, 2004.

[50] M Van Hecke. Jamming of soft particles: geometry, mechanics, scaling and isostaticity. *Journal of Physics: Condensed Matter*, 22(3):033101, 2009.

[51] Daniel Vågberg, Peter Olsson, and S Teitel. Universality of jamming criticality in overdamped shear-driven frictionless disks. *Physical review letters*, 113(14):148002, 2014.

[52] Pinaki Chaudhuri, Ludovic Berthier, and Srikanth Sastry. Jamming transitions in amorphous packings of frictionless spheres occur over a continuous range of volume fractions. *Physical review letters*, 104(16): 165701, 2010.

[53] AW Lees and SF Edwards. The computer study of transport processes under extreme conditions. *Journal of Physics C: Solid State Physics*, 5(15):1921, 1972.

[54] Gary P Morriss and Denis J Evans. *Statistical Mechanics of Nonequilbrium Liquids*. ANU Press, 2013.

[55] Loic Vanel, Daniel Howell, D Clark, RP Behringer, and Eric Clément. Memories in sand: Experimental tests of construction history on stress distributions under sandpiles. *Physical Review E*, 60(5):R5040, 1999.

[56] Masahiro Toiya, Justin Stambaugh, and Wolfgang Losert. Transient and oscillatory granular shear flow. *Physical review letters*, 93(8):088001, 2004.

[57] Donald W Marquardt. An algorithm for least-squares estimation of nonlinear parameters. *Journal of the society for Industrial and Applied Mathematics*, 11(2):431–441, 1963.

[58] William H Press. *Numerical recipes 3rd edition: The art of scientific computing*. Cambridge university press, 2007.

[59] William H Press, Saul A Teukolsky, William T Vetterling, and Brian P Flannery. *Numerical recipes in C*, volume 2. Cambridge university press Cambridge, 1996.

[60] Harry H Ku. Notes on the use of propagation of error formulas. *Journal of Research of the National Bureau of Standards*, 70(4), 1966.

[61] DJ Durian. Foam mechanics at the bubble scale. *Physical review letters*, 75(26):4780, 1995.

[62] Daniel Vågberg, Peter Olsson, and S Teitel. Universality of jamming criticality in overdamped shear-driven frictionless disks – Supplemental material. *Physical review letters*, 113(14):148002, 2014.

[63] Carl F Schreck, Ning Xu, and Corey S O'Hern. A comparison of jamming behavior in systems composed of dimer-and ellipse-shaped particles. *Soft Matter*, 6(13):2960–2969, 2010.

[64] Daniel Vågberg, Peter Olsson, and S Teitel. Dissipation and rheology of sheared soft-core frictionless disks below jamming. *Physical Review Letters*, 112(20):208303, 2014.

[65] Ken Shoemake. Quaternions. www.cs.ucr.edu/~vbz/resources/quatut.pdf. Department of Computer and Information Science, University of Pennsylvania.

[66] LD Landau and EM Lifshitz. *Mechanics, Course of theoretical physics*, volume 1. 1976.

[67] Wikipedia. Ellipsoid — Wikipedia, the free encyclopedia. https://en.wikipedia.org/wiki/Ellipsoid, 2017. [Online; accessed 12-May-2017].

[68] Kenneth G Wilson. Renormalization group and critical phenomena. i. renormalization group and the kadanoff scaling picture. *Physical review B*, 4(9):3174, 1971.

[69] Kenneth G Wilson and John Kogut. The renormalization group and the ϵ expansion. *Physics Reports*, 12 (2):75–199, 1974.

[70] Kenneth G Wilson. Renormalization group methods. *Advances in Mathematics*, 16(2):170–186, 1975.

[71] Nigel Goldenfeld. Lectures on phase transitions and the renormalization group. 1992.

[72] Wikipedia. Cusp (singularity) — Wikipedia, the free encyclopedia. https://en.wikipedia.org/wiki/Cusp_(singularity), 2016. [Online; accessed 10-July-2017].

Appendices

A | Quaternions

A.1 Definition

Quaternions were introduced by Hamilton as extension of complex numbers [65]:

$$q = q_0 + \sum_{i=1}^{3} q_i e_i, \text{ with } \begin{cases} e_m^2 = -1 \\ e_m e_n = \varepsilon_{mnk} e_k \quad , m \neq n \end{cases} \text{ and } q_0, q_1, q_2, q_3 \in \mathbb{R} \tag{A.1}$$

For convenience, we will write $q \equiv [\vec{q}, q_0]$ with $\vec{q} = (q_1, q_2, q_3) \in \mathbb{R}^3$, and $\mathbb{H}$ the quaternions' space.

Moreover, we will identify vectors $\vec{v}$ from $\mathbb{R}^3$ with $[\vec{v}, 0]$ and scalars w from $\mathbb{R}$ with $[0, w]$. We will assume this identification throughout the document without notification.

A.2 Properties

Addition $\boxed{q + q' = [\vec{q} + \vec{q'}, q_0 + q_0']}$

Multiplication $\boxed{qq' = [\vec{q} \times \vec{q'} + q_0\vec{q'} + q_0'\vec{q}, q_0 q_0' - \vec{q} \cdot \vec{q'}]}$

$$qq' = (q_0 + \sum_{i=1}^{3} q_i e_i)(q_0' + \sum_{i=1}^{3} q_i' e_i) = q_0 q_0' + \underbrace{q_0 \sum_{i=1}^{3} q_i' e_i}_{q_0\vec{q'}} + \underbrace{q_0' \sum_{i=1}^{3} q_i e_i}_{q_0'\vec{q}} + \underbrace{\sum_{i=1}^{3} q_i q_i' \underbrace{e_i e_i}_{-1}}_{-\vec{q}\cdot\vec{q'}} + \underbrace{\sum_{\substack{i,j \\ i \neq j}} q_i q_j' \underbrace{e_i e_j}_{\varepsilon_{ijk} e_k}}_{\vec{q}\times\vec{q'}}$$

$$= [\vec{q} \times \vec{q'} + q_0\vec{q'} + q_0'\vec{q}, q_0 q_0' - \vec{q} \cdot \vec{q'}]$$

Multiplication by a scalar $\boxed{\lambda q = [\lambda\vec{q}, \lambda q_0]}$

Bilinearity $\boxed{q''(\lambda q + \lambda q') = \lambda q'' q + \lambda q'' q'}$

Associative property $\boxed{(qq')q'' = q(q'q'')}$

Conjugate $\boxed{q^* = [-\vec{q}, q_0]}$

$$q^* = (q_0 + \sum_{i=1}^{3} q_i e_i)^* = q_0 - \sum_{i=1}^{3} q_i e_i$$
$$= [-\vec{q}, q_0]$$

Conjugation property $\boxed{(qq')^* = q'^* q^*}$

$$\begin{aligned} (qq')^* &= ([\vec{q}, q_0][\vec{q'}, q_0'])^* \\ &= ([\vec{q} \times \vec{q'} + q_0\vec{q'} + q_0'\vec{q}, q_0 q_0' - \vec{q} \cdot \vec{q'}])^* \\ &= [\underbrace{-\vec{q} \times \vec{q'}}_{(-1)\vec{q'} \times (-1)\vec{q}} + q_0(-\vec{q'}) + q_0'(-\vec{q}), q_0 q_0' - (-1)\vec{q} \cdot (-1)\vec{q'}] \\ &= [-\vec{q'}, q_0'][-\vec{q}, q_0] \\ &= q'^* q^* \end{aligned}$$

Norm $\boxed{N^2(q) = \sum_{i=0}^{3} q_i^2}$

$$\begin{aligned} N^2(q) = qq* &= [\vec{q}, q_0][-\vec{q}, q_0] = [\cancel{-q_0\vec{q}} + \cancel{q_0\vec{q}}, q_0q_0 + \vec{q}\cdot\vec{q}] \\ &= [0, \sum_{i=0}^{3} q_i^2] = \sum_{i=0}^{3} q_i^2 \end{aligned}$$

Inverse $\boxed{q^{-1} = q^*/N^2(q)}$

$$q\frac{q*}{N^2(q)} = \frac{q*}{N^2(q)}q = 1 \Leftrightarrow q^{-1} = \frac{q*}{N^2(q)}$$

Action of an unit quaternion From the property of the inverse of a quaternion, it is trivial that the action of any quaternion q

$$\begin{aligned} \mathcal{A}_q &: \mathbb{H} \to \mathbb{H} \\ &p \longmapsto qpq^{-1} \end{aligned}$$

will be the same as the action of the associated unit quaternion $q/N(q)$. Therefore, we will only consider unit quaternion from now on and use q^* instead of q^{-1}.

We then have that for any $p = [\vec{v}, w]$, $\boxed{qpq^* = [\vec{v'}, w]}$ with $N(\vec{v}) = N(\vec{v'})$

Indeed, with $S(q) \equiv \frac{q+q^*}{2}$ the scalar part of any quaternion q we have

$$\begin{aligned} &2S(qpq^*) \\ &= qpq^* + (qpq^*)^* = qpq^* + qp*q^* \\ &= q\underbrace{(p+p^*)}_{2w}q^* = 2wq\cancel{qq^*} = 2w \\ &= 2S(p) \end{aligned}$$

The conjugation property ensures that the multiplication conserves the norm, then $N(qpq^*) = N(p)$, hence the property.

Therefore the action of any quaternion on any vector of $\mathbb{R}^3$ is a vector of $\mathbb{R}^3$.

A.3 Actions and rotations

Consider $\vec{v_0}, \vec{v_1} \in \mathbb{R}^3$ with $\vec{v_0} \times \vec{v_1} \neq 0$ and $N(\vec{v_0}) = N(\vec{v_1}) = 1$. We define $q \equiv \vec{v_1}\vec{v_0}^* = [\vec{v_0} \times \vec{v_1}, \vec{v_0} \cdot \vec{v_1}]$, $\theta \equiv (\vec{v_0}; \vec{v_1})$ and $\vec{v} = \frac{\vec{v_0} \times \vec{v_1}}{||\vec{v_0} \times \vec{v_1}||}$ so that $q = [\vec{v}\sin\theta, \cos\theta]$. We want to know what is the action of q, $\mathcal{A}_q$, on any vector of $\mathbb{R}^3$.

We have $(\vec{v_0}, \vec{v_1}, \vec{v})$ a basis of $\mathbb{R}^3$. Thanks to the bilinearity of the product of quaternions, we can infer $\mathcal{A}_q(\vec{u}) \forall \vec{u} \in \mathbb{R}^3$ from the action of q on this basis. The following demonstration was originally made in [65].

Action on $\vec{v}$

$$\begin{aligned} \mathcal{A}_q(\vec{v}) &= q\vec{v}q^* \\ &= [\vec{v}\sin\theta, \cos\theta][\vec{v}, 0][-\vec{v}\sin\theta, \cos\theta] \\ &= [\vec{v}\cos\theta, -\underbrace{|\vec{v}|^2}_{=1}\sin\theta][-\vec{v}\sin\theta, \cos\theta] \\ &= [\underbrace{\vec{v}\sin^2\theta + \vec{v}\cos^2\theta}_{=\vec{v}}, \cancel{-\sin\theta\cos\theta} + \underbrace{|\vec{v}|^2}_{=1}\cancel{\sin\theta\cos\theta}] \\ &= [\vec{v}, 0] \\ &= \vec{v} \end{aligned}$$

Action on $\vec{v_0}$ We define $\vec{v_2} \equiv \mathcal{A}_q(\vec{v_0}) = q\vec{v_0}q^*$ and notice that

$$\begin{aligned}
\vec{v_2}\vec{v_1}^* &= (q\vec{v_0}q^*)\vec{v_1}^* \\
&= (q\vec{v_0}(\vec{v_1}\vec{v_0}^*)^*)\vec{v_1}^* \\
&= q\vec{v_0}(\vec{v_0}\vec{v_1}^*)\vec{v_1}^* \\
&= q\underbrace{(\vec{v_0}\vec{v_0})}_{=-1}\underbrace{(\vec{v_1}^*\vec{v_1}^*)}_{=-1} \\
&= q = \vec{v_1}\vec{v_0}^*
\end{aligned}$$

so $\begin{cases} \vec{v_1} \times \vec{v_2} &= \vec{v_0} \times \vec{v_1} \\ \vec{v_1} \cdot \vec{v_2} &= \vec{v_0} \cdot \vec{v_1} \end{cases}$. Therefore, $\vec{v_0}, \vec{v_1}$ and $\vec{v_2}$ belong to the same plane and furthermore, $(\vec{v_1}; \vec{v_2}) = (\vec{v_0}; \vec{v_1}) = \theta$. Then, $\vec{v_2}$ is the rotation of $\vec{v_0}$ of an angle 2θ around $\vec{v}$.

Action on $\vec{v_1}$ We define $\vec{v_3} \equiv \mathcal{A}_q(\vec{v_1}) = q\vec{v_1}q^*$ and notice that

$$\begin{aligned}
\vec{v_3}\vec{v_2}^* &= (q\vec{v_1}q^*)(q\vec{v_0}q^*)^* \\
&= (q(q\vec{v_0})q^*)(q\vec{v_0}q^*)^* \\
&= q(q\vec{v_0}q^*)(q\vec{v_0}q^*)^* \\
&= q = \vec{v_1}\vec{v_0}^*
\end{aligned}$$

so $\begin{cases} \vec{v_2} \times \vec{v_3} &= \vec{v_0} \times \vec{v_1} \\ \vec{v_3} \cdot \vec{v_3} &= \vec{v_0} \cdot \vec{v_1} \end{cases}$. Therefore, $\vec{v_0}, \vec{v_1}, \vec{v_2}$ and $\vec{v_3}$ belong to the same plane and furthermore, $(\vec{v_2}; \vec{v_3}) = (\vec{v_0}; \vec{v_1}) = \theta$. Then, $\vec{v_3}$ is the rotation of $\vec{v_1}$ of an angle 2θ around $\vec{v}$.

Finally, we have that $\mathcal{A}_q$ corresponds to the rotation of angle 2θ around $\vec{v}$. The corollary to that property is that

every 3D rotation can be expressed as the action of some unit quaternion.

B | Euler's equation

In this appendix we mean to remind the definitions of the rotation vector, the angular momentum, the tensor of moments of inertia and the establishment of the Euler's equation describing the rotation of a rigid body. All demonstrations are based on [66].

B.1 Rotation vector

Consider a vector $\vec{u}$ on which we apply an infinitesimal rotation of angle $d\theta$ around the axis $\vec{e_z}$ (figure B.1).

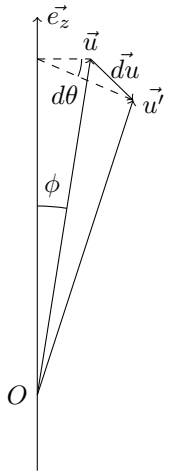

Figure B.1

We then have $\vec{u'} = \vec{u} + \vec{du}$ with $|\vec{du}| = |\vec{u}\,\theta \sin\phi|$ and the direction of $\vec{du}$ being perpendicular to the plane formed by $\vec{e_z}$ and $\vec{u}$, which gives us

$$\vec{du} = d\theta \vec{e_z} \times \vec{u} = d\vec{\theta} \times \vec{u} \tag{B.1}$$

therefore, if the rotation angle is a function of time $\theta(t)$ we have, by consideration that $d\theta(t) = \dot{\theta}(t)dt$, that

$$\frac{\vec{du}}{dt} = \dot{\theta}\vec{e_z} \times \vec{u} \tag{B.2}$$

We can sum infinitesimal rotations therefore, in the general case – with $\frac{d}{dt}|\vec{u}| = 0$ – we can always define a vector $\vec{\omega}$ such that $\dot{\vec{u}} = \vec{\omega} \times \vec{u}$.

A rigid body $\mathcal{O}$ is in rotation if we can define such a vector $\vec{\omega}$ which will be the same for all the points of the body. Therefore, whatever origin we may choose, if $\vec{p}$ and $\vec{q}$ point to two points A and B of the body – which induces that $\frac{d}{dt}|\vec{p} - \vec{q}| = 0$ – we will have that

$$\frac{d}{dt}(\vec{p} - \vec{q}) = \vec{\omega} \times (\vec{p} - \vec{q}) \tag{B.3}$$

which is equivalent to

$$\forall A, B \in \mathcal{O}, \vec{v_B} = \vec{v_A} + \vec{\omega} \times \vec{AB} \tag{B.4}$$

where $\vec{v_A}$ and $\vec{v_B}$ are the velocities of the points A and B.

B.2 Angular momentum

The mechanical properties of a closed system do not vary when it is rotated as a whole in any manner in space. Therefore, the Lagrangian of a rigid body $L(\vec{r_i}, \vec{v_i}, t)$ has to be unchanged by any infinitesimal rotation $\vec{d\theta}$.

One can first notice that the equation B.1 can be applied on any vector of our space, therefore both the positions and velocities are affected by the rotation.

We then have that

$$\begin{aligned}
\forall \vec{d\theta},\ \delta L = L(\vec{r_i} + \vec{dr_i}, \vec{v_i} + \vec{dv_i}, t) - L(\vec{r_i}, \vec{v_i}, t) = 0 \\
\Leftrightarrow \sum_i \left(\underbrace{\frac{\partial}{\partial \vec{r_i}} L}_{\dot{\vec{p_i}}} \cdot \underbrace{\vec{dr_i}}_{\vec{d\theta} \times \vec{r_i}} + \underbrace{\frac{\partial}{\partial \vec{v_i}} L}_{\vec{p_i}} \cdot \underbrace{\vec{dv_i}}_{\vec{d\theta} \times \vec{v_i}} \right) = 0 \\
\Leftrightarrow \sum_i \left(\dot{\vec{p_i}} \cdot \vec{d\theta} \times \vec{r_i} + \vec{p_i} \cdot \vec{d\theta} \times \vec{v_i} \right) = 0 \\
\Leftrightarrow \vec{d\theta} \cdot \sum_i \left(\vec{r_i} \times \dot{\vec{p_i}} + \vec{v_i} \times \vec{p_i} \right) = 0 \\
\Leftrightarrow \vec{d\theta} \cdot \frac{d}{dt} \underbrace{\sum_i \vec{r_i} \times \vec{p_i}}_{\vec{A}} = 0
\end{aligned}$$

therefore the vector

$$\boxed{\vec{A} \equiv \sum_i \vec{r_i} \times \vec{p_i}} \tag{B.5}$$

which we will call *angular momentum*, is conserved for a closed system.

We can give a relation between the angular momentum of the same rigid body in the frame of reference F and the inertial frame of the body F_O – where the centre of mass O is at rest –, the latter moving with velocity $\vec{V}$ relative to the former.

We have to first notice that the velocities of the same point a in these frames are linked by

$$\vec{v_a} = \vec{v_{a,O}} + \vec{V}$$

from we can infer that

$$\begin{aligned}
\vec{A} = \sum_i \vec{r_i} \times \vec{p_i} &= \sum_i (\vec{r_O} + (\vec{r_i} - \vec{r_O})) \times \vec{p_i} \\
&= \vec{r_O} \times \underbrace{\sum_i \vec{p_i}}_{\vec{P}} + \sum_i (\vec{r_i} - \vec{r_O}) \times \vec{p_i} \\
&= \vec{r_O} \times \vec{P} + \sum_i m_i (\vec{r_i} - \vec{r_O}) \times \left(\vec{v_{i,O}} + \vec{V} \right) \\
&= \vec{r_O} \times \vec{P} + \underbrace{\sum_i (\vec{r_i} - \vec{r_O}) \times \vec{v_{i,O}}}_{\vec{A_O}} + \cancelto{0}{\sum_i m_i (\vec{r_i} - \vec{r_O})} \times \vec{V}
\end{aligned}$$

where $\vec{P}$ is the total momentum of the rigid body.

Therefore we have the following relation

$$\boxed{\vec{A} = \vec{r_O} \times \vec{P} + \vec{A_O}} \tag{B.6}$$

B.3 Tensor of moments of inertia

The angular momentum in equation B.5 is more easily expressed in the inertial frame of the body where the centre of mass of the body is at rest. We can then infer the angular momentum in the frame of reference with the mean of equation B.6.

Consider $\vec{\omega}$ the rotation vector of the rigid body, in the inertial frame of the body we then have that the momentum of any point i is

$$\forall i, \vec{p_i} = m\vec{v_i} = m\vec{\omega} \times \vec{r_i}$$

therefore, the angular momentum $\vec{A_O}$ is

$$\begin{aligned}
\vec{A_O} &= \sum_i \vec{r_i} \times \vec{p_i} = \sum_i m_i \vec{r_i} \times (\vec{\omega} \times \vec{r_i}) \\
&= \sum_i m_i \left(\vec{r_i}^2 \vec{\omega} - \vec{r_i} \left(\vec{r_i} \cdot \vec{\omega} \right) \right) \\
&= \sum_k \vec{e_k} \left(\sum_i m_i \left(\vec{r_i}^2 \omega_k - r_{i,k} \sum_l r_{i,l} \omega_l \right) \right) \\
&= \sum_k \vec{e_k} \left(\sum_l \left(\sum_i m_i \left(\vec{r_i}^2 \delta_{k,l} - r_{i,k} r_{i,l} \right) \right) \omega_l \right)
\end{aligned}$$

We can denote the following symmetric matrix

$$\boxed{\forall k, l \in [\![1, 3]\!], \bar{\bar{I}}_{k,l} \equiv \sum_i m_i \left(\vec{r_i}^2 \delta_{k,l} - r_{i,k} r_{i,l} \right)} \tag{B.7}$$

the *tensor of moments of inertia*, which then enables us to write

$$\boxed{\vec{A} = \bar{\bar{I}} \vec{\omega}} \tag{B.8}$$

which remains true if the body is regarded as continuous.

According to the spectral theorem, there exists an orthonormal base of space $(\vec{u_1}, \vec{u_2}, \vec{u_3})$ in which $\bar{\bar{I}}$ is diagonal with

$$\forall k, l \in [\![1, 3]\!], \bar{\bar{I}}_{k,l} = \delta_{k,l} I_k \tag{B.9}$$

these axes are then called the *principal axes of inertia* of the body.

B.4 Conservation of the angular momentum

From equation B.5 we can write that

$$\frac{d}{dt}\vec{A} = \frac{d}{dt} \sum_i \vec{r_i} \times \vec{p_i} = \sum_i \left(\underbrace{\dot{\vec{r_i}}}_{\vec{v_i}} \times \vec{p_i} + \vec{r_i} \times \underbrace{\dot{\vec{p_i}}}_{\vec{F_i}} \right) = \sum_i \vec{r_i} \times \vec{F_i}$$

where $\vec{F_i}$ is the total force exerted on the point i of the rigid body.

We will denote

$$\vec{M} = \sum_i \vec{r_i} \times \vec{F_i} \tag{B.10}$$

the total *torque* exerted on the rigid body, then the following equation

$$\boxed{\frac{d}{dt}\vec{A} = \vec{M}} \tag{B.11}$$

formulates the conservation of the angular momentum.

B.5 Euler's equation

We have that the angular momentum $\vec{A}$ in equation B.11 is hard to express in any frame of reference – see equations B.7 and B.8.

For a given rigid body $\mathcal{O}$, we then choose to write the conservation of the angular momentum in the system of coordinates corresponding to the principal axes of inertia $(\vec{u_1}, \vec{u_2}, \vec{u_3})$ of $\mathcal{O}$, where the tensor of moments of inertia is diagonal. In this frame, the derivative of the angular momentum relatively to the fixed frame of reference can be decomposed in a first part

$$\frac{d'}{dt}\vec{A} = \sum_k \frac{d}{dt}\Big(\underbrace{\vec{A}\cdot\vec{u_k}}_{A_k}\Big)\vec{u_k}$$

corresponding to the rate of change of $\vec{A}$ relatively to the rotating frame and a second part

$$\vec{\omega} \times \vec{A}$$

corresponding to the change of $\vec{A}$ due only to the rotation of the frame.

We can infer from equations B.8 and B.9 that

$$\forall k \in [\![1, 3]\!], A_k = I_k \omega_k$$

with all the I_k being constant, therefore, with $\vec{M} = \sum_k M_k \vec{u_k}$ the total torque exerted on $\mathcal{O}$, we can finally write the following Euler's equation

$$\boxed{\forall k \in [\![1, 3]\!],\ I_k \dot{\omega_k} + \varepsilon_{k,l,m}\omega_l I_m \omega_m = M_k} \tag{B.12}$$

which rules the rotation of a rigid body.

We can note that the tensor of moments of inertia of a spherically symmetric body is a scalar matrix, therefore the equation B.11 can be directly solved without the considerations of this part.

C | Ellipsoids

C.1 Definition

An ellipsoid is a surface that may be obtained from a sphere by deforming it by means of directional scalings, or more generally, of an affine transformation [67].

Within a Cartesian coordiante system in which the origin is the center of the ellipsoid and the coordinate axes are axes of the ellipsoid, a vector $\vec{r} = \begin{pmatrix} x \\ y \\ z \end{pmatrix} \in \mathbb{R}^3$ belongs to the surface of the ellispoid if and only if

$$\frac{x^2}{a^2} + \frac{y^2}{b^2} + \frac{z^2}{c^2} = 1 \tag{C.1}$$

where a, b and $c \in \mathbb{R}$ are the the semi-axes of the ellipsoid.

Equivalently to equation C.1, an ellipsoid $\mathcal{A}$ can be defined by a positive definite matrix $A \in \mathcal{M}_3(\mathbb{R})$ and a vector $\vec{v} \in \mathbb{R}^3$ such that

$$\boxed{\forall \vec{r} \in \mathbb{R}^3, \vec{r} \in \bar{\mathcal{A}} \Leftrightarrow (\vec{r} - \vec{v})^T A (\vec{r} - \vec{v}) = 1} \tag{C.2}$$

The eigenvectors of A then define the principal axes of $\mathcal{A}$ and the associated eigenvalues are the reciprocals of the squares of the semi-axes. The vector $\vec{v}$ defines the center of the ellipsoid.

C.2 Homogeneous coordinates

C.2.1 Quick reminder

A vector $\vec{r} = \begin{pmatrix} x \\ y \\ z \end{pmatrix} \in \mathbb{R}^3$ is equivalent to its homogeneous form $\begin{pmatrix} x \\ y \\ z \\ 1 \end{pmatrix} \in E^3$ where E^3 is the Euclidean 3D projective space.

Moreover, we have that in E^3, $\forall \lambda \in \mathbb{R}^*$ and $\forall (x, y, z) \in \mathbb{R}^3$, $\begin{pmatrix} x \\ y \\ z \\ 1 \end{pmatrix}$ and $\begin{pmatrix} \frac{x}{\lambda} \\ \frac{y}{\lambda} \\ \frac{z}{\lambda} \\ 1 \end{pmatrix}$ represent the exact same point. Therefore, we will always assume that the last coordinate of our vectors in E^3 is 1.

From the property above, you naturally have that any point in E^3 whose last coordinate would be 0 is then infinitely far from the origin $\begin{pmatrix} 0 \\ 0 \\ 0 \\ 1 \end{pmatrix}$.

C.2.2 Useful affine transformations

C.2.2.1 Translation

We define in $\mathbb{R}^3$ the translation of vector $\vec{u} \in \mathbb{R}^3$ as

$$\begin{aligned} \mathcal{T}_{\vec{u}} \colon \mathbb{R}^3 &\to \mathbb{R}^3 \\ \vec{v} &\longmapsto \vec{v} + \vec{u} \end{aligned}$$

In E^3, this function $\mathcal{T}_{\vec{u}}$ is represented by the matrix $T_{\vec{u}}$:

$$\boxed{T_{\vec{u}} = \begin{pmatrix} \mathbb{1}_3 & \vec{u} \\ \vec{0}^T & 1 \end{pmatrix}} \tag{C.3}$$

C.2.2.2 Dilatation

We define in $\mathbb{R}^3$ the dilatation of factor $a \in \mathbb{R}$ as

$$\begin{aligned} \mathcal{X}_a \colon \mathbb{R}^3 &\to \mathbb{R}^3 \\ \vec{v} &\longmapsto a\vec{v} \end{aligned}$$

In E^3, this function $\mathcal{X}_a$ is represented by the matrix X_a:

$$\boxed{X_a = \begin{pmatrix} a\mathbb{1}_3 & \vec{0} \\ \vec{0}^T & 1 \end{pmatrix}} \tag{C.4}$$

C.2.2.3 Rotation

We showed in part A.3 that every 3D rotation can be expressed as the action of some unit quaternion.

The product of quaternions being bilinear, we can associate the action of a quaternion to a linear function in a vectorial space and therefore to a matrix [65].

Consider $q = [\vec{q}, q_0], p = [\vec{p}, p_0] \in \mathbb{H}$. According to part A.2, we have $qp = [\underbrace{\vec{q} \times \vec{p}}_{Ap} + \underbrace{q_0\vec{p}}_{Bp} + \underbrace{p_0\vec{q}}_{Cp}, \underbrace{q_0p_0}_{Dp} \underbrace{-\vec{q} \cdot \vec{p}}_{Ep}]$, with

$$A = \begin{pmatrix} \vec{q}\times\bullet & \vec{0} \\ \vec{0}^T & 0 \end{pmatrix}, B = \begin{pmatrix} q_0\mathbb{1}_3 & \vec{0} \\ \vec{0}^T & 0 \end{pmatrix}, C = \begin{pmatrix} 0_3 & \vec{q} \\ \vec{0}^T & 0 \end{pmatrix}, D = \begin{pmatrix} 0_3 & \vec{0} \\ \vec{0}^T & q_0 \end{pmatrix}, E = \begin{pmatrix} 0_3 & \vec{0} \\ -\vec{q}^T & 0 \end{pmatrix}$$

Therefore the left multiplication by q in $\mathbb{H}$ can be represented by the matrix

$$\begin{aligned} L_q &= A + B + C + D + E \\ &= \begin{pmatrix} \vec{q}\times\bullet + q_0\mathbb{1}_3 & \vec{q} \\ -\vec{q}^T & q_0 \end{pmatrix} \end{aligned}$$

Similarly, we have $pq^* = [\underbrace{\vec{q} \times \vec{p}}_{Ap} + \underbrace{q_0\vec{p}}_{Bp} \underbrace{-p_0\vec{q}}_{-Cp}, \underbrace{q_0p_0}_{Dp} + \underbrace{\vec{q} \cdot \vec{p}}_{-Ep}]$, therefore the right multiplication by q^* can be represented by the matrix

$$\begin{aligned} R_{q^*} &= A + B - C + D - E \\ &= \begin{pmatrix} \vec{q}\times\bullet + q_0\mathbb{1}_3 & -\vec{q} \\ \vec{q}^T & q_0 \end{pmatrix} \end{aligned}$$

Consequently, the matrix representing the action of the unit quaternion q in $\mathbb{H}$ is

$$Q_q = L_qR_{q^*} = R_{q^*}L_q = \begin{pmatrix} \mathcal{Q}_q & \vec{0} \\ \vec{0}^T & \underbrace{N^2(q)}_{=1} \end{pmatrix}$$

where

$$\boxed{\mathcal{Q}_q = (\vec{q}\times\bullet + q_0\mathbb{1}_3)^2 + \vec{q}\vec{q}^T} \tag{C.5}$$

is the matrix representing the rotation associated to the unit quaternion q in $\mathbb{R}^3$.

Therefore, the matrix reprensenting the action of q in $\mathbb{H}$ and the rotation associated to q in E^3 are the same and we will note the latter

$$\boxed{Q_q = \begin{pmatrix} \mathcal{Q}_q & \vec{0} \\ \vec{0}^T & 1 \end{pmatrix}} \tag{C.6}$$

C.3 Belonging matrix

C.3.1 Definition

We want to find for any ellipsoid $\mathcal{A}$ a matrix B acting on homogeneous coordinates with the following properties

$$\forall \vec{r} \in E^3, \begin{cases} \vec{r}^T B \vec{r} < 0 & \text{if } \vec{r} \in \mathcal{A} \setminus \bar{\mathcal{A}} \\ \vec{r}^T B \vec{r} = 0 & \text{if } \vec{r} \in \bar{\mathcal{A}} \\ \vec{r}^T B \vec{r} > 0 & \text{if } \vec{r} \notin \mathcal{A} \end{cases} \tag{C.7}$$

which we will call the *belonging matrix* of $\mathcal{A}$.

C.3.2 Expression

We have seen with equation C.2 that the belonging to the surface of an ellispoid could be expressed with a matrix whose eigenvectors define the principal axes of the ellipsoid and whose eigenvalues define the reciprocals of the squares of the semi-axes. Therefore, if we denote $(R_i)_{i=1:3}$ the semi-axes of the ellipsoid, this matrix can be written as $A = P^{-1}\text{diag}(R_1^{-2}, R_2^{-2}, R_3^{-2})P$.

The semi-axes of an ellipsoid define an orthogonal base of $\mathbb{R}^3$. Therefore P is the transition matrix from the orthogonal base formed by the principal axes of the ellipsoid to the original Euclidean base $(\vec{e_i})_{i=1:3}$, and inversely for P^{-1}.

Consequently, we have that $\forall i \in [\![1,3]\!], \vec{v} + R_i P^{-1} \vec{e_i} \in \bar{\mathcal{A}}$ and so

$$\begin{aligned} \forall i \in [\![1,3]\!], & (P^{-1}R_i\vec{e_i})^T A (P^{-1}R_i\vec{e_i}) = 1 \\ \Leftrightarrow & (P^{-1}R_i\vec{e_i})^T P^{-1}\text{diag}(R_j^{-2})_{j=1:3} P (P^{-1}R_i\vec{e_i}) = 1 \\ \Leftrightarrow & R_i\vec{e_i}^T (P^{-1})^T P^{-1}\text{diag}(R_j^{-2})_{j=1:3} \underbrace{PP^{-1}}_{\mathbb{1}_3} R_i\vec{e_i} = 1 \\ \Leftrightarrow & \vec{e_i}^T (P^{-1})^T P^{-1} \underbrace{\text{diag}(R_j^{-2})_{j=1:3} R_i^2 \vec{e_i}}_{\vec{e_i}} = 1 \\ \Leftrightarrow & \vec{e_i}^T (P^{-1})^T P^{-1} \vec{e_i} = 1 \end{aligned}$$

Thus, the norm of every column vector of P^{-1} equals to 1. Therefore, P^{-1}, and equivalently P, is an orthonormal matrix.

If P is an orthonormal matrix, then the principal axes of the ellipsoids are derived from the original Euclidean base through rotations and permutations of axis. Without loss of generality, we can consider that there are no permutations of axis, leading to $P = \mathcal{Q}_q^{-1} = \mathcal{Q}_q^T$ with q the quaternion describing the orientation of the ellipsoid. Equation C.2 thus becomes:

$$\forall \vec{r} \in \mathbb{R}^3, \vec{r} \in \bar{\mathcal{A}} \Leftrightarrow (\vec{r} - \vec{v})^T \mathcal{Q}_q \text{diag}(R_i^{-2})_{i=1:3} \mathcal{Q}_q^T (\vec{r} - \vec{v}) = 1$$

We can get rid of the $\vec{v}$ by using homogeneous coordinates. In E^3, $\vec{r} - \vec{v}$ becomes $T_{-\vec{v}}\vec{r}$ and, to conserve the scalar product, $\text{diag}(R_i^{-2})_{i=1:3}$ becomes $\text{diag}(R_i^{-2}, 0)_{i=1:3}$.

We always assume that the last coordinate of our vectors in E^3 is 1, therefore we can notice that $\forall \vec{u} \in E^3, \vec{u}^T \text{diag}(0,0,0,-1)\vec{u} = -1$. We can then rewrite equation C.2:

$$\begin{aligned} \forall \vec{r} \in E^3, \vec{r} \in \bar{\mathcal{A}} \Leftrightarrow & \vec{r}^T T_{-\vec{v}}^T Q_q \text{diag}(R_i^{-2}, 0)_{i=1:3} Q_q^T T_{-\vec{v}} \vec{r} = 1 \\ \Leftrightarrow & \vec{r}^T \underbrace{T_{-\vec{v}}^T Q_q \text{diag}(R_i^{-2}, -1)_{i=1:3} Q_q^T T_{-\vec{v}}}_{\mathcal{C}} \vec{r} = 0 \end{aligned}$$

The matrix $\mathcal{C}$ is a good candidate for the belonging matrix of $\mathcal{A}$, we then have to understand how it works.

The $T_{-\vec{v}}$ translation and the Q_q^T rotation bring back the principal axes of the ellipsoid to the original Euclidean base and origin. Without loss of generality, we can then consider that the principal axes of the ellipsoids are along $(\vec{e_1}, \vec{e_2}, \vec{e_3})$.

For a vector $\vec{r} = \begin{pmatrix} x \\ y \\ z \end{pmatrix} \in \mathbb{R}^3$, we have

$$\begin{aligned} &\frac{x^2}{R_1^2} + \frac{y^2}{R_2^2} + \frac{z^2}{R_3^2} = \mu^2 \\ \Leftrightarrow &\frac{x^2}{(\mu R_1)^2} + \frac{y^2}{(\mu R_2)^2} + \frac{z^2}{(\mu R_3)^2} = 1 \end{aligned}$$

therefore, μ can be construed as the rescaling factor that has to be applied to the ellipsoid for $\vec{r}$ to be on its surface. Then, $\mu < 1$ if $\vec{r} \in \mathcal{A} \setminus \bar{\mathcal{A}}$, $\mu = 1$ if $\vec{r} \in \bar{\mathcal{A}}$, and $\mu > 1$ otherwise.

Since we have that $\forall \vec{r} \in E^3, \vec{r}^T \mathcal{C} \vec{r} = \mu^2 - 1$, $\mathcal{C}$ is the matrix we have been looking for, and we can define

$$\boxed{B(\vec{v}, q, (R_i)_{i=1:3}) \equiv T_{-\vec{v}}^T Q_q \text{diag}(R_i^{-2}, -1)_{i=1:3} Q_q^T T_{-\vec{v}}} \tag{C.8}$$

One must notice that such a matrix is symmetric. We can also define the *belonging function* of the ellipsoid $\mathcal{A}$

$$\boxed{\begin{aligned} &\mathcal{F}_{\mathcal{A}} \colon E^3 \to \mathbb{R} \\ &\qquad \vec{r} \longmapsto \vec{r}^T B(\vec{v}, q, (R_i)_{i=1:3}) \vec{r} \end{aligned}} \tag{C.9}$$

such that $\forall \vec{r} \in E^3$, $\vec{r} \in \mathcal{A} \Leftrightarrow \mathcal{F}_{\mathcal{A}}(\vec{r}) \leq 0$ and

$$\boxed{\mathcal{F}_{\mathcal{A}}(\vec{r}) = \mu^2(\vec{r}) - 1} \tag{C.10}$$

with $\mu^2(\vec{r})$ the rescaling factor that has to be applied to the ellipsoid for $\vec{r}$ to be on its surface.

C.3.3 Reduced belonging matrix

The equation C.8 is theoretically relevant, however it is not computationally efficient.

On the one side, resorting to homogeneous coordinates and expressing the translation with a translation matrix (equation C.3) leads to more operations than to express the rotation in $\mathbb{R}^3$ directly. On the other side, we have seen in part 1.1.3 that the rotation of a vector was quicker performed when converting the quaternion associated to the rotation to a rotation matrix.

We then introduce, for an ellipsoid $\mathcal{A}$ whose centre is located in $\vec{v}$, whose orientation is described by the unit quaternion q and whose semi-axes are $(R_i)_{i=1:3}$, the associate *reduced belonging matrix*

$$\boxed{\bar{B}(q, (R_i)_{i=1:3}) \equiv \mathcal{Q}_q \text{diag}(R_i^{-2})_{i=1:3} \mathcal{Q}_q^T} \tag{C.11}$$

with $\mathcal{Q}_q$ the $\mathbb{R}^3$ rotation matrix associated to q (equation C.5). One must notice that the reduced belonging matrix is also symmetric. Furthermore, this reduced belonging matrix has the following properties

$$\forall \vec{r} \in \mathbb{R}^3, \begin{cases} (\vec{r} - \vec{v})^T \bar{B} (\vec{r} - \vec{v}) < 1 & \text{if } \vec{r} \in \mathcal{A} \setminus \bar{\mathcal{A}} \\ (\vec{r} - \vec{v})^T \bar{B} (\vec{r} - \vec{v}) = 1 & \text{if } \vec{r} \in \bar{\mathcal{A}} \\ (\vec{r} - \vec{v})^T \bar{B} (\vec{r} - \vec{v}) > 1 & \text{if } \vec{r} \notin \mathcal{A} \end{cases} \tag{C.12}$$

according to equation C.7, which leads to the following expression for the belonging function:

$$\boxed{\begin{aligned} &\mathcal{F}_{\mathcal{A}} \colon \mathbb{R}^3 \to \mathbb{R} \\ &\qquad \vec{r} \longmapsto (\vec{r} - \vec{v})^T \bar{B}(q, (R_i)_{i=1:3})(\vec{r} - \vec{v}) - 1 \end{aligned}} \tag{C.13}$$

C.4 Unit normal vectors

Since the surface of the ellipsoid – the locus of points where $\mathcal{F}_{\mathcal{A}}(\vec{r}) = 0$ – is an isosurface of the function $\mathcal{F}_{\mathcal{A}}$, we have that $\forall \vec{r_S} \in \bar{\mathcal{A}}, \vec{\nabla} \mathcal{F}_{\mathcal{A}}(\vec{r_S})$ is a non-unit outward-facing normal vector to the ellipsoid in $\vec{r_S}$.

Let us note $\forall \vec{r_S} \in \bar{\mathcal{A}}$, $\vec{n}(\vec{r_S})$ the unit outward-facing normal vector to the ellipsoid in $\vec{r_S}$. Then $\vec{n}(\vec{r_S}) // \vec{\nabla} \mathcal{F}_{\mathcal{A}}(\vec{r_S})$, we thus have to find the direction of this gradient.

C.4.1 Expression with the belonging matrix

We have that

$$\begin{aligned}\forall \vec{r} \in E^3, \mathcal{F}_{\mathcal{A}}(\vec{r}+\vec{dr}) &= (\vec{r}+\vec{dr})^T B(\vec{r}+\vec{dr}) \\ &= \underbrace{\vec{r}^T B\vec{r}}_{\mathcal{F}_{\mathcal{A}}(\vec{r})} + \underbrace{\vec{r}^T B\vec{dr} + \vec{dr}^{\,T} B\vec{dr}}_{2\vec{dr}^{\,T} B\vec{r}} + \vec{dr}^{\,T} B\vec{dr}\end{aligned}$$

therefore we can show that

$$\begin{aligned}\forall \vec{r} \in E^3, \forall i \in [\![1,3]\!],\ \mathcal{F}_{\mathcal{A}}(\vec{r}+dr_i\vec{e_i}) - \mathcal{F}_{\mathcal{A}}(\vec{r}) &= 2dr_i\vec{e_i}^T B\vec{r} + dr_i^2 \vec{e_i} B\vec{e_i} \\ \Rightarrow \frac{\partial}{\partial e_i}\mathcal{F}_{\mathcal{A}}(\vec{r}) &= \lim_{dr_i \to 0} \frac{\mathcal{F}_{\mathcal{A}}(\vec{r}+dr_i\vec{e_i}) - \mathcal{F}_{\mathcal{A}}(\vec{r})}{dr_i} = 2\vec{e_i}^T B\vec{r} \\ \Rightarrow \vec{\nabla}\mathcal{F}_{\mathcal{A}}(\vec{r}) &= \sum_{i=1}^{3} \left(\frac{\partial}{\partial e_i}\mathcal{F}_{\mathcal{A}}(\vec{r})\right)\vec{e_i} = 2\underbrace{\sum_{i=1}^{3}(\vec{e_i}^T B\vec{r})\vec{e_i}}_{B\vec{r}}\end{aligned}$$

i.e. $\vec{\nabla}\mathcal{F}_{\mathcal{A}}(\vec{r}) = 2B\vec{r}$. Consequently, we finally have that

$$\boxed{\forall \vec{r_S} \in \bar{\mathcal{A}}, \vec{n}(\vec{r_S}) = \frac{B(\vec{v}, q, (R_i)_{i=1:3})\vec{r_S}}{|B(\vec{v}, q, (R_i)_{i=1:3})\vec{r_S}|}} \tag{C.14}$$

C.4.2 Expression with the reduced belonging matrix

With the same notations while assuming that the centre of the ellipsoid is located in $\vec{v}$, we can notice that replacing $\vec{r}$ by $(\vec{r}-\vec{v})$ in the demonstration of part C.4.1 leads to the following expression

$$\forall \vec{r} \in E^3, \forall i \in [\![1,3]\!],\ \mathcal{F}_{\mathcal{A}}(\vec{r}+dr_i\vec{e_i}) - \mathcal{F}_{\mathcal{A}}(\vec{r}) = 2dr_i\vec{e_i}^T \bar{B}(\vec{r}-\vec{v}) + dr_i^2 \vec{e_i}\bar{B}\vec{e_i}$$

and thus, by analogy, the following result

$$\boxed{\forall \vec{r_S} \in \bar{\mathcal{A}}, \vec{n}(\vec{r_S}) = \frac{\bar{B}(q, (R_i)_{i=1:3})(\vec{r_S}-\vec{v})}{|\bar{B}(q, (R_i)_{i=1:3})(\vec{r_S}-\vec{v})|}} \tag{C.15}$$

D | Renormalisation group theory

The renormalisation group (RG) theory, attributed to Kenneth G. Wilson [68–70], relies on coarse-graining arguments near critical points and gives a genuine way of thinking about critical phenomena and provides a theoretical motivation for scaling assumptions. Moreover, this theory allows one to calculate critical exponent although being particularly technical.

In this appendix, we mean to present the renormalisation group theory and how it leads to the scaling hypothesis we made, focusing on its implications on numerical simulations scaling. All demonstrations and discussions are based on [71] and unpublished documents by Peter Olsson.

D.1 Coarse-graining argument

D.1.1 Block spins

We can easily illustrate the RG theory with the Ising model for spins with nearest neighbours interactions. In this model, a system of spins displays a ferromagnetic transition at the temperature $T = T_C$, where the correlation length diverges.

Consider a system Ω of spins on a d-dimensional hypercubic lattice, with spacing a. We have that the spins are correlated on lengths scales of order ξ, the basic idea is thus to consider that spins on a length scale la, with l satisfying

$$a \ll la \ll \xi$$

act as a single spin, which we will call a *block spin*.

We can then make the assumptions that block spins interact with their nearest block spin neighbours, as do the single spins, with coupling constants – between spins, and between spins and external field – somewhat different. Our block spin system is then described by the same Hamiltonian than the single spin spin. However, the spacing between block spins is l times larger than the spacing between single spins, leading to the correlation length

$$\xi_l = \frac{\xi}{l}$$

smaller than the correlation length of the original system. This tells us that the latter system is further from criticality than the former, leading to a reduced temperature

$$t_l \equiv 1 - \frac{T}{T_{C,l}} = s(l) \underbrace{\left(1 - \frac{T}{T_C}\right)}_{t} < t$$

with s a function to determine.

Since two consecutive scale changes with the factors l_1 and l_2 are equivalent to a single scale change of factor $l_1 l_2$, we have that

$$s(l_1 l_2) = s(l_1) s(l_2)$$

which is satisfied by

$$s(l) = l^y$$

for any y, hence the scaling assumptions.

Furthermore, we realise that the critical temperature, characterising a state where the correlation length is infinite, is a fixed point of the scaling transformation.

D.1.2 Renormalisation group transformations

We need to formalise the scaling transformation we have introduced.

Consider a system Ω described by the general Hamiltonian

$$\mathcal{H} \equiv -\beta H_\Omega = \sum_n K_n \Theta_n\{S\} \tag{D.1}$$

where $\beta = 1/kT$ with k the Boltzmann constant and T the temperature, K_n are the coupling constants, and $\Theta\{S\}$ the local operators on the degrees of freedom $\{S\}$.

We introduce $\forall l > 1$ the *renormalisation group transformation* R_l which acts on the coupling constants $[K] \equiv (K_n)_n$

$$R_l[K] \equiv [K'] \tag{D.2}$$

and which is most often complicated and non-linear. These transformations verify

$$\forall l_1, l_2 > 1,\ R_{l_1 l_2}[K] = R_{l_2} \cdot R_{l_1}[K] \tag{D.3}$$

and do not admit inverses since l has to be greater or equal to 1, therefore RG transformations form a semi-group.

RG transformations are coarse-graining transformations which reduce the number N of degrees of freedom by a factor l^{-d} to $N' = Nl^{-d}$, where d is the dimension of the system. Therefore, the degrees of freedom $\{S_i\}_{1\dots N}$ and the Hamiltonian $\mathcal{H}$ are replaced by *block variables* $\{S'_I\}_{1\dots N'}$ and an effective Hamiltonian $\mathcal{H}'$ for these new degrees of freedom respectively.

We introduce a *projection operator* $P(S_i, S'_I)$ which satisfies

$$e^{\mathcal{H}'\{[K'], S'_I\}} = \mathrm{Tr}_{\{S_i\}} P(S_i, S'_I) e^{\mathcal{H}\{[K], S_i\}} \tag{D.4}$$

where $\mathrm{Tr}_{\{S_i\}}$ denotes the sum over the degrees of freedom $\{S\}$, and must fulfil the following requirements

(i) $P(S_i, S'_I) \geq 0$,

(ii) $P(S_i, S'_I)$ reflects the symmetries of the system,

(iii) $\sum_{\{S'_I\}} P(S_i, S'_I) = 1$.

In the context of part D.1.1, the projection operator P is the function that associates an up or down spin to a block of spins.

We define the free energy Z

$$Z[K] = \mathrm{Tr}_{\{S\}} e^{\mathcal{H}\{[K], S_i\}} \tag{D.5}$$

and the free energy density f

$$f[K] = \frac{1}{L^d} Z[K] \tag{D.6}$$

where L is the characteristic dimension of the system, which is the quotient of the free energy by the volume of the system.

Condition (iii) ensures that the partition function, and thus the free energy, remains unchanged

$$\begin{aligned} Z[K'] &\equiv \mathrm{Tr}_{\{S'_I\}} e^{\mathcal{H}'\{[K'], S'_I\}} \\ &= \mathrm{Tr}_{\{S'_I\}} \mathrm{Tr}_{\{S_I\}} P(S_i, S'_I) e^{\mathcal{H}\{[K], S_i\}} \\ &= \mathrm{Tr}_{\{S_i\}} e^{\mathcal{H}\{[K], S_i\}} \cdot 1 \\ &= Z[K] \end{aligned}$$

while the free energy density f is rescaled

$$\begin{aligned} \frac{1}{L^d} \ln Z[K] &= \frac{l^{-d}}{(L/l)^d} \ln Z[K'] \\ &= l^{-d} \frac{1}{L'} \ln Z[K'] \end{aligned}$$

i.e.,

$$f[K] = l^{-d} f[K'] \tag{D.7}$$

D.2 Renormalisation group flows

D.2.1 Fixed points of the coupling constants space

An infinite number of iterations of the RG transformations is required in order to eliminate all degrees of freedom of a thermodynamic system in the thermodynamic limit $N \to +\infty$. By doing so, singular behaviour may occur.

For any $l > 1$, R_l is a function from the coupling constants $[K]$ space to this same space, which we will denote $\mathcal{K}$. We will call *renormalisation group flows* the trajectories in the coupling constants space which are obtained by iterating RG transformations. It is likely to find fixed points of the RG transformations in $\mathcal{K}$, we will then call the *basin of attraction* of such a fixed point the set of points of $\mathcal{K}$ from which an infinite number of iterations of RG transformations inevitably lead.

We have $\forall l > 1$ that the correlation length ξ transforms under the RG transformation R_l as

$$\xi[K'] = \xi[K]/l \tag{D.8}$$

therefore, for a fixed point $[K^*]$

$$\xi[K*] = \xi[K*]/l$$

which allows us to distinguishes two cases

(i) $\xi[K^*] = 0$, for which we will call $[K^*]$ a *"trivial" fixed point*, and

(ii) $\xi[K^*] = +\infty$, for which we will call $[K^*]$ a *critical fixed point*.

We can then notice that since n iterations of R_l transform the correlation length as

$$\xi[K] = l^n \xi[K^{(n)}]$$

we have that all points in the basin attraction of a critical fixed point $[K^*]$, which satisfy $\xi[K^{(n)}] \xrightarrow[n\to+\infty]{} \xi[K^*] = +\infty$, have infinite correlation length. This basin of attraction is called the *critical manifold*.

We have implicitly that the critical points were isolated, however this is not necessarily the case. In fact, fixed points are classified according to their codimension, but this does not affect the validity of our demonstration.

We note that it is also possible for RG flows to describe limit cycles or strange attractors, but in practice it is almost never the case. We will then neglect these possibilities from now on.

D.2.2 Relevance of variables

We are interested in the behaviour of RG flows in the vicinity of a critical fixed point $[K^*]$.

Consider $[K]$ a point of $\mathcal{K}$ close to $[K^*]$

$$[K] = [K^*] + [\delta K]$$

then $\forall l > 1$, $[K]$ transforms under R_l as $R_l[K] = [K']$ with

$$[K']\{[K^*] + [\delta K]\} = \underbrace{[K']\{[K^*]\}}_{[K^*]} + [\delta K']$$

$$\textit{i.e.,}\ [K']\{[K^*] + [\delta K]\} = [K^*] + \underbrace{\left(\left. \frac{\partial K'_n}{\partial K_m} \right|_{K_m = K^*_m} \right)_{n,m}}_{M^{(l)}} [\delta K] + \mathcal{O}\left([\delta K]^2\right)$$

according to Taylor's theorem, where $M^{(l)}$ is the linearised RG transformation in the vicinity of $[K^*]$ and is a real matrix.

In practice, $M^{(l)}$ is most often diagonalisable with real eigenvalues. For present purposes, we will assume for the rest of our presentation that it is symmetric without further notice. We advise the interested reader to read part 9.4.4 of [71] for corrections to be brought to our theory in the case of a non-symmetric linearised RG transformation.

We will denote the eigenvalues and eigenvectors of $M^{(l)}$ by $\Lambda_l^{(\sigma)}$ and $\vec{e}^{(\sigma)}$ respectively, where $(\vec{e}^{(\sigma)})_\sigma$ is an orthonormal base of $\mathcal{K}$ according to the spectral theorem. We can then infer from the semi-group property of equation D.3 that

$$\begin{aligned} \forall l, l' > 1,\ M^{(l)} M^{(l')} &= M^{(ll')} \\ \Rightarrow \forall \sigma,\ \Lambda_l^{(\sigma)} \Lambda_{l'}^{(\sigma)} &= \Lambda_{ll'}^{(\sigma)} \end{aligned}$$

which we can differentiate with respect to l'

$$\begin{aligned} & \frac{d}{dl'}\left(\Lambda_l^{(\sigma)} \Lambda_{l'}^{(\sigma)}\right) = \frac{d}{dl'} \Lambda_{ll'}^{(\sigma)} \\ \Leftrightarrow & \cancelto{0}{\frac{d\Lambda_l^{(\sigma)}}{dl'}} \Lambda_{l'}^{(\sigma)} + \Lambda_l^{(\sigma)} \frac{d\Lambda_{l'}^{(\sigma)}}{dl'} = \frac{d}{dl'} \Lambda_{ll'}^{(\sigma)} \\ & \Rightarrow \Lambda_l^{(\sigma)} \left.\frac{d\Lambda_{l'}^{(\sigma)}}{dl'}\right|_{l'=1} = \frac{d\Lambda_l^{(\sigma)}}{dl} \end{aligned}$$

and therefore write

$$\Lambda_l^{(\sigma)} = l^{y_\sigma} \tag{D.9}$$

where y_σ is independent of l.

Finally, we have that

$$\begin{aligned} [\delta K'] &= M^{(l)} [\delta K] \\ &= \sum_\sigma \Lambda_l^{(\sigma)} \underbrace{\left(\vec{e}^{(\sigma)} \cdot [\delta K]\right)}_{a^{(\sigma)}} \vec{e}^{(\sigma)} \\ &= \sum_\sigma \underbrace{l^{y_\sigma} a^{(\sigma)}}_{a^{(\sigma)\prime}} \vec{e}^{(\sigma)} \end{aligned} \tag{D.10}$$

for which we will distinguish 3 cases:

(i) $y_\sigma > 0$, which implies that $a^{(\sigma)\prime}$ grows as l increases, and for which we will describe the corresponding eigenvalue/direction/eigenvector as *relevant*,

(ii) $y_\sigma < 0$, which implies that $a^{(\sigma)\prime}$ shrinks as l increases, and for which we will describe the corresponding eigenvalue/direction/eigenvector as *irrelevant*,

(iii) $y_\sigma = 0$, which implies that $a^{(\sigma)\prime}$ does not change as l increases, and for which we will describe the corresponding eigenvalue/direction/eigenvector as *marginal*.

Therefore, if we start at $[K]$ near $[K^*]$, but not in the critical manifold then the flow in directions out of the critical manifold in the vicinity of $[K^*]$ are associated with relevant eigenvalues. The irrelevant eigenvalues correspond to directions into the fixed point, and their corresponding eigenvectors span the critical manifold.

D.2.3 Relation between RG flows and the phase diagram

Starting from any point in $\mathcal{K}$, which is equivalent to the phase space, we can determine to which fixed point an infinite number of iterations of RG transformations leads to. The state of the system described by this fixed point then represents the phase at the original point.

RG theory therefore enables one to investigate the whole phase diagram. We will however focus on critical behaviours and advise the interested reader to read part 9.3.3 of [71] about the global properties of RG flows and the different types of fixed points and their significance.

We have that points that are slightly off the critical manifolds are repelled from it in the relevant directions. Therefore, it is the same eigenvalues that drive all slightly off-critical systems away from the critical fixed point: this is the origin of universality. Furthermore, we have that the critical behaviour is not determined by the initial values of the coupling constants but only by the flow behaviour.

D.3 Critical scaling

D.3.1 Scaling behaviour of the free energy density and its derivatives

We have that the linearised RG transformation R_l close to the critical fixed point $[K^*]$, $M^{(l)}$, is diagonal in the orthonormal base $(\vec{e}^{(\sigma)})_\sigma$ of $\mathcal{K}$. We want to investigate the behaviour of the free energy density f and its derivatives close to this critical fixed point, we will then denote $[K^*] \equiv \sum_\sigma K^*_\sigma \vec{e}^{(\sigma)}$ and introduce $\tilde{f}$ such that

$$\begin{aligned} f[K] = f(K_0, \dots, K_m) \equiv \tilde{f}(\tilde{K}_0, \dots, \tilde{K_m}) = \tilde{f}[\tilde{K}] \\ \forall \sigma \in [\![0, m]\!],\ \tilde{K_\sigma} = \begin{cases} \frac{K_\sigma - K^*_\sigma}{K^*_\sigma} & \text{if } K^*_\sigma \neq 0 \\ K_\sigma & \text{if } K^*_\sigma = 0 \end{cases} \end{aligned} \tag{D.11}$$

and which verifies the following property

$$\forall \sigma \in [\![0, m]\!],\ \frac{\partial}{\partial K_\sigma} f[K] = \begin{cases} \frac{1}{K^*_\sigma} \frac{\partial}{\partial \tilde{K}_\sigma} \tilde{f}[\tilde{K}] & \text{if } K^*_\sigma \neq 0 \\ \frac{\partial}{\partial K_\sigma} \tilde{f}[\tilde{K}] & \text{if } K^*_\sigma = 0 \end{cases}$$

which implies

$$\forall \sigma \in [\![0, m]\!],\ \frac{\partial}{\partial K_\sigma} f[K] \propto \frac{\partial}{\partial \tilde{K}_\sigma} \tilde{f}[\tilde{K}] \tag{D.12}$$

this property being also easily demonstrated for cross-derivatives and higher order derivatives.

According to equations D.7 and D.9, the free energy density transforms under n iterations of the RG transformation R_l as

$$f[K] = l^{-nd} f[K'] = l^{-nd} \tilde{f}[\tilde{K}'] = l^{-nd} \tilde{f}(l^{ny_0} \tilde{K}_0, \dots, l^{ny_m} \tilde{K}_m) \tag{D.13}$$

Besides that it has to be greater or equal to 1, there is no restriction to the values l can take, we then introduce b such that

$$l^n = \left(\frac{b}{\tilde{K}_0} \right)^{1/y_0} \geq 1 \tag{D.14}$$

therefore we have the free energy density and its derivatives

$$\begin{aligned} f[K] = \left(\frac{\tilde{K}_0}{b} \right)^{d/y_0} \tilde{f} \left(b, \left(\frac{b}{\tilde{K}_0} \right)^{y_1/y_0} \tilde{K}_1, \dots, \left(\frac{b}{\tilde{K}_0} \right)^{y_m/y_0} \tilde{K}_m \right) \\ \forall \sigma \in [\![0, m]\!],\ \frac{\partial}{\partial K_\sigma} f[K] \propto \left(\frac{\tilde{K}_0}{b} \right)^{(d-y_\sigma)/y_0} \frac{\partial}{\partial K_\sigma} \tilde{f} \left(b, \left(\frac{b}{\tilde{K}_0} \right)^{y_1/y_0} \tilde{K}_1, \dots, \left(\frac{b}{\tilde{K}_0} \right)^{y_m/y_0} \tilde{K}_m \right) \end{aligned} \tag{D.15}$$

for which we will distinguish 2 cases:

(i) $\forall \sigma \in [\![0, m]\!],\ \vec{e}^{(\sigma)}$ is a relevant eigenvector, then if we take $\tilde{K}_\sigma = 0,\ \forall \sigma \in [\![1, m]\!]$, we can rewrite equation D.15 as

$$\begin{cases} f[K] = \left(\frac{\tilde{K}_0}{b} \right)^{d/y_0} \tilde{f}\,(b, 0, \dots, 0) \\ \forall \sigma \in [\![0, m]\!],\ \frac{\partial}{\partial K_\sigma} f[K] \propto \left(\frac{\tilde{K}_0}{b} \right)^{(d-y_\sigma)/y_0} \frac{\partial}{\partial K_\sigma} \tilde{f}\,(b, 0, \dots, 0) \end{cases} \Rightarrow \begin{cases} f[K] & \underset{\tilde{K}_0 \to 0}{\sim} \tilde{K}_0^{c_0} \\ \frac{\partial}{\partial K_\sigma} f[K] & \underset{\tilde{K}_0 \to 0}{\sim} \tilde{K}_0^{c_{0,\sigma}} \end{cases} \tag{D.16}$$

where c_0 and $c_{0,\sigma}$ are constants, hence the power-law scaling of the thermodynamic constants close to criticality.

Therefore, RG theory gives a theoretical explanation of the power-law scaling at criticality, thus supporting our scaling assumptions, and furthermore provides a technique to calculate the corresponding critical exponents. However, as stated in the introduction to this appendix, this calculation remains particularly

technical, "where the renormalization group approach has been successful a lot of ingenuity has been required: one cannot write a renormalization group cookbook" [70]. We advise the interested reader to read part 9.6 of [71] on the application of RG theory to the 2D Ising model.

(ii) $\exists\ \sigma \in [\![1, m-1]\!]$, $\vec{e}^{(0)}, \dots, \vec{e}^{(p-1)}$ are revelant eigenvectors – which implies $y_0, \dots, y_{p-1} > 0$ – and $\vec{e}^{(p)}, \dots, \vec{e}^{(m)}$ are irrelevant eigenvectors – which implies $y_p, \dots, y_m < 0$ –, then we can notice that in equation D.15

$$\forall \sigma \in [\![p, m]\!],\ \left(\frac{b}{\tilde{K}_0}\right)^{y_\sigma/y_0} \tilde{K}_\sigma \xrightarrow[\tilde{K}_0 \to 0]{} 0$$

therefore if $\tilde{f}$ is analytic in the limit of the vanishing coupling constants in the irrelevant directions, then the results of equation D.16 still hold. However, this is often not the case. When $\tilde{f}$ is singular in the limit that a particular irrelevant variable vanishes, the irrelevant variable is termed a *dangerous irrelevant variable*.

We want to draw attention to the fact that in the case of the free energy density depending solely on two relevant variables K_0 and K_1, or on a relevant variable K_0 and a non-dangerous irrelevant variable K_1, we have close to criticality

$$f[K] = \left(\frac{\tilde{K}_0}{b}\right)^{d/y_0} \tilde{f}\left(b, \left(\frac{b}{\tilde{K}_0}\right)^{y_1/y_0} \tilde{K}_1\right) \equiv \tilde{K}_0^{d/y_0} \tilde{f}_1\left(\tilde{K}_0^{-y_1/y_0} \tilde{K}_1\right) \tag{D.17}$$

with a similar result for the derivatives of the free energy density, therefore in the context of numerical simulations of a system close to criticality with two relevant variables not equal to their critical values, it is still possible to determine from the data the fitting function $\tilde{f}_1$ and then the critical exponent.

In the case of K_1 being a relevant variable, we will call $\Delta \equiv y_1/y_0$ the *crossover scaling critical exponent* and $z \equiv \tilde{K}_1/\tilde{K}_O^{\Delta}$ the *crossover scaling variable* [4]. What happens if z is non-neglible is that this variable is able to drive the system from the neighbourhood of one fixed point to that of another. Therefore, we may not observe the correct assymptotic behaviour when neglecting the term associated with K_1, hence the importance of this correction.

Furthermore, what has been eluded in our demonstration is that to verify equation D.14, b has to be of the same sign as $\tilde{K}_0$, therefore in equation D.16 the value and most importantly the sign of $\tilde{f}(b, 0, \dots, 0)$ and its derivatives, and thus the sign of the asymptotic approximation, may change depending on the sign of $\tilde{K}_0$. What is most often observed is a scaling behaviour at criticality of the type

$$\begin{aligned} f[K] &\underset{\tilde{K}_0 \to 0}{=} A_\pm^{(0)} |\tilde{K}_O|^{c_0} + o\left(|\tilde{K}_O|^{c_0}\right) \\ \frac{\partial}{\partial K_\sigma} f[K] &\underset{\tilde{K}_0 \to 0}{=} A_\pm^{(0,\sigma)} |\tilde{K}_O|^{c_{0,\sigma}} + o\left(|\tilde{K}_O|^{c_{0,\sigma}}\right) \end{aligned} \tag{D.18}$$

where the values of $A_\pm^{(0)}$ and $A_\pm^{(0,\sigma)}$ may change depending on the sign of $\tilde{K}_0$.

D.3.2 Corrections to scaling

Consider for a given Hamiltonian that the RG transformation R_l close to the critical fixed point $[K^*]$ is diagonal in the orthonormal base $(\vec{e}^{(0)}, \vec{e}^{(1)})$ with $\vec{e}^{(0)}$ a relevant eigenvector and $\vec{e}^{(1)}$ an irrelevant eigenvector. We then have, with the notation of equations D.15 and D.17, and in the framework of equation D.18, the following relation

$$\begin{aligned} f[K] &\equiv \left|\tilde{K}_0\right|^{d/y_0} \tilde{f}_1^{\pm}\left(\left|\tilde{K}_0\right|^{-y_1/y_0} \tilde{K}_1\right) \\ \forall \sigma \in [\![0, 1]\!],\ \frac{\partial}{\partial K_\sigma} f[K] &\equiv \left|\tilde{K}_0\right|^{(d-y_\sigma)/y_0} \tilde{f}_{1,\sigma}^{\pm}\left(\left|\tilde{K}_0\right|^{-y_1/y_0} \tilde{K}_1\right) \end{aligned} \tag{D.19}$$

In practice, it is very difficult to access the asymptotic critical regime $\tilde{K}_0 \to 0$, therefore the irrelevant variable may not be negligible and corrections have to be brought to our scaling assumptions.

A solution is to assume that $\tilde{f}_1$ and/or $\tilde{f}_{1,\sigma}$ are analytic functions in the limit that their argument, which we will call x for convenience, vanishes – assumption which is valid if $\tilde{K}_1$ is not a dangerous irrelevant variable. Therefore, we have a new assymptotic behaviour

$$\begin{aligned} f[K] &\underset{\tilde{K}_0 \to 0}{=} \left|\tilde{K}_0\right|^{d/y_0} \left(A_1 + B_1 \left|\tilde{K}_0\right|^{-y_1/y_0} \tilde{K}_1 + \mathcal{O}\left(x^2\right)\right) \\ \forall \sigma \in [\![0,1]\!],\ \frac{\partial}{\partial K_\sigma} f[K] &\underset{\tilde{K}_0 \to 0}{=} \left|\tilde{K}_0\right|^{(d-y_\sigma)/y_0} \left(A_{1,\sigma} + B_{1,\sigma} \left|\tilde{K}_0\right|^{-y_1/y_0} \tilde{K}_1 + \mathcal{O}\left(x^2\right)\right) \end{aligned} \tag{D.20}$$

according to Taylor's theorem, where A_1, B_1, $A_{1,\sigma}$ and $B_{1,\sigma}$ are – non-universal – constants.

As expected, the leading behaviour as $\tilde{K}_0 \to 0$ is a power-law in $\tilde{K}_0$. We may then distinguish 2 cases:

(i) $|y_1|/y_0 > 1$, which implies that the correction becomes smaller as $\tilde{K}_0 \to 0$,

(ii) $|y_1|/y_0 < 1$, which implies that the correction may not be negligible for small but non-zero $\tilde{K}_0$. This first order correction is actually singular, since it gives rise to a cusp [72] at $\tilde{K}_0 = 0$. Such a correlation is referred as a *confluent singularity*.

D.3.3 Finite-size scaling

Numerical simulations use finite systems of which we will denote L the characteristic length. As the system approaches a critical fixed point, its correlation length ξ diverges, therefore when L and ξ are comparable, the thermodynamic properties of the system can not be considered as being those of an infinite system anymore. What is observed is that the transition associated with the critical fixed point appears less sharp.

To address this issue, one has to include the characteristic length of the system – or rather its inverse $1/L$ which vanishes as the system approaches the critical fixed point associated with an infinite system – in the variables of the free energy density, which will then transform under n iteration of the RG transformation R_l as

$$f[K] = l^{-nd} f[K'] = l^{-nd} \tilde{f}[\tilde{K}'] = l^{-nd} \tilde{f}(l^{ny_0} \tilde{K}_0, \ldots, l^{ny_m} \tilde{K}_m, l^n L^{-1}) \tag{D.21}$$

A crossover scaling analysis, as described in the discussion of equation D.17, can then be performed.